University of Alberta

Liquid Degassing Using Fine Droplets and Micro Bubbles

by

Yiming Ji

A thesis submitted to the Faculty of Graduate Studies and Research
in partial fulfillment of the requirements for the degree of

Master of Science
in
Chemical Engineering

Department of Chemical and Materials Engineering

Fall 2011
Edmonton, Alberta

Abstract

This project was initiated to study the H_2S removal process from liquid sulfur and later extended to generic liquid degassing scenarios. Enersul Hyspec™ Degassing Process was first field tested so that comparison could be made with new units to be engineered. Two new degassing units were modelled and lab-tested. The first one used fine poly-dispersed droplets, and the other added micro bubbles to the traditional approach of mechanical agitation. A single unit using one of the degassing techniques could achieve >90% efficiencies in a cost-effective manner. Higher degassing requirements can be met by operating multiple units in series. Degassing using mono-dispersed droplets was also studied to provide a better understanding of the contributing parameters for the poly-dispersed droplet system. Linear correlations of the Sherwood number in relation to the Peclet number were derived. Finally, kinetic parameters, the diffusion coefficient and reaction rate constants of H_2S in liquid sulphur, were determined.

Acknowledgements

Three years of a Master's program has been a long journey for me, during which I have owed my gratitude to countless people.

My appreciation first goes to Dr. Zhenghe Xu, my supervisor. Dr. Xu is such an amazing professor and probably the most hardworking guy I have ever seen. The most valuable virtue I learnt from Dr. Xu and the biggest reason why I feel lucky to work with him is that he is so humble that he makes the gap between a student and a world-renown professor hardly noticeable. Besides his consistent supports, I especially appreciate his "bold" decision on taking on me into this master's program three years ago when even myself doubted my not-so-engineering background.

Dr. Zhongchao Tan, my co-supervisor, is also on the very top of the long list. My gratitude to him cannot be described by any word whatsoever. Without his consistent and patient guidance, encouragement and trust ever since the first day we met each other almost four years ago, I would never have gone this far and found my journey this enjoyable. My career probably would have gone a totally different way. I enjoyed every single conversation I had with him on a daily basis. More importantly, Dr. Tan has also been a tremendous mentor and friend to me outside the academic world. He sets such a great example to me as to how a man should balance his work and family responsibilities while working hard towards being the top.

My thanks also go to Drs. Yadi Maham, Sean Sanders, and John Shaw. It was a great fun taking their courses and/or being their teaching assistant.

Moreover, beyond all, I have a strong sense of the debt of love that I owe to my dear Mom, Yanjun Wang, and Dad, Yongchun Ji. Every time I heard them teasing my two years' absence from home by saying "We know you don't miss us at all and probably wouldn't even be able to recognize us next time you come back home", I feel like nothing but crying. Two years and a half is too long for me, too, but it is their tremendous understanding, care, and support that have carried me over all the hard times I had. This debt of love is also extended to Juan Zhang, my dear girlfriend. There have been way too many hard times for our long distance relationship but we somehow managed to get through them all. We've got plenty of good reasons to continue our life journey on together.

Many thanks should also be given to my friends in Edmonton and Calgary for their encouragement and help. I did have a great time working with my gorgeous officemates at Edmonton and group mates in Calgary. I thank my buddies all over the world, too, for their continued friendship. Their success always sets a bar for me to measure myself and keeps me aiming high and never giving up.

Finally, I would like to acknowledge Natural Sciences and Engineering Research Council (NSERC) of Canada and Enersul Inc. for their financial and technical support.

All in all, if I were to be asked to use one word to summarize what I've learned through my master's program, I would definitely say "patience". Most of the times, success and happiness are about nothing but being patient with everything you have and anything you are wishing for.

Table of Contents

List of Tables

List of Figures

CHAPTER 1 : INTRODUCTION

1.1 Background

Hydrogen sulfide (H_2S) is a byproduct of a number of operations in petrochemical industries. It is usually converted to elemental sulfur (S) via Claus Process, also referred to as a "sulfur recovery process". This process world-widely supplies 47 million tonnes of elemental sulfur annually [1]. Claus Process is composed of two-step reactions — the partial combustion of H_2S to SO_2 and the synproportionation reaction between hydrogen sulfide and sulfur dioxide [2]:

$$H_2S + \frac{3}{2}O_2 \rightarrow SO_2 + H_2O \qquad (1)$$

$$2H_2S(g) + SO_2(g) \leftrightarrow \frac{3}{n}S_n(g) + 2H_2O(g) \qquad (2)$$

However, some thermodynamic limitations exist. In order to get high conversion efficiency, this exothermic process requires a low operation temperature, which leads to low reaction rates. Elemental sulfur is then condensed, but inevitably some dissolved H_2S retains in the liquid products. Ismagilova et al. [3] reported the amount of this H_2S to be about 240-380 ppmw.

H_2S is a notoriously toxic and flammable gas so that most governments require the liquid sulfur to be de-H_2S-ed to a level lower than 10 ppmw [4] before it can be stored or transported to the end users. Liquid sulfur serves as a key element in many industrial processes such as the production of carbon disulfide, rubber, pharmaceuticals, and sulfuric acid [5].

H_2S should also be well controlled in the feedstock used for treatment of hydrocarbons in the oil and gas industry because it poisons most of the catalysts.

Therefore, there is a need to have an efficient and cost-effective design of a sulfur degassing apparatus. What makes this H_2S-sulfur system more complicated is that, simultaneously, H_2S is reacting with liquid sulfur. First noticed by Fanelli [6], unlike most gases, the solubility of H_2S in liquid sulfur increased with the temperature. This phenomenon is resulted from the reaction between H_2S and liquid sulfur and the solubility of the product, H_2S_x (x=2-5), increases significantly with the temperature. The sulfur-H_2S-H_2S_x system is, therefore, described as:

$$H_2S_x \underset{k_{-1}}{\overset{k_1}{\rightleftharpoons}} H_2S_{(sol)} \underset{k_{-2}}{\overset{k_2}{\rightleftharpoons}} H_2S_{(gas)} \tag{3}$$

The direction to which this system shifts is determined by the reaction and mass transfer rate constants k_1, k_{-1}, k_2, and k_{-2}. k_1 and k_{-1} describe the reversible chemical reactions, whereas k_2, and k_{-2} are for the physical mass transfer processes. This equation also describes the sulfur degassing process since H_2S_x is considered a non-diffusive species in liquid sulfur. More specifically, a liquid sulfur degassing process is composed of four steps:

1. decomposition of H_2S_x to H_2S,
2. diffusion of H_2S to the sulfur surface,
3. mass transfer of H_2S through the interface, and
4. removal of H_2S from the surrounding environment.

The third and fourth steps are usually a few orders of magnitude faster than the second one. Besides, the decomposition of H_2S_x, even though kinetically very slow, can be greatly promoted by adding certain catalysts in practice. Therefore,

the second step, usually limited by the interfacial area, determines the rate of the whole degassing process. Various degassing techniques are in existence aiming to improve this point but not many of them address this problem well.

In order to enhance the degassing efficiency, it is of great importance to conduct fundamental studies such as analytical modeling. Essentially, degassing is a specific example of a general liquid-gas mass transfer process. The contributing factors can be investigated separately and well integrated into the design of the equipment. Equally important is to look into the fundamental parameters that determine/affect the rates and limits of the mass transfer such as the diffusion coefficient, reaction rate constants and solubility.

1.2 Motivations/Existing degassing techniques

There are various degassing techniques being used or patented by different oil and gas companies. Some typical processes are as follows.

Enersul Hyspec^{TM} Degassing Process

Enersul LP (Limited Partnership) is a major sulfur player in Canada and owns a patented Hyspec^{TM} sulfur degassing process, operating in between of 135 and 145 °C. As shown in Figure 1-1, this degassing unit is comprised of 4 tanks operating in series. Liquid sulfur flows through each degassing tank and is vigorously agitated by an impellor. Large bubbles, forming through the openings on a shroud, are also expected to enhance the degassing efficiency. Sweep gas is injected in and carries away the H_2S removed from the liquid product. One of the

biggest advantages of this design is a much shortened residence time (about 10 minutes in each tank). Each tank has a capacity of about 2.5 tons of sulfur and the sulfur flow rate is designed to be 45 tons per hour. The actual working load is 800 tons per day. In addition, 5 to 10 ppmw of catalyst is continuously injected in the first tank. When the total H_2S concentration in the feed is about 120-135 ppmw, field tests showed that the final concentration is below 5 ppmw [7].

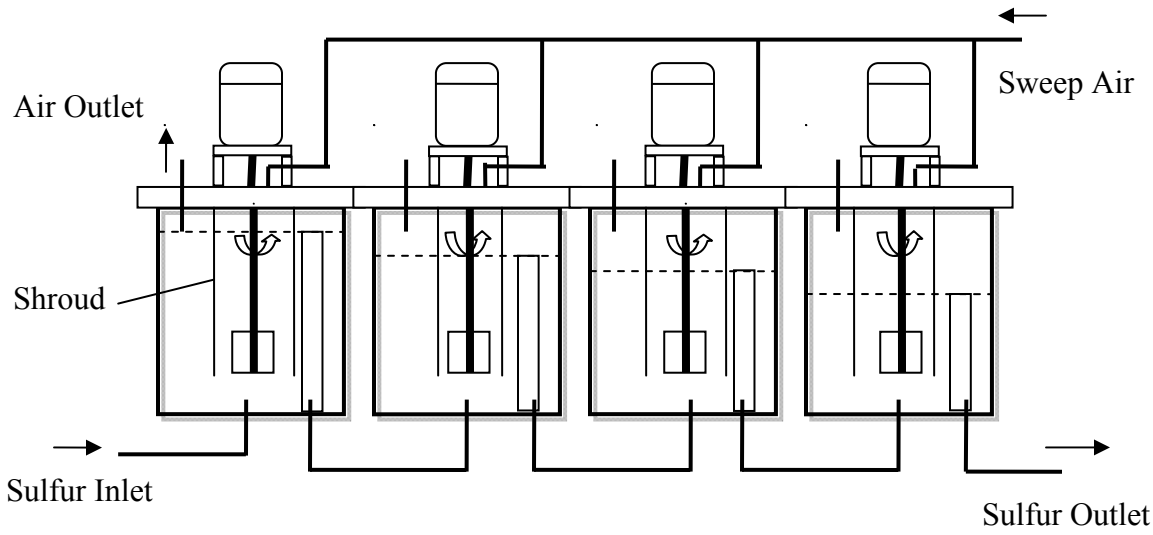

Figure 1-1 Schematic of the Enersul Hyspec^{TM} degassing process

D'GAASS Degassing Process

D'GAASS is another common degassing technique patented by Goar, Allison & Associates, Inc. [8]. The key part of this process is a vessel as shown in Figure 1-2. It is a pressurized system such that compressed air (>60 psig) is injected in to be in contact with sulfur within special fixed vessel internals. The elevated pressure is expected to favor the H_2S oxidization process. Therefore, the size of the reactor and the residence time are effectively reduced, while recycle of the

overhead stream becomes more feasible. Its capacity is about 60 tons of sulfur per day.

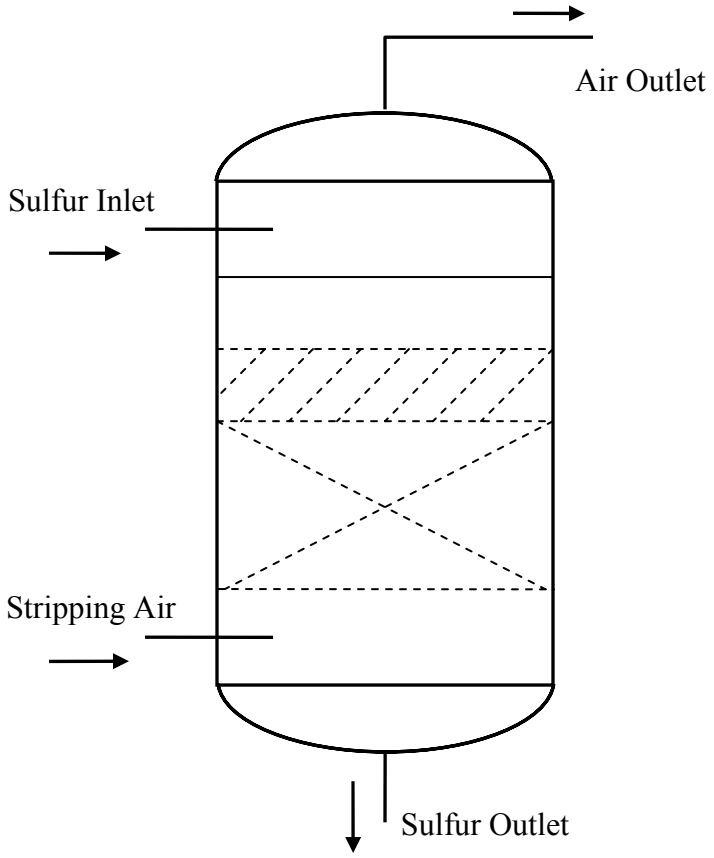

Figure 1-2 Schematic of the D'GAASS degassing process

Shell Degassing Process

Shell Global Solutions, as one of the biggest oil and gas players, offers one of the most sophisticated sulfur degassing solutions. The concentration of the H_2S in their liquid sulfur coming from the Claus process was reported to be 250 - 300 ppmw [9]. Worldwide there have been more than 120 of it in operation and their capacities range from 3 to 4000 tons of sulfur per day. The schematic of the degassing unit is shown in Figure 1-3. Liquid sulfur is circulating in a big stripper column agitated by preheated stripping air injecting from the bottom. Meanwhile,

H_2S_x is oxidized to H_2S, significantly facilitating the degassing process. H_2S removed from the sulfur is then taken carried away by the sweep air to an incinerator.

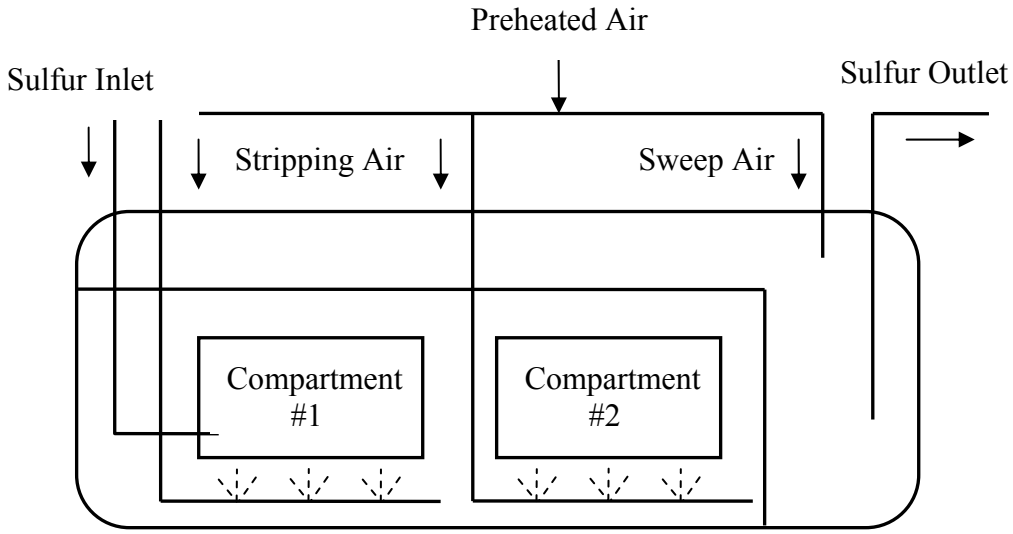

Figure 1-3 Schematic of the Shell degassing process

ExxonMobil Degassing Process

ExxonMobil Liquid Sulfur Degassing™ technology includes three types of processes: air only, catalyst only, and a combination of air and catalyst. The core design of the equipment is almost identical to the Shell one, where stripping gas forms small bubbles to facilitate both the mass transfer and agitation. An air only system is ideal as it has no negative effect on the sulfur product quality but the combination system is the most common one when adequate residence time is not permitted.

SNEA Aquisulf Degassing Process

SNEA Aquisulf Degassing Process is another technique that mainly relies on catalyst addition [10]. The equipment design, as shown in Figure 1-4, is quite similar to Shell's degassing unit. Sulfur is circulating within two compartments in mix with certain catalysts. Instead of sparging stripping gas, this unit uses a spray method to agitate sulfur. It is a technique that has been used world-widely for a long time, but the major concern falls on the residue catalyst concentration in the final sulfur product.

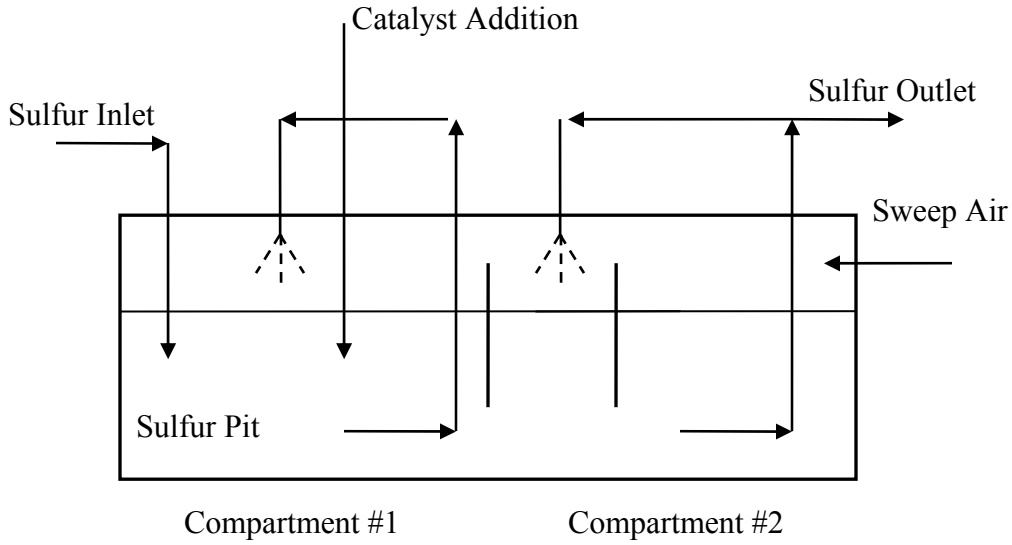

Figure 1-4 Schmatic of the SNEA Aquisulf degassing process

Texasgulf Degassing Process

As shown in Figure 1-5, the Texasgulf degassing process is an example of increasing the contact area to improve the degassing performance. Its design employs a baffle plate column [10]. Liquid sulfur gets agitated and releases H_2S while it is running down from the top. Addition of the catalyst is not common for this system but, in some plants, air is injected in to assist remove the H_2S from the

airspace. This column is installed on a sulfur tank from which the sulfur is recycled. An obvious advantage of this unit is a low construction and maintenance cost and low energy consumption. However, it requires a longer residence time to meet high degassing requirements.

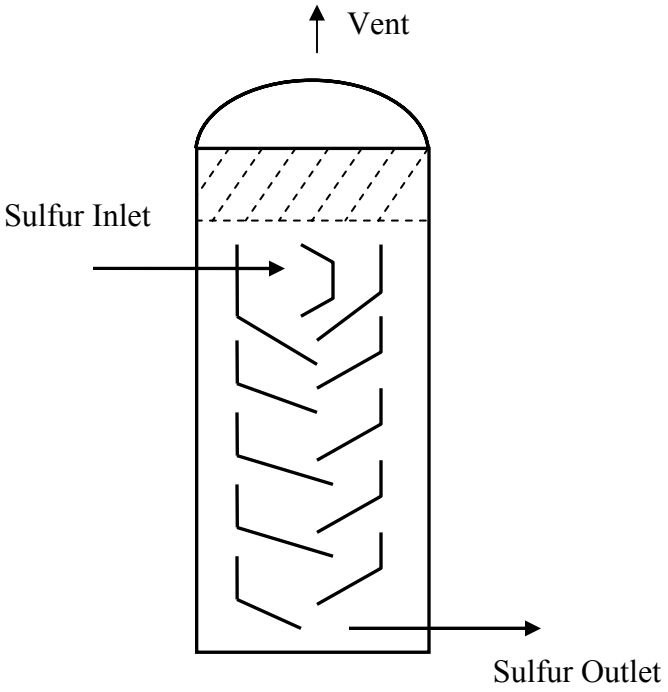

Figure 1-5 Schematic of the Texasgulf degassing process

Almost all the studies of sulfur degassing techniques were purely result driven. There have hardly been any systematic research available in literature—little lab work has been reported, feasibility of using continuous reactors to shorten the residence time has rarely received any attention, and lots of fundamental parameters are missing so that detailed engineering cannot be easily verified.

1.3 Objective

As introduced above, a sulfur degassing process is comprised of a chemical process of H_2S_x decomposition and a physical process of diffusion. Since the first step can be successfully accomplished by adding a trace amount of catalyst, this study was conducted mainly against the second step and a water-oxygen system was used in the laboratory to simulate the process. Since the physical diffusion is essentially a mass transfer process where the most important factor is the surface to volume ratio, the idea was to maximize the interfacial contact area by generating fine liquid droplets or, conversely, micro inert gas bubbles. A continuous reactor is expected to be engineered to efficiently treat the liquid in a cost-effective manner.

The detailed tasks of this study are as follows:

- field-evaluate the existing degassing process;
- design and lab-test a new degassing system using fine (poly-dispersed) liquid droplets;
- conduct fundamental studies on a degassing unit using mono-dispersed droplets;
- lab-test a new degassing system using micro bubbles;
- analytically evaluate all previous three systems;
- design a scale-up pilot degassing unit for field tests; and
- determine the diffusion coefficient and reaction rate constants in an H_2Sx-H_2S -liquid sulfur system.

1.4 Thesis structure

This thesis is written in a paper format where each of chapters 2 to 5 is an independent paper dealing with a specific topic. Chapter 2 is focused on determining the diffusion coefficient of H_2S in liquid sulfur. The diffusion coefficient of H_2S in liquid sulfur is a key kinetic parameter that has been missing in literature. In this chapter, a pressure decay method was applied to measure the diffusion coefficients of H_2S in liquid sulfur at 403 and 423 K. The solubility of H_2S in liquid sulfur at 403 and 423 K were also calculated and the results agreed with the semi-empirical correlation lately reported in literature. This study further extended the validity of the correlation to higher partial H_2S pressure conditions. A version of this chapter has been published in the journal of *Fluid Phase Equilibria* [11].

Chapter 3 is about degassing using poly-dispersed and mono-dispersed droplets. Liquid degassing using mono-dispersed and poly-dispersed fine droplets (148.6 and 264.8 μm) falling in inert gas was experimentally and analytically studied. The system using poly-dispersed droplets was designed for an industrial degassing process and a number of operating parameters were therefore studied. The mono-dispersed droplet system was set up for fundamental studies of contributing factors. A version of this chapter is under preparation for journal submissions [12].

Chapter 4 brings a specific application of the degassing technique using droplets using fine droplets in water treatment. Optimizing the working conditions is of main interest in this paper. A version of this Chapter was presented at Air and Waste Management Association (A&WMA)'s 103rd annual conference [13].

Chapter 5 experimentally and analytically studies a degassing system using a combination of micro inert gas bubbles and mechanical agitations. This degassing unit could be operated as either a batch or a continuous reactor and was later on tested in Talisman's gas plant in Edson with satisfactory results.

Chapter 6 provides all other important technical details such as field tests to evaluate the latest HySpec™ degassing process at the Edson gas plant, design of a pilot degasser using fine droplets, unreported data in the pressure decay experiments, and more information about the mono-dispersed droplet system.

Finally, conclusions and future work recommendations are summarized in Chapter 7.

References

[1] R. A. Marriott, E. Fitzpatrick, K. L. Lesage, Fluid Phase Equilibria 269 (2008) 69-72.

[2] M. P. Elsner, M. Menge, C. Muller, D. W. Agar, Catalysis Today 78-79 (2003) 487-494.

[3] Z. F. Ismagilova, R. R. Safin, F. R. Ismagilova, Chem. Technol. Fuels Oils 40 (2004) 279-283.

[4] Tengizchevroil Environmental Communications Group, Sulfur Production and Sales Handbook (2007).

[5] W. Nehb, K. Vydra, Sulfur, Lurgi AG, Frankfurt/Main (2006).

[6] R. Fanelli, Ind. Eng. Chem. 41 (1949) 2031-2033.

[7] P. Crawford, Hydrocarbon Engineering (2009).

[8] E. Nasato, Unite States Patent 5,632,967 (1997).

[9] J. B. Rajani, Treating Technologies of Shell Global Solutions for Natural Gas and Refinery Gas Streams (2004).

[10] J. A. Lagas, Hydro. Process, 61 (1982) 85-89.

[11] Y. Ji, H. Li, Z. Xu, Z. Tan, Fluid Phase Equilibria 307 (2011) 135-141.

[12] Y. Ji, K. Zhang, Z. Xu, Z. Tan (To be submitted).

[13] Y. Ji, Z. Tan, Z. Xu, A&WMA 103rd Annual Conference and Exhibition, June 22-25, 2010, Calgary, Canada.

CHAPTER 2 : THE DIFFUSION COEFFICIENT OF H_2S IN LIQUID SULFUR

1. Introduction

Hydrogen sulfide (H_2S) is a product of a number of operations in petrochemical industries. It is usually converted to elemental sulfur (S) via the Claus reaction, which includes the partial combustion of H_2S to SO_2 (Eq. 1) and the synproportionation reaction between H_2S and sulfur dioxide (SO_2) (Eqn. 2) [1]:

$$H_2S + 3/2\, O_2 \rightarrow SO_2 + H_2O \quad (1)$$

$$2H_2S(g) + SO_2(g) \leftrightarrow \frac{3}{n} S_n(g) + 2H_2O(g); \quad (2)$$

Gaseous sulfur is then condensed to produce elemental sulfur but some amount of residual H_2S is dissolved and retains in the liquid product. Ismagilova et al. [2] reported this concentration to be about 240-380 ppmw. H_2S is toxic and flammable. It is usually required to be removed to a level of 10 ppmw or lower [3] before the liquid sulfur can be transported, stored and delivered to the end users [4]. Furthermore, dissolved H_2S reacts with elemental sulfur to form hydrogen polysulfide (H_2S_x). This reaction facilitates the sulfur deposition and, subsequently, negatively affects the sour gas production and transportation [5, 6]. Therefore, it is of great research and practical importance to fundamentally understand the transport of H_2S in and out of liquid sulfur.

Several studies have focused on the solubility of H_2S in liquid sulfur. It was first noticed by Fanelli [7] that the solubility of H_2S in liquid sulfur

increased uniquely with that of the temperature, which was also resulted from the presence of hydrogen polysulfide. Wiewiorowski and Touro [8] confirmed Fanelli's theory using infrared spectra and proposed the possible chemical reaction mechanism. Recently, Marriott et al. [9] reported the solubility of total H_2S and the ratio of H_2S to H_2S_x at different temperatures and initial partial pressures. They also derived a semi-empirical Henry's law correlation.

However, related kinetic information has been missing in literature. Dissolving H_2S into or releasing it out of the liquid sulfur is essentially a kinetic gas-to-liquid mass transfer process such that the major resistance lies in the liquid phase. The most important parameter that characterizes this kinetic process is the gas diffusion coefficient, which is a function of pressure, temperature, and the specific chemical composition [10, 11]. In addition, the formation and decomposition of H_2S_x have not been studied systematically either. Of the most importance and interest in this reversible process are the reaction rate constants.

Some existing studies on diffusion of H_2S reported in literature have focused on glycol or water as the diffusing medium. For example, Ferrando et al. [12] studied the solubility and diffusion coefficient of H_2S in polyethylene glycol at 373, 393, and 413 K. Halmour and Sandall [13] conducted his research of H_2S diffusing in water in a temperature range of 288 K to 308 K under the atmospheric pressure using a laminar jet method. Tamimi et al. [14] tested a wider temperature range for more gas diffusions (H_2S, N_2O, and CO_2) in water using a wetted-sphere method. Indirect techniques for diffusion coefficient measurements, using correlating indicators such as volume, pressure, and refraction of electromagnetic radiation, have been developed.

They are usually less intrusive and more cost-effective than the direct techniques which involve measurements of the in-situ concentrations of the target gas in the liquid. The pressure decay method [15] is one of the indirect methods using pressure as an indicator. This method has been variously improved and widely adopted in the oil and gas industry and related research areas [12, 16-19].

The main objective of this study is to find the diffusion coefficient as well as the kinetics (e.g. chemical reaction rate constants) of H_2S in elemental liquid sulfur using the pressure decay method. The experiments will be conducted at 403 and 423 K (130 and 150 ºC), which are the most common industrial operation temperatures. The solubility of H_2S in liquid sulfur under the equilibrium partial pressure in the pressure decay tests is also to be investigated and compared with the existing studies.

2. Theory

For H_2S dissolved in liquid sulfur, diffusion and reversible chemical reactions occur simultaneously as:

$$H_2S_{(sol)} \underset{k_{-1}}{\overset{k_1}{\rightleftharpoons}} H_2S_X \tag{3}$$

where k_1 and k_{-1} are the reaction rate constants of the forward and backward reactions, respectively. They are in connection with the equilibrium concentrations (c_{eH_2S} for H_2S and $c_{eH_2S_x}$ for H_2S_x) by [20]:

$$\frac{c_{eH_2S}}{c_{eH_2S} + c_{eH_2S_x}} = \frac{k_{-1}}{k_1 + k_{-1}} \tag{4}$$

$$\frac{c_{eH_2S_x}}{c_{eH_2S} + c_{eH_2S_x}} = \frac{k_1}{k_1 + k_{-1}} \tag{5}$$

Thus, the ratio of the equilibrium concentrations of H_2S and H_2S_x can be calculated if the ratio of the reaction rate constants is known, and vice versa.

Meanwhile mass transfer takes place at the interface between H_2S and liquid sulfur. Consider a system as illustrated in Figure 2-1, where pressurized H_2S is in the headspace above the liquid sulfur. The height of the liquid sulfur is *a* and that of the headspace is *b*.

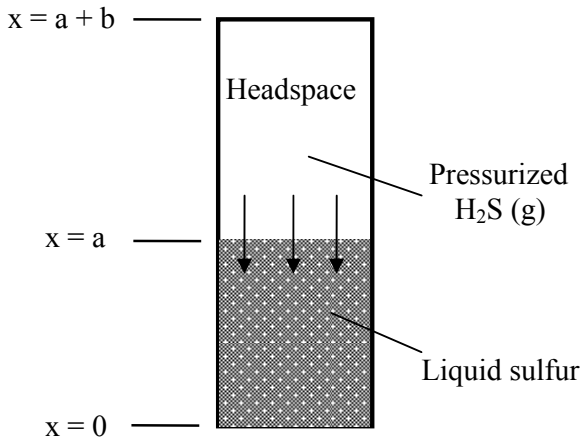

Figure 2-1 Schematic of the diffusion process in a reactor.

The following assumptions are made in order to analytically model this mass transfer process: the temperature is homogenous in the whole gas and liquid phases and steady over the mass transfer process; the diffusion coefficient and reaction rate constants of H_2S in liquid sulfur do not change with the increased concentration of the dissolved H_2S at a constant temperature; H_2S_x is non-diffusive (immobilized substance) in liquid sulfur; and the liquid sulfur is stagnant (no convections), non-volatile (low vapor pressure), non-decomposable, and does not expand because of the dissolved

H_2S (low solubility). Then the partial differential equation for the diffusion is expressed by:

$$\frac{\partial c_{H_2S}}{\partial t} = D_g \frac{\partial^2 c_{H_2S}}{\partial x^2} - \frac{\partial c_{H_2S_x}}{\partial t} \tag{6}$$

where D_g is the diffusion coefficient of H_2S in liquid sulfur, c_{H_2S} and $c_{H_2S_x}$ denote the concentrations of H_2S free to diffuse and H_2S_x, respectively. Since both the forward and backward reactions (Eqn. 3) are of the first order, the concentrations are related to the reaction rate constants by:

$$\frac{\partial c_{H_2S_x}}{\partial t} = k_1 c_{H_2S} - k_{-1} c_{H_2S_x} \tag{7}$$

Substituting Eqn. 7 into Eqn. 6 gives:

$$\frac{\partial c_{H_2S}}{\partial t} = D_g \frac{\partial^2 c_{H_2S}}{\partial x^2} - k_1 c_{H_2S} + k_{-1} c_{H_2S_x} \tag{8}$$

Initially, the liquid sulfur is free of H_2S and H_2S_x, which corresponds to the initial condition:

$$c_{H_2S} = c_{H_2S_x} = 0, \quad (0 < x < a, \ t = 0) \tag{9}$$

For impermeable walls, the corresponding boundary conditions are:

$$\nabla c_{H_2S} = 0, \quad (t \geq 0) \tag{10}$$

The boundary condition at the gas-liquid interface, however, according to Tharanivasan et al.'s study [16], is still up for debate. Tharanivasan et al. classified the Dirichlet-type boundary conditions (BC) used in literature without chemical reactions into three categories: equilibrium BC, quasi-equilibrium BC, and non-equilibrium BC. It was further concluded that there was a most suitable boundary condition for each specific diffusion system. No

studies have been reported about the BC selections for an inorganic diffusion system with chemical reactions. Herein, we adopted the quasi-equilibrium BC and it is easier to write it in a form of the Newman-type boundary equation as:

$$b\frac{\partial c_{H_2S}}{\partial t} = -D_g \frac{\partial c_{H_2S}}{\partial x}, \quad (x = a,\ t \geq 0) \qquad (11)$$

The physical meaning of this BC is that the rate H_2S leaves the headspace is equal to that it enters into the liquid sulfur. An assumption behind this BC is that H_2S is always homogeneous in the headspace. The concentration of the H_2S at the interface ($x = a$) is essentially defined as a function (i.e. the saturation concentration) of the in-situ headspace pressure which decreases as the diffusion proceeds.

For this one-dimensional diffusion, with initial and boundary conditions (Eqns. 9, 10, and 11), the partial differential Eqn. 8 was solved by Crank [21] as:

$$c = \frac{bc_0}{b + \left(k_1 \diagup k_{-1}\right)a} + \sum_{n=1}^{\infty} \frac{c_0 \exp\left(p_n t\right)}{1 + \left[1 + \frac{k_1 k_{-1}}{\left(p_n + k_{-1}\right)^2}\right]\left(\frac{a}{2b} + \frac{p_n}{2D_g q_n{}^2} + \frac{p_n{}^2 ab}{2D_g{}^2 q_n{}^2}\right)} \frac{\cos q_n x}{\cos q_n a}$$

(12)

where p_n's are the non-zero roots of equation, and the roots are sorted from the smallest to the biggest as p_1, p_2, $p_3 \ldots p_n$; and q_1, q_2, $q_3 \ldots q_n$ in the modeling equation's summation terms:

$$\frac{bp_n}{D_g} = q_n \tan q_n a, \quad q_n{}^2 = -\frac{p_n}{D_g}\frac{p_n + k_1 + k_{-1}}{p_n + k_{-1}}$$

(13)

and c_0, in this case, is defined as the molar H_2S molar density under the initial H_2S pressure (P_i) in the headspace, following the ideal gas law:

$$c_0 = \frac{P_i}{RT} \tag{14}$$

If the headspace pressure is not high, the ideal gas law is also applicable to the headspace:

$$PV = nRT \tag{15}$$

where P is the H_2S pressure, V is the volume of the headspace, n is the amount of H_2S in moles, R is the ideal gas law constant, and T is the operation temperature. Differentiating Eqn. 15 gives:

$$\frac{\partial P}{\partial t} V = \frac{\partial n}{\partial t} RT \tag{16}$$

and combining Eqn. 16 with Eqn. 11 at $x=a$ gives:

$$\frac{\partial P}{\partial t} = -D_g \frac{RT\rho_s}{bM} \frac{\partial c_{H_2S}}{\partial x} \qquad (x = a) \tag{17}$$

where M is the molecular weight of H_2S, and ρ_s is the density of liquid sulfur.

Meanwhile, differentiating Eqn. 12 with respect to x, at $x=a$, gives:

$$\frac{\partial c_{H_2S}}{\partial x} = -\sum_{n=1}^{\infty} \frac{c_0 q_n \exp(p_n t)}{1 + \left[1 + \frac{k_1 k_{-1}}{(p_n + k_{-1})^2}\right]\left(\frac{a}{2b} + \frac{p_n}{2D_g q_n{}^2} + \frac{p_n{}^2 ab}{2D_g{}^2 q_n{}^2}\right)} \tan(q_n a) \quad (x = a) \tag{18}$$

Finally, substituting Eqn. 18 into Eqn. 17 and integrating both sides with respect to time, from 0 to t, gives:

$$\int_0^t \frac{\partial P}{\partial t} dt = \int_0^t \left[D_g \frac{RT\rho_s}{bM} \sum_{n=1}^{n} \frac{c_0 q_n \exp(p_n t)}{1 + \left[1 + \frac{k_1 k_{-1}}{(p_n + k_{-1})^2}\right]\left(\frac{a}{2b} + \frac{p_n}{2D_g q_n{}^2} + \frac{p_n{}^2 ab}{2D_g{}^2 q_n{}^2}\right)} \tan(q_n a) \right] dt \quad (x = a) \tag{19}$$

and

$$P(t)-P_i = D_g \frac{RT\rho_S}{bM} \sum_{n=1}^{\infty} \frac{c_0 q_n \tan(q_n a)}{1+\left[1+\frac{k_1 k_{-1}}{\left(p_n + k_{-1}\right)^2}\right]\left(\frac{a}{2b}+\frac{p_n}{2D_g q_n{}^2}+\frac{p_n{}^2 ab}{2D_g{}^2 q_n{}^2}\right)}\left[\exp\left(p_n t\right)-1\right] \quad (20)$$

where P_i is the initial pressure of H_2S in the headspace. Essentially, Eqn. 20 relates the diffusion process (with a reversible chemical reaction) in the liquid sulfur to the thermodynamic parameters of the H_2S gas phase in the headspace. Therefore, the gas diffusion coefficient D_g can be calculated if the headspace pressure decay history with respect to time is known.

However, the key to solve this problem involves finding the solutions for Eqns. 12 and 13, which is mathematically challenging. The physical significance of the solutions is not obvious, and the exact analytical solutions cannot be obtained without knowing the specific values of D_g, k_1, and/or k_{-1}. For a much simpler case, Zhang et al. [17] employed nonlinear regression to numerically fit their experimental data.

Considering the fair complexity of the problem, finite element method (FEM) was employed to solve the problem for approximate solutions. Commercial software, COMSOL and Matlab, was used to assist the FEM simulation. In the simulation, the criterion of the convergence was set as 10^{-12}. Based on the aforementioned analysis, the boundary conditions as well as the meshing strategy are presented in Figure 2-2. The concentration of H_2S was calculated on each meshing point. Meanwhile, in the simulation of the liquid part, extra memory space was applied to store the concentration of H_2S_x at each step. The pressure of the gas was obtained by submitting the integration of the concentration of H_2S in the headspace into the Eqn.14. Since k_1 and k_{-1} are also missing in literature, a genetic optimization method was employed to

obtain the optimized values. Comparing with other optimization methods, genetic algorithm has the advantage of global searching and escaping from a local optimization. The objective function used to guide the optimization process is the same as the one used by Tharanivasan et al. [22]:

$$\Delta P_{ave} = \sqrt{\frac{\sum_{i=1}^{n} \left| P_{cal}(t_i) - P_{\exp}(t_i) \right|^2}{n}}$$

(21)

where t_i denotes any measurement time point (i=1, 2, 3,…n). This equation presents the average pressure difference between the theory and experiments and D_g, k_1 and k_{-1} can be determined from the best matched curve. More information on this algorithm can be found in Mitsuo's book [23].

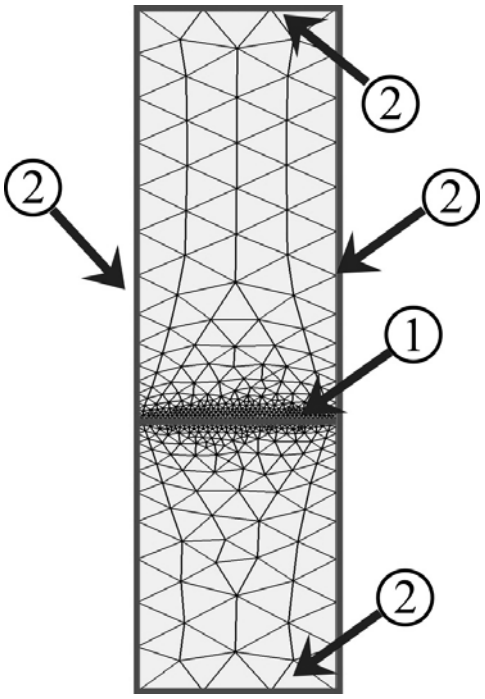

Figure 2-2 Schematic of the meshing strategy where the boundary denoted by 1 follows Eqn.11 and the boundaries denoted by 2 follow the Eqn. 10.

3. Experimental

The experimental setup was shown in Figure 2-3 and the key part is a pressure transducer (GP: 50 Model 211) from Inter Technology Inc. The pressure signal was transferred through a National Instruments Data Acquisition Card (NI USB-6210) and logged by LabVIEW (SignalExpress). A 300 ml cylindrical reactor (Model 316L-50DF4-300, Skagelok) was mounted into a fluidized sandbath (IFB-51, Techne®) in a fume hood for safety purposes. The whole system was designed to be a sealed system controlled by five needle valves (Skagelok). Valve #1 adjusted the flow rate of compressed air to fluidize the sands, which is a function of the operating temperatures; Valve #3 and #4 controlled the inlet and outlet flows, respectively; while the line with Valve #2 and #5 was connected to a vacuum pump.

Sulfur samples were provided by Enersul Inc. with a purity of 99.95%. The purity was determined using a modified ASTM (American Society of Testing and Materials) method. This new method incorporated elemental sulfur into a standard carbon/ash analysis procedure. In addition, Fourier transform infrared spectroscopy (FTIR) tests showed that the sulfur samples contained less than 3.5 ppmw total H_2S. Differential **s**canning **c**alorimetry (DSC) test was also conducted at a heating rate of 5 K/min in comparison with the 99.998% trace metals basis sulfur sample from Sigma-Aldrich. Each test was conducted consecutively twice. 215.48 g and 213.41 g solid sulfur samples were then weighed for diffusion tests at 403 K and 423 K, respectively, such that the liquid sulfur would occupy 40% of the space in the reactor by volume. The weighed sulfur was placed at the bottom of the reactor at first. The sandbath was turned on with a continuous compressed air supply (207 kPa), and 1 hour was allowed for it to reach a steady operating

temperature. Another half an hour was allowed after the reactor was put into the sandbath so that the solid sulfur completely melted and reached the same temperature as the sandbath. Then, with Valves #3/#4 being closed and Valve #2/#5 being open, the reactor was vacuumed by the vacuum pump. Valve #2 was closed after the vacuum pressure gauge read -30 inch Hg. By doing vacuuming, not only the air in the system was removed, the seal of the system could also be verified. Then H_2S gas (99.6% pure from Praxair) was slowly introduced into the system with Valve #5 being closed and Valve #3 being open. Valve #3 was closed after the pressure transducer indicated a headspace pressure of about 345 kPa (50 psi). Pressure decay happened instantly and became slower as more H_2S diffused into the sulfur. The process was monitored and recorded every five seconds. Since this sampling rate is higher than other studies reported in literature, this decay history was deemed to be more reliable. Unchanged pressure readings indicated the equilibrium state. However, the time required to reach the equilibrium is considerably long, and it is arguably more accurate to use linear regression method to predict the equilibrium pressure [17]. After each test, valve #4 was slowly opened to release the pressurized H_2S into the fume hood. The liquid sulfur sample cooled down and solidified at room temperature in the fume hood before re-melting in a furnace.

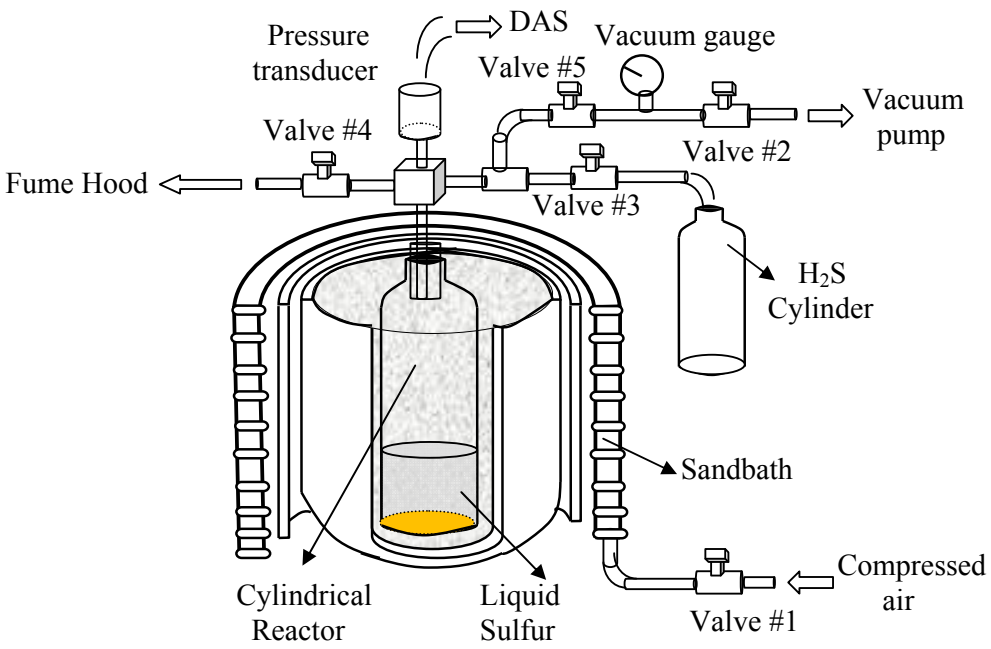

Figure 2-3 Experimental setup of the pressure-decay system.

4. Results and discussion

4.1 Physical properties of the sulfur sample

Elemental sulfur itself is a complex system as it has several different isotropic forms which have their unique physical properties. Thus it is necessary to characterize the sulfur sample before running the diffusion experiments. The DSC test result in Figure 2-4 shows that the physical properties for the sample used in this study and for the 99.998% pure sulfur are almost identical, especially in the first melt down. This verified the high purity of the sulfur sample in this study. It was also found that the sulfur occurred in the monoclinic β-form which had a melting point of 391.72 K. Literature reported this value between 392.3 to 387.5 K [24]. For the second run after the sulfur cooled down and re-melted, the melting point of the sulfur shifted to 375.65 K, which is corresponding to elemental sulfur's nacreous γ-

form. Valves reported in literature were between 376.4 and 379.8 K [24]. The sulfur used in the diffusion tests was in the same condition as it was in the first run, therefore is expected to be in the monoclinic β-form. It is also important to see that the temperatures chosen for diffusion coefficient measurements, 403 and 423 K, are both in a relatively steady region in Figure 2-4. Higher temperatures are out of the scope of this study, but Figure 2-4 also provides information that sulfur polymerization should happen, in this case, at ca. 163.12 to 174.14 °C. This temperature marks the starting point a sharp increase in viscosity due to formation of the amorphous μ-form sulfur.

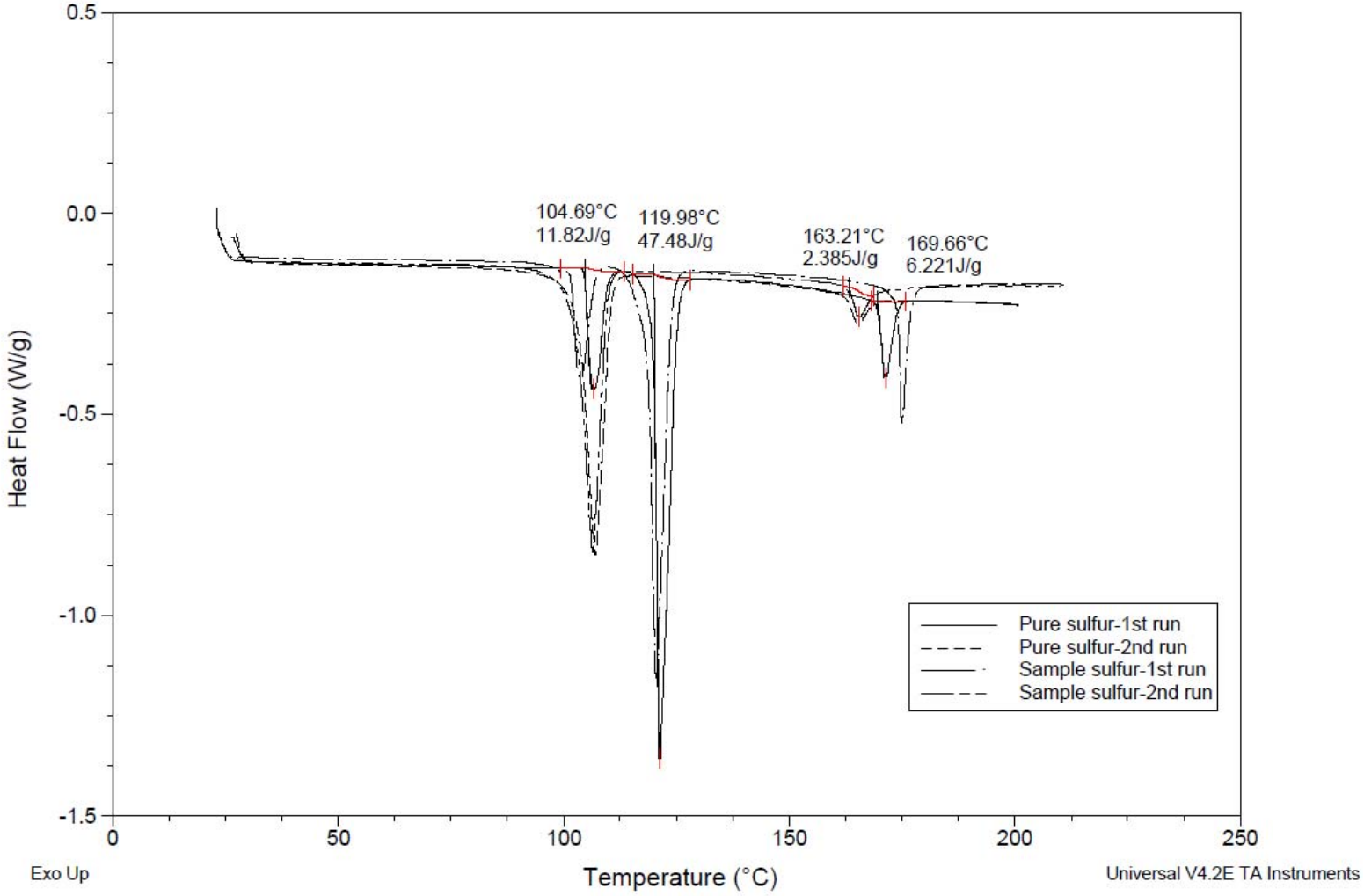

Figure 2-4 DSC test of the elemental sulfur sample.

4.2 Numerical optimization

The ratio of the forward and backward rate constants was one of the parameters in the objective equation and it was calculated from the equilibrium data following the discussion in section 2.1. The equilibrium concentrations at different temperatures were reported in Wiewiorowski and Touro's study [8]. Their results indicated that, below the sulfur polymerization transition temperature (432 K), the ratio of H_2S to the total amount of H_2S and H_2S_x was linearly decreasing with the increase of temperature by:

$$x_{H_2S} = -0.0148T + 6.7255 \quad R^2 = 0.9965$$

(22)

Later on, Marriott et al. [9] showed that the terms at the left hand side of Eqn. 4 and 5 were independent of the headspace H_2S partial pressure. Therefore, these two equations were used herein in the optimization process. Some calculated and known parameters used in the numerical optimization are summarized in Table 2-1:

Table 2-1 Parameters used for model calculations.

Constants	***T = 403 K***	***T= 423 K***
R = 8.31 J/(K mol)	ρ_s = 1,795.7 kg/m^3	ρ_s = 1,778.4 kg/m^3
a = 0.0827m	P_i = 344,442.3 Pa	P_i = 363,250.9 Pa
b = 0.124 m	c_0 = 102.85 mol/m^3	c_0 = 103.34 mol/m^3
M = 0.034 kg/mol	$\frac{k_1}{k_{-1}} = 0.314$	$\frac{k_1}{k_{-1}} = 1.150$

A system with a high (> 1 atmospheric pressure) headspace H_2S partial pressure so far has not been studied. In a pressure decay experiment, a higher

initial pressure usually means a longer time to reach the equilibrium, but it provides a more reliable pressure decay history for a given sampling rate. Also considering factors such as safety and applicability of the ideal gas law, the initial pressures were set to be around 3.45×10^5 Pa (50 psi).

The measured pressure decay data and the best matched curve given from the aforementioned numerical optimization were plotted in Figure 2-5 and Figure 2-6 for 403 and 423 K, respectively The ΔP_{ave}'s in this study was small and comparable to those calculated with the best boundary condition in Tharanivasan et al.'s study [22]. Therefore, both figures indicate that Eqn. 20 and the chosen boundary conditions are proper in characterizing this dynamic H_2S-H_2S_x-sulfur system. It can also be seen that the pressure decay rate in the 403 K system is greater than that in the 423 K system. A greater pressure decay rate suggests a lower diffusion coefficient as well as a lower forward reaction rate constant. A higher pressure for the 403 K system at larger times approaching the equilibrium is due to a lower total H_2S (in the forms of H_2S and H_2S_x) solubility. Furthermore, Figure 2-7 and Figure 2-8 more showed the history of what happened in the reaction by plotting the H_2S concentration distributions in the reactor at different times. While H_2S was leaving the homogenous gas phase, the concentration gradients of the total dissolved H_2S were becoming less insignificant in the liquid phase. The concentration difference at the interface is the first-step drive force of this pressure decay process. It explains why it took a long time for the system to reach equilibrium and why the corresponding curves in Figure 2-5 and Figure 2-6 are getting less sharp with respect to time. The distribution of dissolved H_2S became

homogenous in the liquid sulfur at the equilibrium and the concentration is determined by the Henry's law.

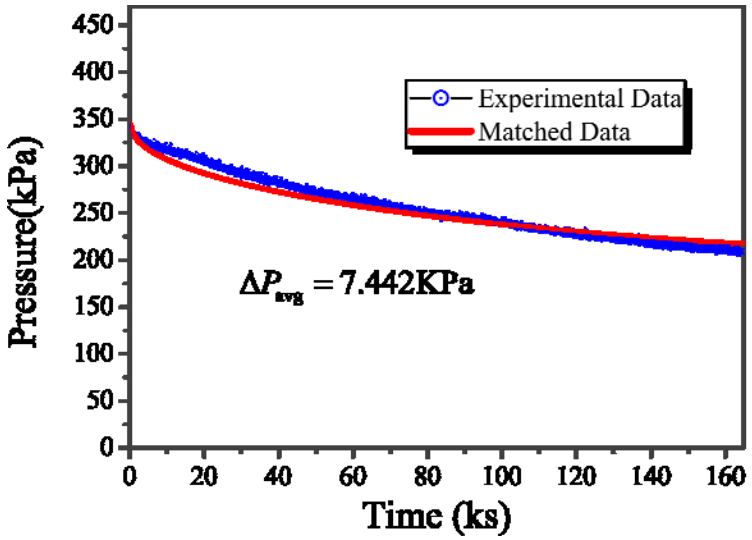

Figure 2-5 Experimental pressure decay data and the numerically matched curve for T=403K.

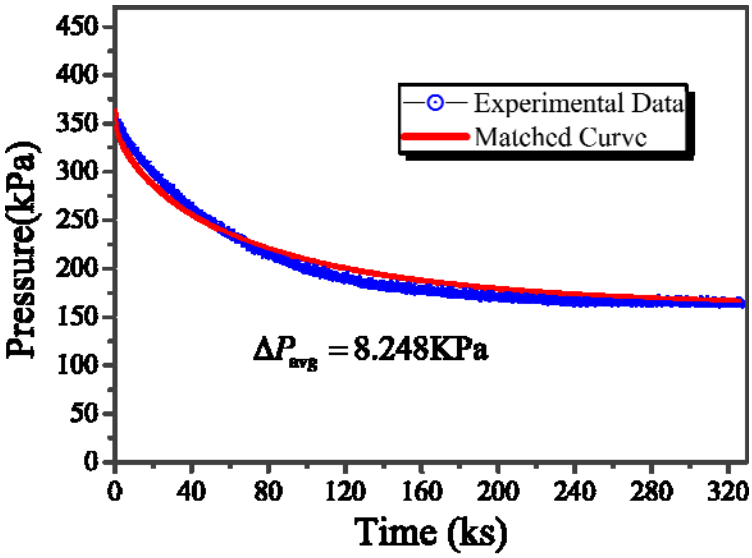

Figure 2-6 Experimental pressure decay data and the numerically matched curve for T=423K.

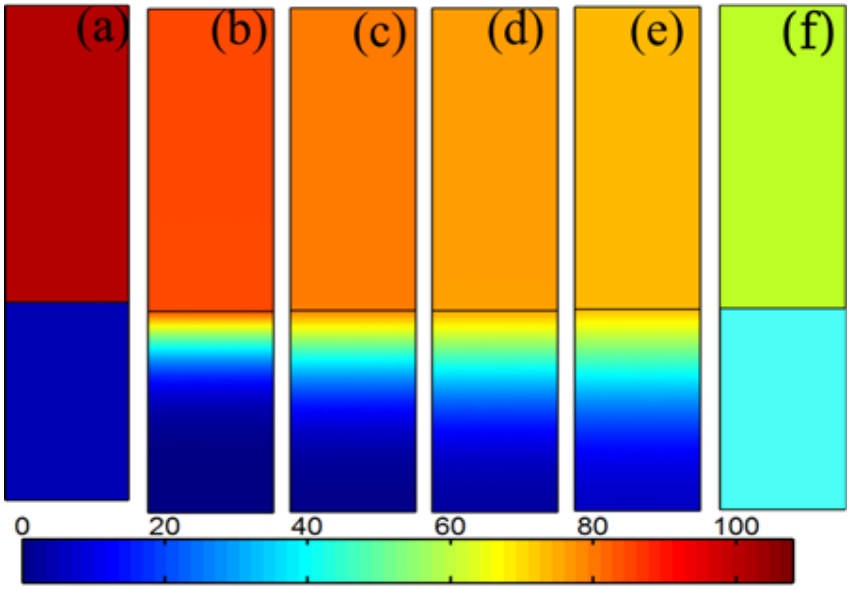

Figure 2-7 The variances of H_2S concentration distributions in the reactor versus time at 403 K (The unit of the color-map is [mol/m^3]). (a) t=0s; (b) t=4×10^{4}s; (c) t=8×10^{4}s; (d) t=12×10^{4}s; (e) t=16×10^{4}s; (f) t=∞ (equilibrium).

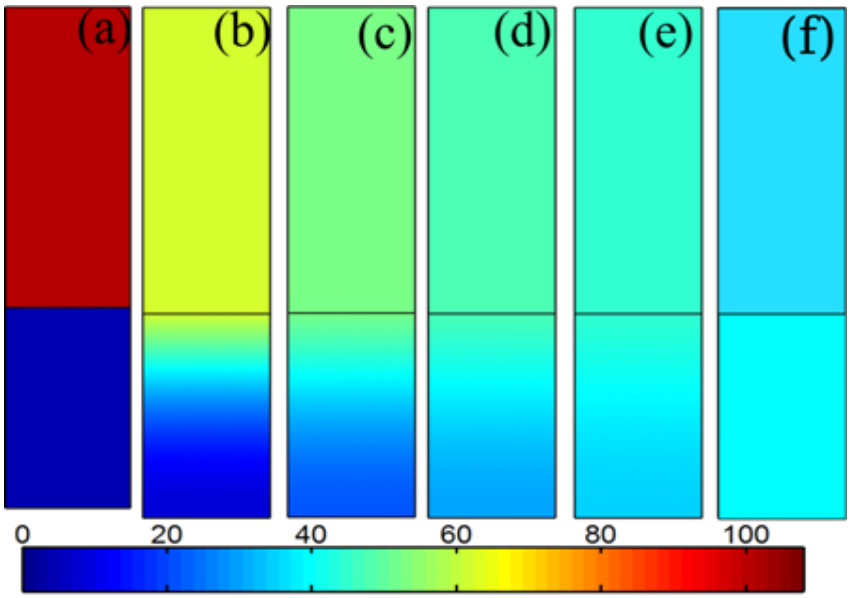

Figure 2-8 The variances of H_2S concentration distributions in the reactor versus time at 423 K (The unit of the color-map is [mol/m^3]). (a) t=0s; (b) t=8×10^{4}s; (c) t=16×10^{4}s; (d) t=24×10^{4}s; (e) t=32×10^{4}s; (f) t=∞ (equilibrium).

The determined diffusion coefficients and the reaction rate constants for each of the two temperatures are given in Table 2-2. It can be seen that the system at 423 K corresponds to a much greater diffusion coefficient. Besides

the well acknowledged temperature dependence of the diffusion coefficient, it is also worthwhile to mention two other important factors. First is that the viscosity of the sulfur usually reaches its minimum value when the temperature is around 423 K [24]. The other factor is the structural change/deformation of the sulfur—as more radicals and less rings of elemental sulfur are present at a higher temperature, less diffusion resistance is placed at the molecular scale. More free radicals available for the forward reaction, in addition to the well-known Arrhenius equation, also contributes to the higher rate to form H_2S_x (k_1) and the ratio of the reaction rate constants are significantly higher at 423 K than those at 403 K. Nevertheless, as shown in Table 2-2, the order of magnitude of the rate constants is between 10^{-6} and 10^{-5}, which still suggests relatively slow reactions at both temperatures.

Table 2-2 Diffusivities of H_2S in liquid sulfur and reaction rate constants between H_2S and liquid sulfur at *T*= 403 and 423 K.

Temperature, K	Diffusivity, D_g, 10^{-8} m^2/s	Reaction rate k_1, $10^{-5}s^{-1}$	Reaction rate k_{-1}, $10^{-5}s^{-1}$	Equilibrium pressure, 10^5Pa
403	1.70	*0.579*	*1.84*	*1.84*
423	2.91	2.77	*2.41*	*1.49*

4.3 The solubility of total H_2S in liquid sulfur

Although there has been no study of the diffusion coefficient reported, the solubility of H_2S in liquid sulfur has been studied with a partial pressure of H_2S no greater than one atmospheric pressure. Marriott et al. [9] derived a semi-empirical correlation for the Henry's law correlation. When the

concentration (in ppmw) of H_2S is much smaller than the unity, the correlation can be simplified as:

$$c = \frac{P}{1000 \times \exp\left(-1.93 + \frac{-3.35}{1+\exp\left(\left(436.3-T\right)/8.32\right)}\right)} \quad (23)$$

Meanwhile, the solubility can also be derived in this study at equilibrium where the pressures were between 1 and 2 atmospheric pressure, for 403 and 423 K, by:

$$c = \frac{M\left(P_i - P_{eq}\right)V_g}{RTm_s} \quad (24)$$

The calculation results are summarized in Table 2-3 and can be used to compare with predictions from Marriott et al.'s [9] correlation.

Table 2-3 Validation of Marriott et al.'s (2008) correlation about the solubility of total H_2S in liquid sulfur.

Temperature, K	Equilibrium pressure, 10^5Pa	Total equilibrium H_2S concentration, ppmw		
		Eqn. 24	This study	
403	1.84	1346.2	1360.7	403
423	1.49	1803.3	1747.9	423

It can be seen that the results derived from this study agree with Marriott et al.'s [9] correlation with minimal deviations, which verifies the validity of the experiments and simulation in this study. Vice versa, this study complements the correlation by extending its valid conditions to a higher partial pressure of H_2S.

5. Conclusions

As the single most important and fundamental kinetic parameter for a H_2S- H_2S_x-Sulfur system, the diffusion coefficient has been missing in literature. In this study, the diffusion coefficient of H_2S in liquid sulfur was studied at two temperatures, 403 and 423 K. An indirect measurement method, a pressure decay method, was experimentally employed. Key experimental design includes a stainless steel reactor, a sandbath, a highly sensitive pressure transducer, and a LabView data acquisition system. A H_2S-H_2S_x-Sulfur system has only been studied for a partial H_2S pressure lower than one atmospheric pressure, but experiments in this study were conducted in a pressurized system (initial headspace environment >3 atm) in order to get a more reliable pressure decay history. Analytical modeling was performed considering the simultaneous diffusion and reversible chemical reactions between H_2S and liquid sulfur. The diffusion coefficient and reaction rate constants were then numerically optimized through matching the experimental pressure decay data using Finite Element Method and Genetic Algorithm. Small deviations of the best matched curve and the experimental data verified the analytical model and a proper selection of boundary conditions. The diffusion coefficients were found to be 1.70×10^{-8} m^2/s and 2.91×10^{-8} m^2/s for 403 and 423 K, respectively; whereas the forward reaction rate constant between H_2S and liquid sulfur were 5.79×10^{-6} s^{-1} and 2.77×10^{-5} s^{-1}, respectively. Besides the classic theories about the dependence of these two kinetic parameters on temperature, the significant increases were also due to the decrease in sulfur viscosity and change in elemental sulfur's structure. Finally, the solubility of total H_2S in liquid sulfur under the equilibrium was also calculated for 403 and

423 K. The calculated equilibrium concentrations were in excellent accordance with a semi-empirical correlation that has recently been available in literature. This verified the experiments and simulation in this study. Vice versa, this study extended the validity of the correlation to a higher headspace partial pressure (149 and 184 kPa) of H_2S.

References

[1] M. P. Elsner, M. Menge, C. Muller, D. W. Agar, Catalysis Today 79-80 (2003) 487-494.

[2] Z. F. Ismagilova, R.R. Safin, F. R. Ismagilova, Chem. Technol. Fuels Oils 40 (2004) 279-283.

[3] Tengizchevroil Environmental Communications Group, Sulfur Production and Sales Handbook, 2007.

[4] J. B. Hyne, Sulphur Technical Data sheet and Accompany Commentary for Canadian Petroleum Association and Sultran Ltd., 1990, ASR #294-90-91.

[5] X. Guo, Z. Du, X. Yang, Y. Zhang, D. Fu, Pet. Sci. 6 (2009) 405-414.

[6] P. D. Clark, K. L. Lesage, P. Sarkar, Energy Fuels 3 (1989) 315-320.

[7] R. Fanelli, Ind. Eng. Chem. 41 (1949) 2031-2033.

[8] T. K. Wiewiorowski, F. J. Touro, J. Phys. Chem. 70 (1966) 234-238.

[9] R. A. Marriott, Ed Fitzpatrick, K. L. Lesage, Fluid Phase Equilib. 269 (2008) 69-72.

[10] R. B. Bird, W. E. Steward, E. N. Lightfoot, Transport phenomena, 2nd Edition. Wiley, Toronto, 2001.

[11] M. R. Riazi, C. H. Whitson, Ind. Eng. Chem. Res. 32 (1993) 3081-3088.

[12] N. Ferrando, P. Mougin, D. Defiolle, H. Vermesse, Oil Gas Sci. Technol. 63 (2008) 343-351.

[13] N. Haimour, O. C. Sandall, Chem. Eng. Sci. 39 (1984) 1791-1796.

[14] A. Tamimi, E. B. Rinker, O. C. Sandall, J. Chem. Eng. Data 39 (1994) 330-332.

[15] M. R. Riazi, J. Pet. Sci. Eng. 14 (1996) 235-250.

[16] A. K. Tharanivasan, C. Yang, Y. Gu, J. Pet. Sci. Eng. 44 (2004) 269-282.

[17] Y. P. Zhang, C. L. Hyndman, B. B. Maini, J. Pet. Sci. Eng. 25 (2000) 37-47.

[18] S. R. Upreti, Ph.D. dissertation, University of Calgary, 2000.

[19] S. R. Upreti, A. K. Mehrotra, Ind. Eng. Chem. Res. 39 (2000) 1080-1087.

[20] H. Metiu, Physical Chemistry Kinetics, Taylor & Francis, New York, 2006.

[21] J. Crank, The Mathematics of Diffusion, second ed., Oxford University Express, New York, 1979.

[22] A. K. Tharanivasan, C. Yang, Y. Gu, Energy Fuels 20 (2006) 2509-2517.

[23] G. Mitsuo, Genetic algorithms and engineering optimization, John Wiley& Sons, New York, 2000.

[24] W. Nehb, K. Vydra, Sulfur, Lurgi AG, Frankfurt/Main, 2006.

CHAPTER 3 : LIQUID DEGASSING USING MONO-DISPERSED AND POLY-DISPERSED DROPLETS

1. Introduction

Liquid degassing is a critical step in many industrial processes in the oil and gas, metallurgy, food and beverage, and municipal water treatment industries. A degassing process is to remove undesired gases dissolved in a liquid to improve the purity of the respective liquid products, to reduce the potential environmental or health impact, and to extract valuable substances from liquids. The examples include, respectively, removal of oxygen from water [1]/beverages [2-3] or hydrogen from molten aluminum [4], removal of H_2S or volatile organic compounds (VOCs) from heavy oil [5-6], and recovery of hydrogen gas from post-processing of salt cakes [7].

A liquid degassing process is essentially an interfacial mass transfer process where a solute (target gas) moves in between two immiscible phases. There are a variety of apparatus that can be used for industrial processes of this sort, such as stirred tank reactors, packed bed columns, bubble columns, and spray columns. These apparatus are easy to construct, operate and maintain therefore, often considered cost-effective and energy-efficient. Some more advanced devices that were developed recently include widely used membrane contactors [8-10] and micro-channels [11]. Great research interests have been placed on the mass transfer phenomena that involve dispersed fluid spheres and a continuous external flow due to the large (interfacial) surface to volume ratio. Existing studies were focused more on a gas adsorption process where aqueous solutions (in form of droplets) were used to capture the target gas such as

SO_2/CO_2 absorption into water drops [12-13], water vapor absorption into aqueous solution of LiBr [14], and H_2S absorption into methyldiethanolamine solution [11]. With similar principles a lot more studied were conducted and proved to be successful on liquid-liquid extraction systems with either of the liquid phases being dispersive [15-18]. However, use of fine droplets (<300 μm) were rarely reported in any of the aforementioned studies.

On the other hand, very few have applied this mass transfer principle to liquid degassing. Among the scarce ones, Wu et al. [4] experimentally studied removal of hydrogen from aluminum using spray droplets and provided preliminary analytical analysis. However, they did not fully investigate the contributing parameters that affected the degassing efficiency such as the droplet size, gas to liquid flow rate ratio, and atomizer type. In addition, Wu et al. [4] also over simplified the analytical model without dynamic details and. Therefore, there is a need for more systematic studies, both experimentally and analytically, of this liquid degassing method using droplets.

Furthermore, the experimental methodology of studying liquid degassing, as well as other mass transfer processes between dispersed fluid spheres and the surrounding immiscible phase in literature was to use either poly-dispersed (spray) droplets [12-13; 19] or a single drop [18; 20-21]. However, it is still subject to debate whether or not the knowledge for mass transfer obtained from a single drop system (a pendent droplet immersed in another solution or a suspended droplet in a wind tunnel) is applicable to a swarm of poly-dispersed droplets. Despite of rare numerical works [22-23], there have been no experimental studies reported using a system that fell between these two systems, especially for degassing: a system using mono-dispersed liquid

droplets, where the mass transfer process may be different. Seeing that it is still difficult to predict the mass transfer due to its inherences with mechanical dynamics and heat transfer, a mono-dispersed droplet system allows for more fundamental studies, such that a better understanding of the contributing parameters can be established. This is particularly important for understanding and improving industrial processes using spray columns (poly-dispersed droplets) because quite a few tangled parameters [24] are possible to be separated and studied independently in a mono-dispersed droplet system. For example, droplets size, gas to liquid flow ratio, target gas partial pressure, surface-active material additions, wall effects, etc. It is also believed that a mono-dispersed droplets system resemble (e.g. continuous reactors) a poly-dispersed droplet system more compared to a single drop system.

The objectives of this study are a) to design and experimentally studied degassing systems using mono-dispersed droplets and poly-dispersed droplets, b) to develop an analytical degassing model and generalize the mass transfer process using dimensionless numbers, and c) to verify the correlation between mono-dispersed and poly-dispersed droplets and compare the results with those in literature. Different methods of measuring dissolved oxygen (DO) are to be evaluated and possibly modified for each specific case. Equally important, the performance of the system using poly-dispersed droplets is also of interest such that it will be evaluated by its feasibility to be used in industrial degassing processes.

2. Theory

2.1 Model based on mass transfer coefficient

The degassing process considered herein is mass transfer of the dissolved gas from liquid droplets (the dispersed phase) to the surrounded inert gas (the continuous phase). Governed by the well-known Fick's law, and the flux, j, is expressed by:

$$j = k\left(c_d - c_g\right) \tag{1}$$

where k is the mass transfer coefficient, c_d and c_g are concentrations of the dissolved gas in the droplet and inert gas, respectively. Considering that evaporation effects, as shown in Lim et al.'s studies [25], were minor in a short time for less volatile liquids (e.g. water) when the droplet size was small, the general mass balance of the mass transfer process is written as:

$$-V\frac{dc_d}{dt} = A_d j = A_d k(c_d - c_g) \tag{2}$$

where V is the volume of a single droplet, and A_d is the interfacial area between the droplet and the liquid.

It is assumed that physically the concentration of the dissolved gas in the continuous phase is equal to that at the interface (hypothetical gas film), as illustrated in Figure 3-1. The corresponding interfacial boundary condition, as discussed by Tharanivasan et al. [26], varied with different systems. Herein it is assumed that the interface maintains a saturated concentration under the in-situ partial pressure of the target gas in the surrounding environment, which was referred to as a quasi-equilibrium condition. The saturated concentration is governed by Henry's law:

$$c_g = PK_H \tag{3}$$

where P is the partial pressure of the target gas in the surrounding environment, and K_H is the temperature-dependent Henry's law constant.

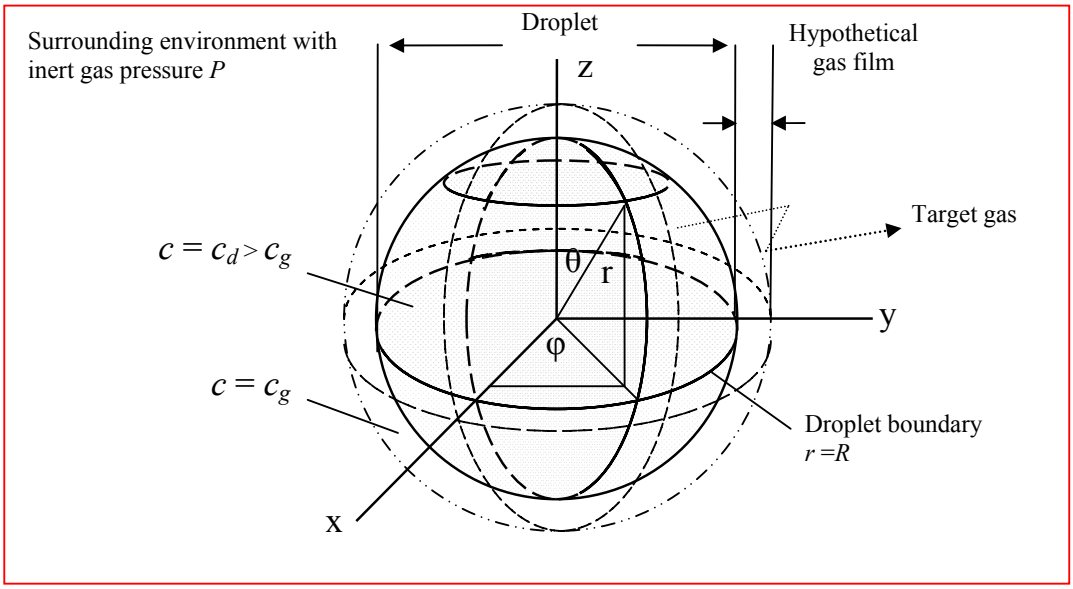

Figure 3-1 Schematic illustration of a degassing process from a liquid droplet with a spherical coordinate system.

When the inert sweep gas used is not 100% pure; initially, it contains certain amount of the target gas with a volume ratio of s. This amount, though little, cannot be ignored when the solubility of the target gas in the liquid is also very small. More importantly, it was commonly ignored in the previous analytical analysis that the target gas removed from the droplets accumulates in the surrounding environment. Its concentration (volume ratio s_c) is determined by the gas to liquid flow ratio:

$$s_c = \frac{V_{removed}}{V_{sweep}} = \frac{(c_i - c_d)m_L / \rho_T}{Q_G t} = \frac{(c_i - c_d)Q_L t \rho_L / \rho_T}{Q_G t} = \frac{(c_i - c_d)Q_L \rho_L}{Q_G \rho_T} \qquad (4)$$

where the gas concentrations are in unit of ppmw. Then equation (3) can be re-written as:

$$c_g = P_0(s + s_c)K_H = \left[s + (c_i - c_d)\frac{Q_L \rho_L}{Q_G \rho_T} \right] K_H P_0 \qquad (5)$$

where c_r, c_i and c_d are the removed gas concentration, dissolved gas concentrations in the droplet at the beginning and at the time t, respectively. Q_L

and Q_G represent the liquid and sweep gas flow rates. ρ_L and ρ_T denote the densities of the liquid and the target gas, respectively. While P_0 is the total pressure in the sweep gas phase, equal to the atmospheric pressure when it is operated as an open system.

Substituting equation (5) into (2) gives:

$$-V\frac{dc}{dt} = Ak\left[c_d - K_H P_0 s - \frac{Q_L\rho_L}{Q_G\rho_T}K_H P_0(c_i - c_d)\right] \tag{6}$$

Integrating equation (6) with the boundary conditions of c_0=c_i and c_t=c_f, one can get:

$$\frac{K_H P_0\left(s + \frac{Q_L\rho_L}{Q_G\rho_T}c_i\right) - \left(1 + K_H P_0\frac{Q_L\rho_L}{Q_G\rho_T}\right)c_f}{K_H P_0 s - c_i} = \exp\left[-\frac{6k}{d}\left(1 + \frac{Q_L\rho_L}{Q_G\rho_T}K_H P_0\right)t\right] \tag{7}$$

Subsequently, the degassing efficiency is calculated as:

$$\eta = 1 - \frac{c_f}{c_i} = 1 - \frac{K_H P_0\left(\frac{s}{c_i} + \frac{Q_L\rho_L}{Q_G\rho_T}\right) - \left(K_H P_0\frac{s}{c_i} - 1\right)\exp\left[-\frac{6kt}{d}\left(1 + \frac{Q_L\rho_L}{Q_G\rho_T}K_H P_0\right)\right]}{1 + \left(K_H P_0\frac{Q_L\rho_L}{Q_G\rho_T}\right)} \tag{8}$$

where the initial and final gas concentrations are both in unit of ppmw, and K_H is in unit of Pa^{-1}. This equation infers that the degassing efficiency depends on not only the well known mass transfer coefficient but also the residence time and the droplet size. The latter two are of greater significance as they are in the exponential term. It is also shown that thermodynamically the upper degassing efficiency is lowered with an increase of the initial target gas concentration in the inert gas. Even with a 100% pure inert gas (where s =0), the efficiency could not reach 100% due to the increase of partial pressure of the target gas in the surrounding gas phase. This is indicated in the equation by the denominator, which is always greater than 1. The duration and amount of accumulation are

affected by the gas/liquid flow ratio. Unlike a single droplet degassing model, equation (8) brought in the gas and liquid flow rates, thus is valid for a continuous system with mono-dispersed droplets. It can also be used for a continuous system with poly-dispersed droplets with a properly defined mean droplet size. In this case, where the interfacial phenomena are of importance, the surface to volume mean should be used. A better modeling method for the poly-dispersed droplet system is to integrate the degassing process against the detailed size distribution. However, to get the information about the detailed size distribution required additional tests from the nozzle supplier and it therefore was not incorporated in the scope of this project.

It has been acknowledged that liquid droplets tend to follow the same drag relationship as solid particles for a Reynolds number of up to 500 [32-33]. When spherical droplets move through another fluid with a comparable viscosity, they usually can not maintain a spherical shape due to the shear stresses created by their motion. On the other hand, for liquid droplets falling in the surrounding gas, the surface tension is high enough to preserve their spherical shape [34]. Therefore, the general dynamic equations such as those for the Reynolds number, drag coefficient, and relaxation time for rigid particles can also be applied. However, there is one key difference of the poly-dispersed droplets from mono-dispersed droplets—analogous to hindered particle settling, the slip velocity is used to characterize the poly-dispersed droplets' falling process. The slip velocity is written as:

$$V_{bs} = V_t \alpha_g^{n-1} \tag{9}$$

Where α_g is volumetric fraction of the inert gas, and n is a function of the terminal Reynolds number Re_t [27]. Following Khan and Richardson's suggestion, n is calculated from the Galileo number by:

$$n = 4.8\frac{1+0.0215Ga^{0.57}}{1+0.043Ga^{0.57}}$$

(10)

Then the Reynolds number can be calculated as:

$$\mathrm{Re} = \frac{\rho_g d}{\mu_g} V_{bs} \tag{11}$$

2.2 Sherwood number

In order to determine the mass transfer coefficient, a number of dimensionless parameters were introduced in literature. Sherwood number, in particular, which represents the extent of the convective mass transfer to the diffusive mass transfer, was directly related to the mass transfer coefficient by:

$$Sh = \frac{kd}{D_g} \tag{12}$$

On the other hand, the formula reported in literature based on experimental or numerical results usually wrote the Sherwood number in terms of the Reynolds number (*Re*) and the Schmidt number (*Sc*) [27-29]: Others proposed correlations to include only one variable, the Peclet number (*Pe*), which is the product of *Re* and *Sc* [23; 28; 30-31]. Of the most widely used ones, Steiner [27] correlated results from 13 different mass transfer systems reported in literature without considering internal circulation with the following equation:

$$Sh = 2.43 + 0.775 * \mathrm{Re}^{1/2}\, Sc^{1/3} + 0.0103\,\mathrm{Re}\, Sc^{1/3} \tag{13}$$

It was further pointed out that Higbie's equation had been acknowledged as the theoretical equation for droplets with fully-developed internal circulation:

$$Sh = \left(2/\sqrt{\pi}\right) Pe^{1/2} \tag{14}$$

More recently, Saboni et al. [28] also numerically modeled the steady state situation by:

$$Sh = \frac{1}{3+k_v}\left\{\begin{array}{l} 1.65 + 0.67\left[\sqrt{Pe} + \dfrac{0.67\,\mathrm{Re}}{\mathrm{Re}+15}\left(\sqrt{Pe}-1\right)\right] \\ + k_v\left[1 - 0.12\,\mathrm{Re}^{1/3} + (1+Pe)^{1/3}\left(1+0.12\,\mathrm{Re}^{1/3}\right)\right] \end{array}\right\} \tag{15}$$

These correlations usually had a complicated form and a number of them lacked of experimental validations, especially for small droplets and droplets with not-fully-developed internal circulation. The principle will be adopted here so that new correlations for the Sherwood number can be derived from both mono-dispersed droplet and poly-dispersed droplet degassing tests. The correlations will be in a simple form, aiming for more practical use.

3. Experimental

3.1 Experimental setup using mono-dispersed droplets

A water-oxygen system with nitrogen gas serving as the sweep gas was used in this study to verify the aforementioned theories. The main part of the experimental setup in this study, as shown in Figure 3-2, was a mono-size droplet generator (TSI, MGD100). De-ionized ultra-filtered (DIUF) water was pumped from a water pump (Teledyne, Model 500D, controlled by a d-series controller) into the generator head. This generator head contained a liquid reservoir and an orifice outlet. A square wave was continuously sent to the generator head from a multiple frequency generator (coming with the generator)

at the side. Water leaving the generator head, was broken up and continued as a uniform string of droplets. The size of the droplets (d) was adjusted by the orifice size and could be calculated from the liquid flow rate (Q) and the excitation frequency (f) from the frequency generator as:

$$d = \left(\frac{6Q}{\pi f} \right)^{1/3} \tag{16}$$

Orifices of two different diameters were used in the tests: 50 and 100 μm. With these two orifices, the controllable size range of the droplets was between 148.6 and 264.8 μm. This size range was designed firstly because fine droplets were rarely used in the previous studies. It was chosen also to be compatible with the mean diameter of the droplets in the poly-dispersed droplet system. These droplets fell through the center line of a 35 cm long acrylic column (inner diameter of the column is 1.9 cm) into a sampling chamber at the bottom. Since the initial velocity of the droplet is a lot larger than its terminal velocity the residence time is defined by:

$$t = \frac{LA_o}{Q_L} \tag{17}$$

where L is the length of the column, and A_o is the area of the orifice.

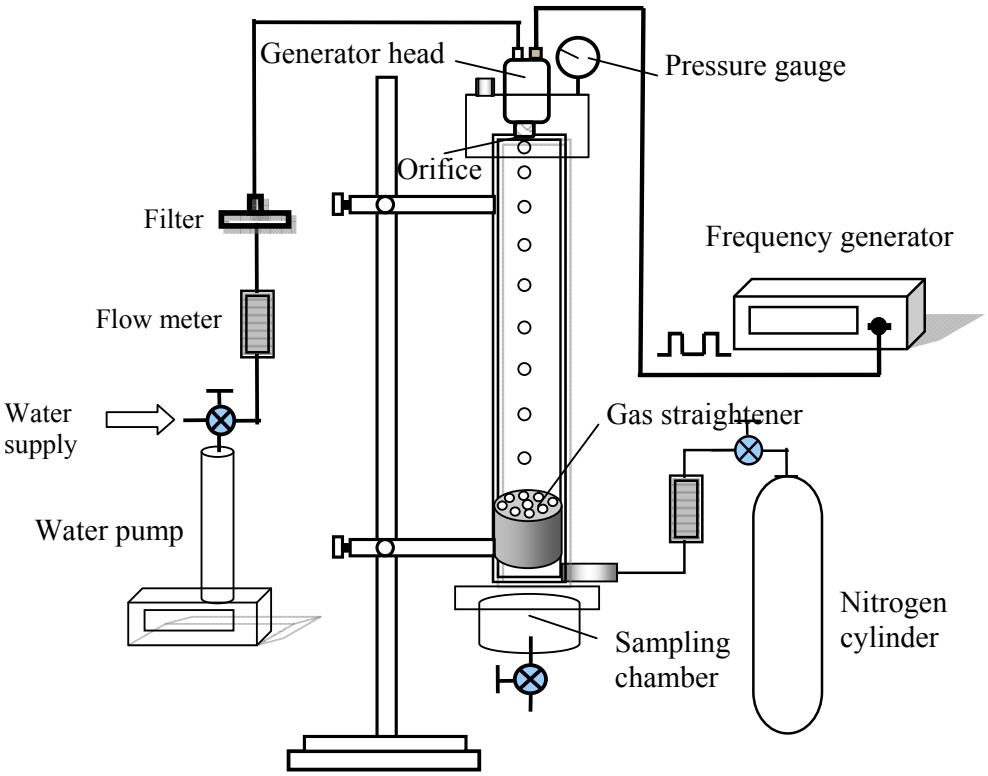

Figure 3-2 Laboratory degassing system using mono-dispersed droplets.

The column was continuously swept from the bottom to the top by nitrogen gas (industrial grade, 99.5%, Praxair) controlled by a gas flow meter (Cole Parmer, RK-32460). The nitrogen gas flow was first straightened by a home-made gas-straightener made of aluminum, as shown in Figure 3-3. The diameter of the hole at the center of the straightener was large enough to allow droplets to fall through freely. Located above the chamber were the gas outlet and a pressure gauge used to measure the stagnant gas pressures when the system was operated as a sealed system. The effective degassing distance was defined as the distance from the orifice to the bottom of the air straightener.

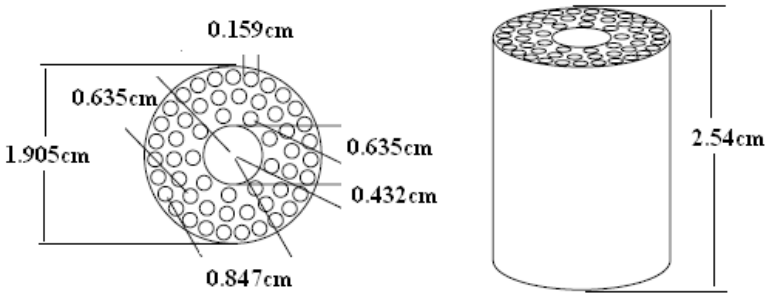

Figure 3-3 Schematic design of the gas straightener.

Before the water supply and the frequency generator were turned on, the system was purged with the nitrogen gas for 10 minutes to remove the air (oxygen). The purging gas was maintained for another 5 minutes after droplets were generated to assure that the system was at steady state. With water flow rates varying from 66 to 200 ml/hr, the nitrogen gas flow rates tested were from 100 to 500 ml/min. A bulk water sample was taken immediately using a syringe for DO measurements once the volume exceeded 1 ml in the bottom chamber. Each DO measurement was repeated three times, and the experimental degassing efficiency was defined as:

$$\eta_E = 1 - \frac{C_{outlet}}{C_{inlet}} \tag{18}$$

3.2 Experimental setup using poly-dispersed droplets

The schematic of the experimental setup using poly-dispersed droplets in a large spray column is shown in Figure 3-4. Filtered tap water was pumped into the system, due to the large volume required for continuous tests, controlled by a water flow meter (Cole-Parmer, RK series). Downstream of the top flange fitting was the main part of the system- a 121.92 cm tall acrylic column with an

inner diameter of 30.48 cm. A home-made metal sheet (316 SS) was used to seal the top of the tube while its bottom was connected to a spray nozzle. The nozzle tested in this study was a 90 degree full-cone fog type one from John Brooks Co. Ltd. (1/4PRSXJB120). It was chosen because it could generate finer droplets than other commonly used industrial nozzles and they were compatible in size with the droplets used in the mono-dispersed system above. In this study, most droplets were expected to be in the range of 50 to 400 μm (number mean diameter) in diameter, according to the calibration of the nozzle supplier. The surface to volume mean diameter was used in model calculations by:

$$d_{vs} = \frac{d_v^{\,3}}{d_s^{\,2}} \tag{19}$$

where d_v and d_s are the volume and surface mean diameters, respectively.

Nitrogen gas (industrial grade, 99.5% from Praxair) was introduced into the system at the bottom and carried the removed oxygen gas out from the top gas outlet. Therefore, the effective degassing distance was 86.68 cm, from the nozzle to the inert gas inlet. The upward flow was straightened through a special unit with paralleled plates, which is also expected to result in minor extra degassing from thin liquid film to the gas phase. Droplets were collected at the bottom, and the degassed water was controlled by a T-valve to go back to the sink or to a sampling container as needed. Experiments were conducted with water flow rates between 120.62 to 220.8 ml/s, and nitrogen flow rates between 197 to 1180 ml/s and each test was repeated 4 times. The wall effect was also taken into account by revising the gas to liquid flow ratio with the spray coverage information:

$$\alpha = \frac{Q_G}{Q_L}\frac{A_s}{A_c} \tag{20}$$

where A_s (experimentally determined herein as 1418.62 cm^2) and A_c are cross-sectional areas of the largest spray coverage and the spray column, respectively..

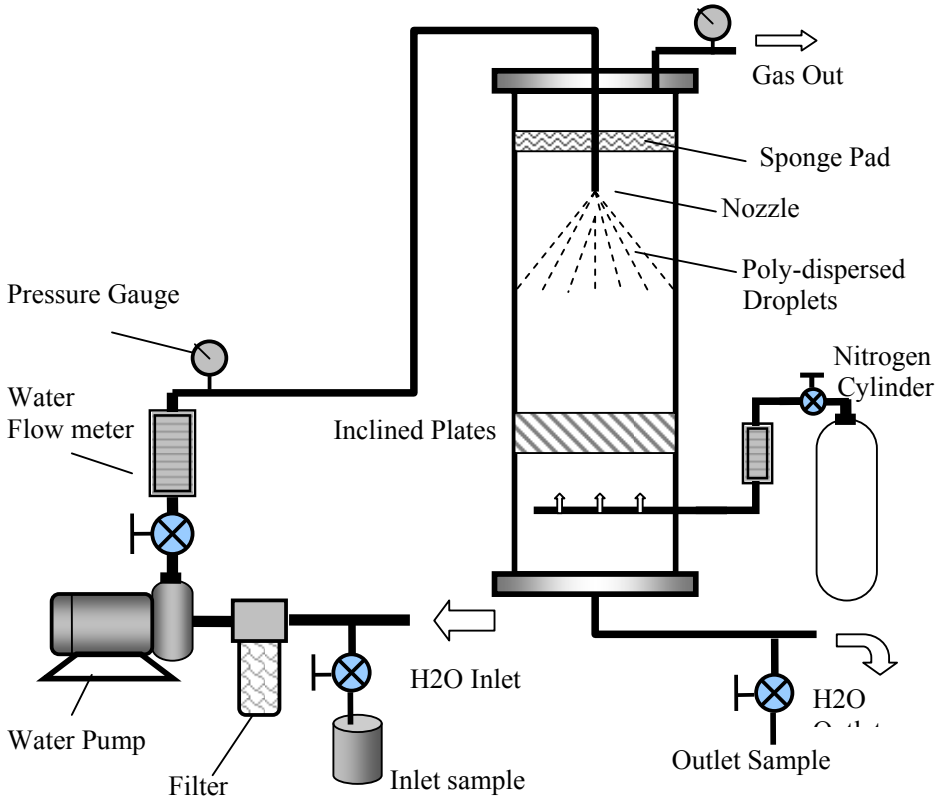

Figure 3-4 Laboratory degassing system using poly-dispersed droplets in a spray column.

3.3 Dissolved oxygen measurements

Measurement of the concentration of the dissolved oxygen in water is another equally important issue that needs to be addressed. As to evaluating the DO removal efficiency in a droplet system, the method must meet two requirements. Firstly, it should require only a small volume of liquid sample because the droplet size is small. The method should also have a short response

time such that it converts the dissolved gas into a stable form instantaneously at the time of sampling. In this way the measurement is valid without being affected by a secondary (extra) degassing/aeration process.

In this study, measurements of the dissolved oxygen concentration were conducted by a simplified system, coupling the Winkler titration method [40-41] with an Ultraviolet-visible (UV/Vis) spectroscopy [42]. A Genesys 10 scanning UV/vis spectrometer (Thermo Fisher Scientific Inc.) was used to determine the end point of each titration. All the chemicals were obtained from Sigma-Aldrich and the solutions were prepared in DIUF (De-Ionized Ultra-Filtered) water: a 2.15 mol/l manganese sulfate solution, an alkaline iodide solution with 12.5 mol/l NaOH, 0.9 mol/l KI (ACS reagent ≥99.0%), and 0.15 mol/l NaN_3 (≥99.5%), a sodium thiosulfate solution with 3.9 mmol/l $Na_2S_2O_3$ (≥98.0%) and 0.0125 mol/l NaOH, and a phosphoric acid solution with 50 wt% ca. H_3PO_4 crystals (reagent grade, ≥98%).

Each DO measurement was completed by drawing 940 µl water sample, 20 µl manganese sulfate and 20 µl alkaline iodide solutions into a 1000 µl syringe, then gently shaking the syringe until the precipitation was complete. 20 µl phosphoric acid was then drawn into the same syringe, and gently shaken until the precipitate was completely dissolved. The final solution was injected into a 1.4 ml UV quartz cuvette. This solution was then titrated with sodium thiosulfate in a 500 µl syringe until the UV/vis spectrometer did not show any more absorbance of the 350 nm wavelength, which indicated the end of the titration.

This titration method was first compared with the measurements using a Hach DO meter (Model WU-53013-10 from Cole-Parmer) and was deemed to be acceptable. For calibration purpose, bulk water samples before and after the DO removal using the spray column were measured using both methods. The concentrations of the bulk water (>300 ml) measured with the DO meter was to compare to that of the respective 1 ml water sample using the titration method. This series of tests were conducted to prove that the modified Winkler titration method was suitable to precisely measure small water samples, both for high and low DO concentrations, as to be introduced shortly.

4. Results and Discussion

4.1 Validation of the modified micro-titration method

The comparison of the DO meter method and the modified micro-Winkler titration method used in this study is shown in Figure 3-5. The experimental data measured by the titration method showed great linearity and were well fitted by the ideal line $y = x$. The titration method barely had some small over-predictions ($\leq 3\%$) at very low DO concentrations (1 and 2 ppmw). However, the titration method is probably the more precise one when it comes to the lower range, since it quickly transformed oxygen into a more stable form and shortened the exposure time of the water sample to the atmospheric contamination. Therefore, this titration method was considered accurate and appropriate for all the tests with mono-dispersed droplets. In addition, by using both methods, the DO concentrations of the inlet water samples for both mono-dispersed and poly-dispersed droplet tests were found to be steady, around 8 ppmw.

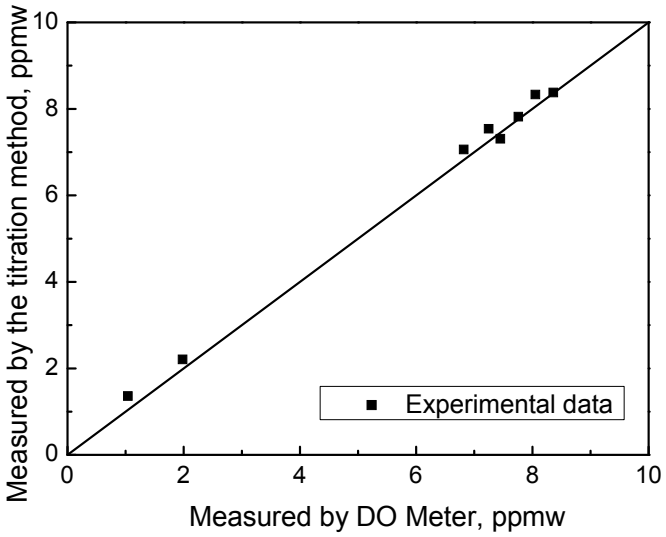

Figure 3-5 Comparison of DO concentrations measured by the titration method and a DO meter.

4.2 Mono-dispersed droplets

4.2.1 Degassing efficiency using mono-dispersed droplets

The degassing efficiency in relation with the droplet diameter at a nitrogen flow rate of 100 ml/min is shown in Figure 3-6. It can be seen that the degassing efficiency decreases with the increase of the droplet size. This is consistent with the aforementioned analytical analysis. Contact time could be another reason for this decrease, but herein it is more influenced by the orifice size, rather than the droplet diameter.

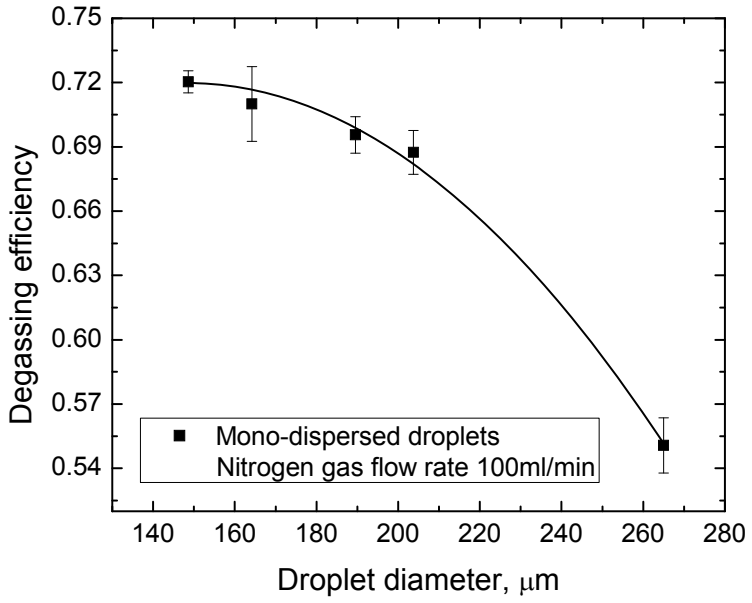

Figure 3-6 Degassing efficiency vs. droplet diameter in the system using mono-dispersed droplets.

One of the arguments existing in literature is about internal circulation. Clift et al. [31] claimed in their classic textbook that when the viscosity difference was large between two fluids (e.g. water sphere falling in air), the internal circulation could be neglected, especially for fine droplets. However, experimental data from different authors were sometimes distinctly different from one another. There is lots of work concerning the internal circulation and the diffusion-convection mechanism, but experiments always seem to indicate a more complex nature. Sometimes, even experimentally confirmed non-circulating droplets were in agreement with the equations derived for droplets with well-developed internal circulation (Ladislav, 1986). Inevitable surfactants and other surface-active materials are said to contaminate water and have shown an impact on interfacial mass transfer in a liquid-liquid extraction system [17; 31; 37]. The authors in this study believe that the possible mechanism should

combine three factors: the coated surfactants placed mass transfer resistance at the interface, the absolute interfacial area increased with the existence of surfactants, and the concentration gradient of the surfactant depressed the internal circulation. As pointed out previously, these factors could rarely be concerns in the mono-dispersed droplet tests herein. By using DIUF water and well-controlled working conditions, Figure 3-6 is expected to set a steady state background for poly-dispersed droplet tests.

4.2.2 Correlation for Mono-dispersed droplets

To find a correlation between the mass transfer coefficient and the dimensionless dynamic parameters, k, Sh, Re, Sc, and Pe were calculated based on the following conditions: atmospheric pressure was 1.01325×10^5 Pa, oxygen gas density was 1.25 kg/m^3, water density was 1000 kg/m^3, K_H was 4.95×10^{-10} Pa^{-1} [43], and s was 0.5% for an industrial grade nitrogen gas. Along with the mass transfer coefficients calculated for five droplet diameters, the results are summarized in Table 3-1.

Table 3-1 The mass transfer coefficient and related dynamic parameters calculated for mono-dispersed droplet correlation derivation.

Droplet diameter, (μm)	Gas flow rate, (ml/min)	Liquid flow rate, (ml/hr)	*Residence time*$\times 10^2$, *(s)*	$k\times 10^2$, (cm/s)	*Sh*	*Re*	*Pe*
148.6	100	66	3.85	8.99	84.6	98.9	42988.6
164.2	100	133	7.45	4.86	50.5	55.1	23945.5
189.5	100	100	9.91	4.04	48.4	47.8	20786.8
203.7	100	100	9.91	4.24	54.6	51.4	22344.4
264.8	100	100	9.91	3.75	62.8	66.9	29068.6
264.8	1000	100	10.06	3.99	66.8	67.9	29502.7
264.8	3000	100	10.42	4.05	67.9	70.1	30467.4
264.8	5000	100	10.79	4.07	68.2	72.3	31432.0
264.8	0	100	9.90	3.66	61.4	66.7	29020.7

The Schmidt number is constant for a given degassing system, therefore the Peclet number is solely determined by the Reynolds number, which were found to be in a medium range (45-100). The mass transfer coefficient increases with the increase of the droplet size because it was, to a greater extent, influenced by the surrounding gas flow pattern at different Reynolds numbers. The order of magnitude of the mass transfer coefficients herein are matching Jeannot and. Cantwell's single drop experiments (1997).

Based on the data in Table 3-1, a new and simple linear correlation between the Sherwood number and the Peclet number was derived accordingly as:

$$Sh = 0.0016Pe + 15.297 \quad (20000<Pe<45000)$$

$$(R^2=0.951) \qquad (21)$$

It was more convenient to use a single parameter Peclet number than two parameters, Reynolds number and Schmidt number, to predict the Sherwood number, especially considering that Schmidt number is a constant for a given system. It is noticed herein that no matter how complex the diffusion-convection mechanism (i.e. the internal circulation) is as it was discussed in the previous sections, the correlation for the mass transfer coefficient could still maintain a simple form as it was for a rigid particle. This correlation also has a simpler form than most of those described in literature [23; 28; 30-31].

4.3 Poly-dispersed droplets

4.3.1 Degassing efficiency using poly-dispersed droplets

Information provided by John Brooks Co. Ltd, the droplets generated by nozzle PJB120 showed normal size distributions based on the number, surface area or volume. These distributions are also dependent on the inlet water

pressure and, consequently, the water flow rate. The mean droplet diameters showed a power relationship with respect to the water flow rate, and different types of mean droplet diameter were calculated from the distribution and plotted in Figure 3-7. It is worth mentioning that this mean diameter only characterizes the size distribution of the droplets generated at the nozzle. Droplet coalescence as well as other types of droplet interactions is expected to happen due to the difference of the terminal settling velocities for droplets of different sizes.

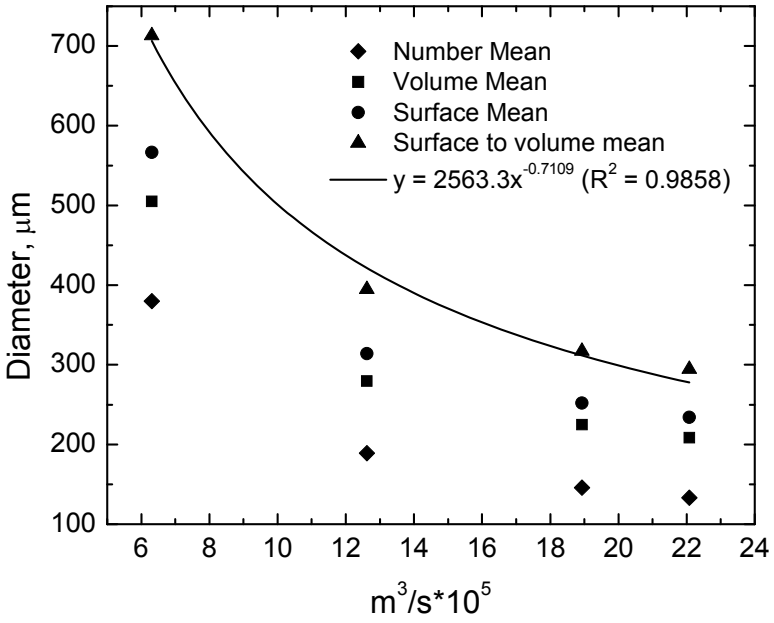

Figure 3-7 Different types of mean diameters of the poly-dispersed droplets.

The correction factor for the wall effect in this study was found to be 0.514. Water sprayed directly onto the column wall went though a film degassing process while running down. Film degassing was considered much less efficient compared to droplet degassing, and was therefore negligible in contributing to the degassing efficiency. Besides, the type of spray nozzle was selected as that the coverage of the spray could make the best use of the cross sectional area of

the spray tower. One of the most important parameters in characterizing a spray column-involved industrial process is gas to liquid flow ratio. Hence, the degassing efficiency with respect to the inter gas to water flow ratio was plotted in Figure 3-8. Similar to the analysis for the mono-droplet tests, the group of dimensionless numbers along with other working conditions are calculated and summarized in Table 3-2. It is indicated in Figure 3-8 that the degassing efficiency increases significantly with respect to the increase of the inert gas to liquid flow ratio. This is because a higher inert gas to liquid flow ratio either results a longer contact (residence) time or a bigger local Reynolds number, both of which are in favor of the mass transfer process. The system reached its limit, caused by thermodynamic and other factors, when the gas/liquid flow ratio was greater than about 15. This performance, 93% ca., matches the most up-to-date industrial degassing techniques such as a combination of inert gas bubbles and mechanical agitation [44]. Higher degassing requirements can be met by operating multiple units of this sort in series. Hence, the spray column is believed to be one of the most cost-effective liquid degassing solutions.

Table 3-2 Mass transfer coefficient and related dynamic parameters calculated for poly-dispersed droplet correlation derivation.

Gas to liquid flow rate ratio	Water flow, $m^3/s * 10^5$	Mean diameter, (μm)	*Residence time, (s)*	$k \times 10^2$, (cm/s)	Sh	Re	Pe
1.73	22.08	294.42	0.748	1.141E-04	21.26	9.09	3950.68
3.03	12.62	394.94	0.534	2.236E-04	55.90	26.35	11455.97
3.46	22.08	294.42	0.748	1.282E-04	23.89	14.06	6112.90
4.04	18.93	317.37	0.684	1.736E-04	34.88	18.01	7832.63
5.20	22.08	294.42	0.748	1.384E-04	25.78	16.62	7228.18
6.06	12.62	394.94	0.534	3.150E-04	78.73	33.99	14782.79
6.06	18.93	317.37	0.684	1.985E-04	39.86	20.79	9039.19
6.93	22.08	294.42	0.748	1.715E-04	31.96	18.17	7900.47

8.08	18.93	317.37	0.684	2.179E-04	43.77	22.42	9747.94
8.66	22.08	294.42	0.748	1.937E-04	36.09	19.20	8348.61
9.09	12.62	394.94	0.534	3.472E-04	86.80	37.32	16224.85
10.10	18.93	317.37	0.684	2.361E-04	47.42	23.49	10213.28
10.39	22.08	294.42	0.748	2.007E-04	37.39	19.94	8668.33
12.13	12.62	394.94	0.534	3.654E-04	91.33	39.16	17027.47
12.13	18.93	317.37	0.684	2.407E-04	48.35	24.24	10541.97
15.16	12.62	394.94	0.534	4.036E-04	100.87	40.34	17538.36
18.19	12.62	394.94	0.534	4.004E-04	100.08	41.15	17892

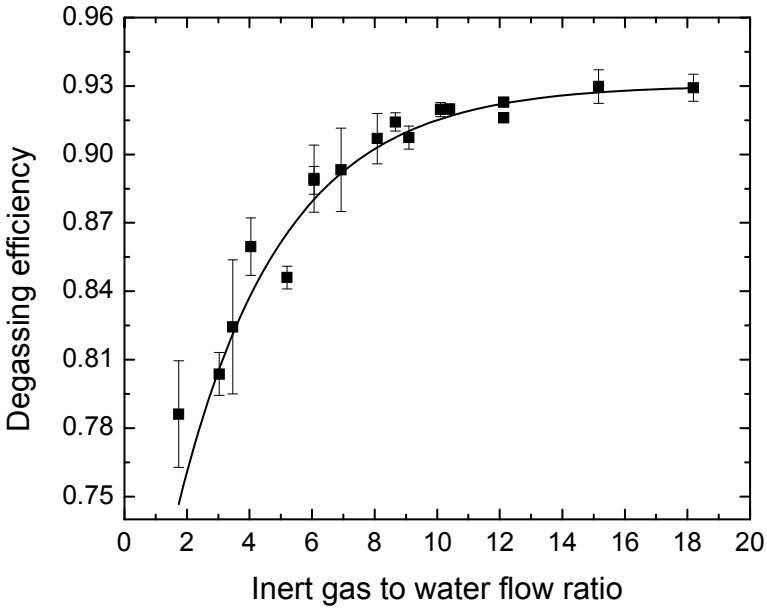

Figure 3-8 Degassing efficiency vs. the gas to liquid flow rate ratio using poly-dispersed droplets.

4.3.2 Correlation for Poly-dispersed droplets

Similar to the result for the mono-dispersed droplet tests, the relationship between the Sherwood number and the Peclet number is also linear in two ranges of Peclet numbers:

$$Sh = 0.00676Pe - 21.337 \quad (7500<\text{Pe}<20000) \quad (\text{with } R^2=0.996) \quad (22)$$

$$Sh = 0.00136Pe + 15.822 \quad (\text{Pe}<7500) \quad (\text{with } R^2=0.984) \quad (23)$$

The correlations derived in this study are plotted together with the correlations mentioned in literature in Figure 3-9. Figure 3-9 shows that at all range of the Peclet number, the correlation derived from the mono-dispersed droplet tests does not deviate much from the either Eqn 13 derived from experiments or Eqn 15 derived from numerical work for a steady state mass transfer. Mathematically it indicates that a simple linear function can be used in lieu of the complex correlations to describe the mass transfer at or close to

steady state; while physically it means that the internal circulation in the mono-dispersed droplets was not significant. This conclusion is especially sound for low Peclet number circumstances and, for a given system with low Reynolds numbers. On the other hand, the correlation derived from the tests using poly-dispersed droplets was mostly far away from the steady state curve. However, the lower Peclet number part of the correlation perfectly agreed with the correlation derived for mono-dispersed droplets. This proves the inherent connection between the physical behaviors of the mono-dispersed droplets and poly-dispersed droplets—the mono-dispersed droplet tests could provide fundamental basis for the poly-dispersed droplet tests when the Peclet number is smaller than 7500. Poly-dispersed droplets behave more differently from they are at steady state when the Peclet number is higher than 7500, which is most likely due to the development of internal circulation. More intense internal circulation means stronger effects of mass transfer by convection, and consequently, a higher Sherwood number. This difference from the mono-dispersed droplets is due to interactions between high concentrations of droplets, and a better contact of the droplets with the inert gas flow. From the industrial point of view, this favors the degassing process. However, in this study ($Pe<20000$), fully developed internal circulation was never formed in the poly-dispersed droplets. It is also worth mentioning that quantitatively estimating the internal circulation between the steady state and full development solely based on the Peclet number might not be of generality because the mass transfer is very likely affected by other factors for a spray column such as the nozzle type and the droplet size distribution.

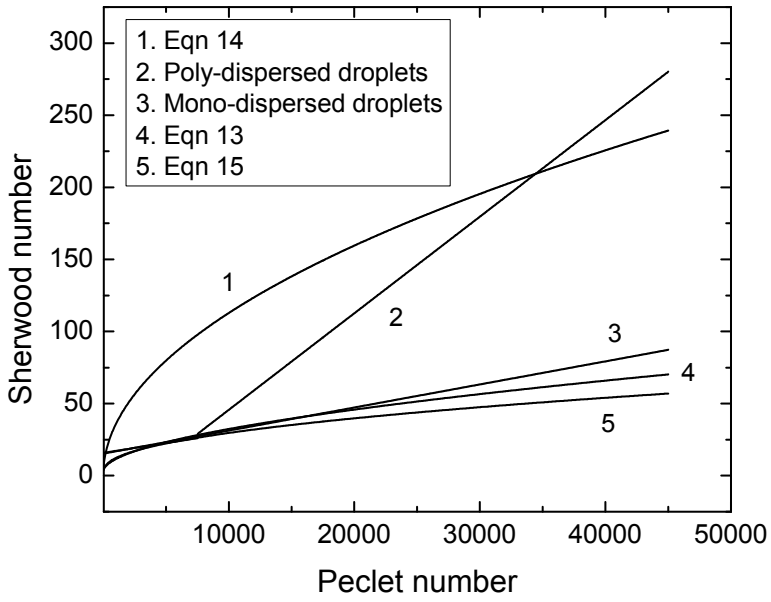

Figure 3-9 Comparison of the correlations in this study with those correlations used in literature.

For comparison reasons, a 60 degree full-cone spiral type (1/4HHSJSXJB6007, John Brooks Co. Ltd.) nozzle was also tested and the results are shown in Figure 3-10. When the flow rate is 63.1 m/s, the spiral-type and the fog-type nozzles were performing almost identical with respect to different sweep gas flow rate. Interestingly, however, when there was a higher inlet water load, 126.2 ml/s, for the fog-type nozzle, the degassing efficiency also increased at each nitrogen flow rate. This could be true only if water was not fully atomized by the fog-type nozzle at lower flow rates (pressures). The significant improvement of the degassing efficiency from using a spiral-type nozzle for lower water load to using a fog-type nozzle for a higher water load proved the fog-type nozzle's superiority. This superiority was most likely resulted from the fact that the droplets came out finer from the fog-type nozzle and had better contacts with the sweep gas.

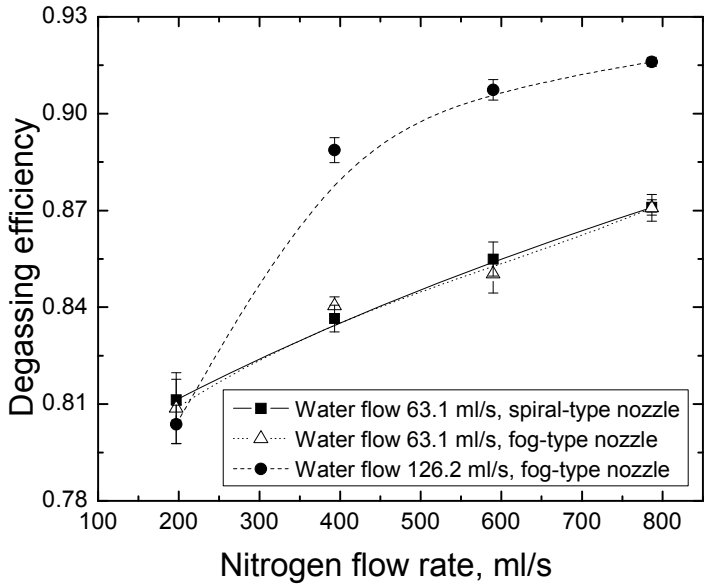

Figure 3-10 Effects on the degassing efficiency using a spiral type and a fog type nozzle.

5. Conclusions

Degassing using mono-dispersed and poly-dispersed fine liquid droplets falling in inert gas was investigated in this study. In the tests using mono-dispersed droplets, fine droplets with a diameter between 148.6 and 264.8 μm were employed. With a high inert gas to liquid flow ratio, the degassing efficiency significantly decreases with the increase of the droplet size. This system using mono-dispersed droplets such that it has more similarities (i.e. dynamic and continuous systems) with a system using poly-dispersed droplets compared to a single droplet system. The droplet size was chosen to be compatible with the size of the droplets in the poly-dispersed tests. In the tests using poly-dispersed droplets, a wide range (0-20) of inert gas to liquid flow rate ratio was systematically studied for 3 different water flow rates (which led to 3 different droplet size distributions). With a full cone fog-type nozzle (also proven to be superior to a full cone spiral nozzle), a system degassing limit of about 93% was reached when the gas to liquid flow ratio was greater than 15. Matching the most up-to-date degassing techniques such as a combination of bubble stripping and mechanical agitation in a cost-effective manner, this system is believed to be applicable to industrial degassing processes.

The degassing process was also analytically modeled by the mass transfer equations taking into the flow rate ratio and the impurity of the inert gas into consideration. Furthermore, a new and simple correlation for the Sherwood number with respect to the Peclet number was derived for the system using mono-dispersed droplets, $Sh = 0.0016\mathrm{Pe} + 15.297$ (20000<Pe<45000). It was compared and showed good consistence with the previous work based on different experimental systems and numerical simulations, especially when Pe is

small, which indicates a steady state mass transfer process. As to the system using poly-dispersed droplets, it was found that $Sh = 0.00136Pe + 15.822$ when Pe is smaller than 7500 and $Sh = 0.00676Pe - 21.337$ when Pe is up to 20000. The lower part of this correlation converges with the correlation for mono-dispersed droplets, while the upper part of it was greatly larger. For the whole range of Pe tested, the correlation for the system using poly-dispersed droplets was never close to the situation with fully-developed internal circulation. Internal circulation was believed to exist in the poly-dispersed droplets due to the high droplets concentration and a better contact with the sweep gas, which are all in favor of a degassing process. However, quantitatively describing the intensity of the internal circulation is still up for debate and out of the scope of this study.

Another contribution of this study is that a faster yet simpler micro-Winkler titration method was applied to measure the dissolved oxygen concentration in water. The method was compared, and showed good consistence with the measurements using a DO meter. The particular advantages include: cost effective equipment, a smaller water sample requirement and a short response time even for low DO concentration measurements. Both of these advantages prevented the measurements from being affected by undesired secondary degassing/aeration processes.

Nomenclature

A_d	surface area of a droplet (m^2)
c_d	concentration of the target gas in the droplet (ppmv)
c_i	initial concentration of the dissolved gas in the droplet (ppmw)
c_f	final concentration of the dissolved gas in the droplet (ppmw)
c_g	concentration of the dissolved gas in the sweep gas (ppmw)
D_g	gas diffusion coefficient in a liquid ($m^2\ s^{-1}$)
f	excitation frequency (s^{-1})
j	flux of the solute transferred from the liquid to the bubbles (kg m^{-2} s^{-1})
k	mass transfer coefficient (m s^{-1})
K_H	Henry's law constant (Pa^{-1})
P	partial pressure of the target gas in the headspace (Pa)
P_0	atmospheric pressure (Pa)
Pe	Peclet number
Q_G	gas flow rate ($m^3\ s^{-1}$)
Q_L	liquid flow rate ($m^3\ s^{-1}$)
r	radius of the droplet (m)
Re	Reynold number
s	initial concentration of the target gas in the sweep gas
Sh	Schmidt number
Sh	Sherwood number
U	falling droplet velocity with respect to the sweep gas (m s^{-1})
V	volume of a droplet (m^3)

Greek symbols	
ρ_L	liquid density (kg m^{-3})
ρ_T	target gas density (kg m^{-3})
η	degassing efficiency
ψ	stream function of the internal circulation in the droplet

References

[1] G. T. Vladisavljevic, Use of polysulfone hollow fibers for bubbleless membrane oxygenation/deoxygenation of water. Sep. Purif. Technol. 17 (1999) 1-10.

[2] B. W. Breitschopf F, Dittrich S, and Koukol R, A new kind of water deaeration based on hollow fiber membranes. Brauwelt International (1997) 431-433.

[3] S. R. Anil Kumar Pabby, Ana Maria Sastre, Handbook of membrane separations: chemical, pharmaceutical, food, and biotechnological applications, CRC press, Boca Raton, 2008.

[4] R. Wu, D. Shu, B. Sun, J. Wang, F. Li, H. Chen, and Y. Lu, Theoretical analysis and experimental study of spray degassing method. Mater. Sci. Eng., A 408 (2005) 19-25.

[5] M. J. Semmens, D. M. Foster, and E. L. Cussler, Ammonia removal from water using microporous hollow fibers. J. Membr. Sci. 51 (1990) 127-140.

[6] N. N. Nassar, and M. M. Husein, Ultradispersed particles in heavy oil: Part I, preparation and stabilization of iron oxide/hydroxide. Fuel Process. Technol. 91 (2010) 164-168.

[7] W. J. Bruckard, and J. T. Woodcock, Recovery of valuable materials from aluminium salt cakes. Int. J. Miner. Process. 93 (2009) 1-5.

[8] T. Leiknes, and M. J. Semmens, Vacuum degassing using microporous hollow fiber membranes. Sep. Purif. Technol. 22-23 (2001) 287-294.

[9] A. Sengupta, P. A. Peterson, B. D. Miller, J. Schneider, and C. W. Fulk Jr, Large-scale application of membrane contactors for gas transfer from or to ultrapure water. Sep. Purif. Technol. 14 (1998) 189-200.

[10] K. Li, I. Chua, W. J. Ng, and W. K. Teo, Removal of dissolved oxygen in ultrapure water production using a membrane reactor. Chem. Eng. Sci. 50 (1995) 3547-3556.

[11] H. Su, S. Wang, H. Niu, L. Pan, A. Wang, and Y. Hu, Mass transfer characteristics of H2S absorption from gaseous mixture into methyldiethanolamine solution in a T-junction microchannel. Sep. Purif. Technol. In Press, Accepted Manuscript.

[12] B. Dou, W. Pan, Q. Jin, W. Wang, and Y. Li, Prediction of SO2 removal efficiency for wet Flue Gas Desulfurization. Energy Convers. Manage. 50 (2009) 2547-2553.

[13] B. Rajmohan, S. N. Reddy, and B. C. Meikap, Removal of SO2 from industrial effluents by a novel twin fluid air-assist atomized spray scrubber. Ind. Eng. Chem. Res. 47 (2008) 7833-7840.

[14] T. Elperin, A. Fominykh, and Z. Orenbakh, Coupled heat and mass transfer during nonisothermal absorption by falling droplet with internal circulation. Int. J. Refrig. 30 (2007) 274-281.

[15] A. R. Uribe-RamiÌ rez, and W. J. Korchinsky, Fundamental theory for prediction of single-component mass transfer in liquid drops at intermediate Reynolds numbers ($10 \leq Re \leq 250$). Chem. Eng. Sci. 55 (2000) 3305-3318.

[16] M. Adekojo Waheed, M. Henschke, and A. Pfennig, Mass transfer by free and forced convection from single spherical liquid drops. Int. J. Heat Mass Transfer 45 (2002) 4507-4514.

[17] H. Lohner, C. Czisch, P. Lehmann, and K. Bauckhage, Mass transfer processes in liquid-liquid systems with surfactants. Chem. Eng. Technol. 24 (2001) 1157-1163.

[18] J. Petera, and L. R. Weatherley, Modelling of mass transfer from falling droplets. Chem. Eng. Sci. 56 (2001) 4929-4947.

[19] A. Turpin, A. Couvert, A. Laplanche, and A. Paillier, Experimental study of mass transfer and H2S removal efficiency in a spray tower. Chem. Eng. Process. 47 (2008) 886-892.

[20] M. A. Jeannot, and F. F. Cantwell, Mass Transfer Characteristics of Solvent Extraction into a Single Drop at the Tip of a Syringe Needle. Anal. Chem. 69 (1997) 235-239.

[21] B. P. Leclair, W. D. Hall, A. E. Hamielec, and Pruppach.Hr, Theoretical and experimental study of internal circulation in water drops falling at terminal velocity in air. J. Atmos. Sci. 29 (1972) 728-&.

[22] N. Kishore, R. P. Chhabra, and V. Eswaran, Mass transfer from ensembles of fluid spheres to a power-law liquid at moderate Reynolds and Peclet numbers. Chem. Eng. Sci. 63 (2008) 2484-2499.

[23] N. Kishore, R. P. Chhabra, and V. Eswaran, Mass transfer from ensembles of Newtonian fluid spheres at moderate Reynolds and Peclet numbers. Chem. Eng. Res. Des. 85 (2007) 1203-1214.

[24] J. Kuntz, and A. Aroonwilas, Performance of spray column for CO2 capture application. Ind. Eng. Chem. Res. 47 (2008) 145-153.

[25] E. C. Lim, S. Heng Koh, L. Kuang Lim, S. Hoon Ore, B. Kiat Tay, Y. Ma, and C. H. Wang, Experimental and computational studies of liquid aerosol evaporation. J. Aerosol Sci. 39 (2008) 618-634.

[26] A. K. Tharanivasan, C. Yang, and Y. Gu, Comparison of three different interface mass transfer models used in the experimental measurement of solvent diffusivity in heavy oil. J. Pet. Sci. Eng. 44 (2004) 269-282.

[27] L. Steiner, Mass-transfer rates from single drops and drop swarms. Chem. Eng. Sci. 41 (1986) 1979-1986.

[28] A. Saboni, Mass transfer from spherical bubbles, drops, and particles (review). Journal of the University of Chemical Technology and Metallurgy 43 (2008) 377-382.

[29] C. J. Walcek, and H.R. Pruppacher, On the scavenging of SO2 by cloud and raindrops: I. A theoretical study of SO2 absorption and desorption for water drops in air. J. Atmos. Chem. 1 (1983) 269-289.

[30] Z. G. Feng, and E.E. Michaelides, Heat and mass transfer coefficients of viscous spheres. I Int. J. Heat Mass Transfer 44 (2001) 4445-4454.

[31] J. R. Clift, M.E. Weber, Bubbles, Drops, and Particles, Academic Press, New York, 1978.

[32] C. F. Lapple, Fluid And Particle Mechanics, Vincent Press, Peterborough, 2007.

[33] R. G. Perry, D.W., Perry's Chemical Engineers' Handbook, McGraw-Hill New York, 1997.

[34] E. E. Michaelides, Particles, Bubbles & Drops: Their Motion, Heat And Mass Transfer, World Scientific Publishing Company, Hackensack, 2006.

[35] W. R. Byron Bird, Edwin N. Lightfoot, Transport phenomena, Wiley, New York, 2002.

[36] R. Kronig, and J. C. Brink, On the theory of extraction from falling droplets. Appl. Sci. Res. 2 (1951) 142-154.

[37] L. Mekasut, J. Molinier, and H. Angelino, Effects of surface-active agents on mass transfer inside drops. Chem. Eng. Sci. 34 (1979) 217-224.

[38] D. A. Barry, and J. Y. Parlange, Recirculation within a fluid sphere at moderate Reynolds numbers. J. Fluid Mech. 465 (2002) 293-300.

[39] J. K. Hans R. Pruppacher, Microphysics of clouds and precipitation, Kluwer Academic Publishers, Norwell, 1997.

[40] J. D. Burke, Determination of oxygen in water using a 10-ml syringe. Jour Elisha Mitchell Sci Soc 78 (1962) 145-147.

[41] H. M. Fox, and C. A. Wingfield, A portable apparatus for the determination of oxygen dissolved in a small volume of water. J. Exp. Biol. 15 (1938) 437-445.

[42] L. S. Peck, Two methods for the assessment of the oxygen content of small volumes of seawater. J. Exp. Mar. Biol. Ecol. 141 (1990) 53-62.

[43] T. R. Rettich, R. Battino, and E. Wilhelm, Solubility of gases in liquids. 22. High-precision determination of Henry's law constants of oxygen in liquid water from T = 274 K to t d 328 Ka. J. Chem. Thermodyn. 32 (2000) 1145-1156.

[44] Y. Ji, Lei, H., Tan, Z., Liquid degassing using a combination of micro-bubbles and mechanical agitation. . Sep. Purif. Technol. (Submitted for publication)

[45] A. Saboni, S. Alexandrova, A. Spasic, C. Gourdon, Effect of the viscosity ratio on mass transfer from a fluid sphere at low to very high Peclet numbers, Chemical Engineering Science, 62, 2007, 4742-4750.

[46] A. R. Khan, and J. F. Richardson, Fluid Particle Interactions and Flow Characteristics of Fluidized Beds and Settling Suspensions of Spherical Particles, *Chem. Eng. Commun.* 78, 111-130 (1989)

CHAPTER 4 : WATER DEGASSING USING MONO-/POLY-DISPERSED DROPLETS FALLING IN INERT GAS

1. Introduction

Water degassing is of great importance in a number of industrial processes. Dissolved oxygen, for example, negatively affects the product quality in beverage and electronics industries. Moreover, toxic or corrosive gases such as ammonia, hydrogen sulfide, sulfur dioxide, and carbon dioxide are commonly found in water used to process crude oil and natural gas, to scrub power plant stack gases, and in anaerobic municipal and industrial wastewater treatment processes, etc.[1]. These waters, if not properly treated, could wear down the equipment or release the gases to the atmosphere, causing serious environmental and health issues.

Some of the degassing processes involve chemical reactions, whereas a physical separation process is often considered more economical [1], and less system-intrusive such that it prevents secondary contamination introduced by added reagents. Physical degassing techniques such as membrane contactor degassing [2-6], and ultrasonic degassing [7-8], have been used where ultra-pure water was needed. However, some less intricate and less costly designs found wider applications. The flash vaporization system[1], the Venturi tube system [9], the mechanical stirring system, and the bubbling (inert gas stripping) system [10], etc. fell into this category. More recently, a system with poly-dispersed spray droplets also began to draw attention in degassing [11] and other related mass transfer studies [12-14]. The large surface to volume ratio of a droplet benefits the interfacial mass transfer while

generating fine droplets in a spray column is simple, cost-effective, and energy-efficient. This idea has gained success especially in SO_2 absorption processes [13, 15]. Yet, degassing, a reverse process to gas adsorption, has not been studied systematically in terms of identifying and optimizing the operation parameters. Meanwhile, it is also worth looking into the degassing process using mono-dispersed droplets. Compared to a system with poly-dispersed droplets, it minimizes uncertain factors such as the wall effects, different definitions of mean droplet size, droplet-droplet interaction, etc. There has been no such experimental data reported in literature.

The objective of this study is to design and evaluate a water-degassing (i.e. removal of dissolved oxygen) system with poly-dispersed droplets falling in inert gas. The contributing parameters to the degassing efficiency will be identified and optimized. This degassing system is also to be compared with one that uses inert gas bubble stripping. Finally, a degassing system with mono-dispersed water droplets will be studied in order to strengthen fundamental understanding of the degassing process.

2. Experimental Methods

2.1 Laboratory degassing system using poly-dispersed spray droplets

A laboratory water degassing system using poly-dispersed droplets is shown in Figure 4-1. The main part of this system is a 121.92 cm tall acrylic column with an inner diameter of 30.48 cm. A home-made metal sheet (316 SS) sealed the top of the tube using a flange connection, and its bottom was connected to the water atomizer (spray nozzle). A 90 degree full-cone fog-type nozzle (1/4PRSXJB120, John Brooks Co. Ltd.) was used in this study. It was

chosen because it could generate the finer droplets among the commonly used industrial nozzles. The droplets were expected to be in the range of 50 to 400 μm in diameter, according to the nozzle supplier. The effective degassing distance, defined as from the nozzle to the bottom of the column, was designed to be 101.6 cm. Another special unit with paralleled inclined plates was set near the bottom of the column with the aim of facilitating an extra degassing process in the form of thin water films. This unit also helped to straighten the sweep gas flow injected upward from the bottom of the column. Another special unit, a sponge pad, was placed on top of the nozzle in order to remove the moisture from the outlet gas.

Tap water was sampled to measure the initial concentration of the dissolved oxygen (DO) before entering into a water filtration system, which was used mainly to remove the solids. Filtered tap water was pumped into the system through a water pump, and the flow rate was controlled by a water flow meter (Cole-Parmer, RK series). Inert gases, tested herein included nitrogen and argon (industrial grade, 99.5% from Praxair), were used to sweep the column in a counter-direction of the falling water droplets and its outlet was located at the top. This sweep gas kept the surrounding environment of the droplet at a low oxygen partial pressure, making the degassing process possible. Degassed water droplets were gathered at the bottom, controlled by a T-valve, and then directed to a sampling container as needed for the final DO concentration measurements. All the measurements were conducted by a Hach DO meter (Model WU-53013-10, Cole-Parmer). Experiments were conducted with water flow rates varying from 63.1 to 220.8 ml/s, and nitrogen flow rates between 197 to 1182 ml/s. Each test was repeated 4 times. In addition, the gas outlet was located at the top

with a pressure gauge and a needle valve, so that the column could be operated either as an open or a sealed system. When it was operated as a sealed system, effects of the vacuum degrees (0.5 to 3.5 kPa) and the positive stagnant pressure (6.89 to 34.45) were studied. Finally, the experimental degassing efficiency was calculated as:

$$\eta = 1 - \frac{C_{out}}{C_{in}}.$$

(1)

For comparison purposes, the degassing efficiencies in this study were compared with that using a laboratory bubbling degassing system [16]. The main part of that system was an acrylic bubble column. The dimensions are a height of 45.72 cm, a length and a width of 40.64 cm. Using a porous bubble generator (Model 7610-1/2-06-2-AB, Mott), the nitrogen bubbles were compatible in size with the droplets in this study.

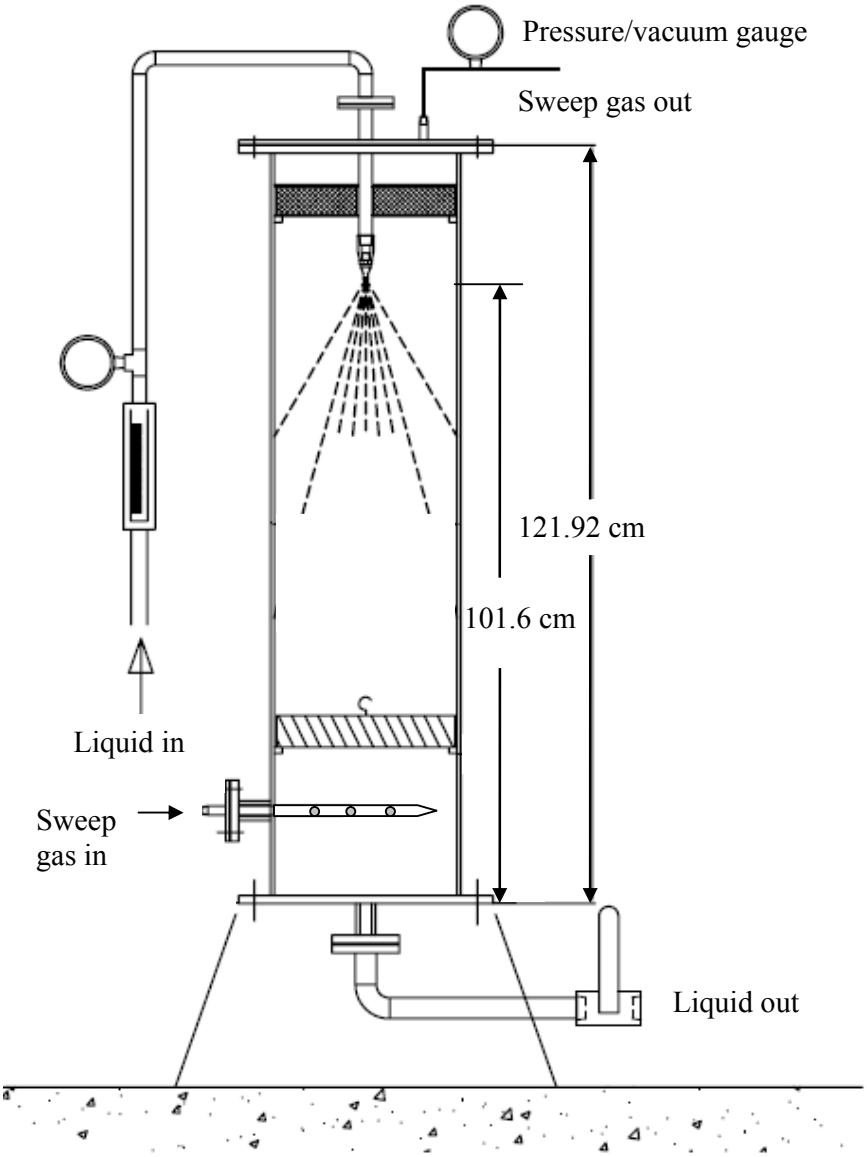

Figure 4-1 Laboratory water degassing system using poly dispersed droplets.

2.2 Laboratory degassing system using mono-dispersed droplets

A laboratory degassing system using mono-dispersed droplets is shown in Figure 4-2, setting up for more fundamental studies. The whole system was designed to be compatible with the system using poly-dispersed droplets. The main part of the experimental setup was a mono-size droplet generator (TSI, MGD100). Water was pumped (Teledyne, Model 500D, controlled by a d-series

flow rate controller) into a generator head, which contained a liquid reservoir and an orifice outlet at the bottom. A square wave was continuously sent to the generator head from a multiple frequency generator at the side. Water leaving the generator head was excited by the wave signal, broken up and continued as a uniform string of droplets.

The droplet size was a function of the liquid flow rate and the excitation frequency. By using orifices of two sizes, 50 and 100 μm, the sizes of the droplets generated in the tests were between 100 and 300 μm in diameter. These droplets fell through the center line of an acrylic column, which had an inner diameter of 1.9 cm, into the sampling chamber. Similar to the poly-dispersed droplet system, the nitrogen sweep gas (industrial grade, 99.5%, Praxair), controlled by a gas flow meter (Cole Parmer, RK-32460), was injected from the bottom of the column and traveled through a home-made gas straightener. The effective degassing distance herein was defined as the distance from the orifice to the bottom of the air straightener, 35 cm. The water flow rates tested in this study varied from 66 to 200 ml/hr while the corresponding nitrogen gas flow rates were from 100 to 500 ml/min. This system using mono-dispersed droplets could also be operated as a sealed system with a minor vacuum or positive pressure, monitored by a pressure gauge mounted at the top. A vacuum pressure of 6.89 kPa was tested.

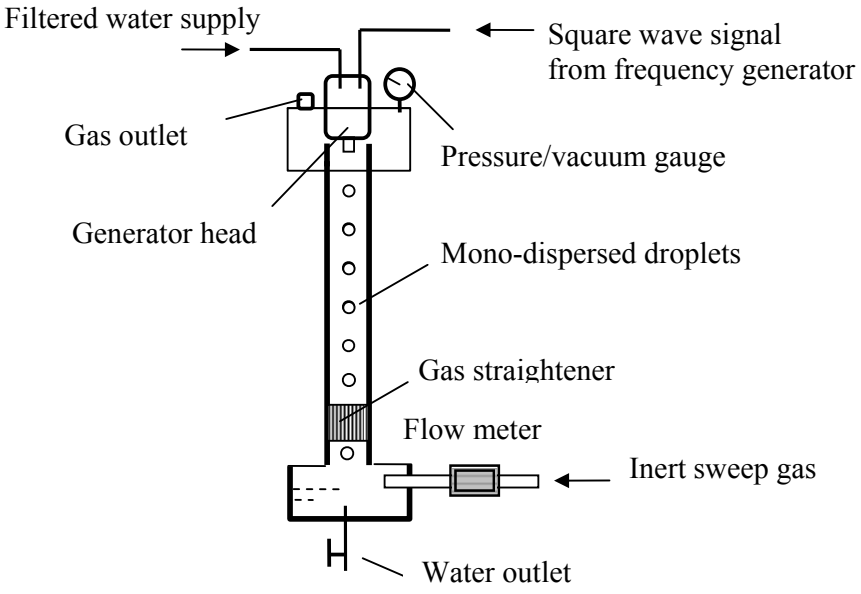

Figure 4-2 Laboratory water degassing system using poly dispersed droplets

DO measurements for this system required a small sample size and a shorter response time to prevent secondary degassing/re-aeration processes. They were realized in this study by using a modified Winkler titration method. Only 1 ml water sample was needed with the help of a Genesys 10 scanning UV/vis spectrometer (Thermo Fisher Scientific Inc.) to determine the end point of titration. Detailed information could be found elsewhere [17] with similar experimental methodology. DO concentration measurements for the same water samples were first conducted and compared with each other both using the titration method and the DO meter before the titration method could be considered accurate and suitable.

3. Results and discussion

3.1 Degassing efficiency with poly-dispersed droplets

3.1.1 Effect of water/inert gas flow rates

Figure 4-3 shows the degassing efficiency vs. the nitrogen sweep flow rates at different inlet water flow rates. When the nitrogen flow rate increased from about 0.2 l/s to 1.2 l/s, the degassing efficiency was improved from about 80% to 92%. This is in contrast with Wu et al.'s study for hydrogen removal from sprayed melt aluminum where they claimed that the sweep gas flow rate had no effect on the degassing efficiency [18]. In addition, with a higher degassing load (higher inlet water flow rate), the degassing efficiency decreased for the same nitrogen flow rate. Nonetheless, the curve for Q_w=63.1 ml/s is not consistent with this trend. It is very likely because at low water flow rates, the water pressures were not high enough to develop full fog-type droplets through the nozzle. Some of the water was injected into the spray column in the form of water streams, negatively affecting the overall degassing efficiency. For all those 4 water flow rates, 1 l/s was approximately the optimal nitrogen flow rate, where a higher sweep gas flow rate did not improve the degassing efficiency significantly. This limit, found to be around 92%, was affected by a number of thermodynamic factors such as the mass transfer coefficient, the temperature, the purity of the inert gas, and the design of the column (e.g. wall effect, effective degassing distance, residence time). Without altering the design, a better degassing performance could be achieved by operating multiple units in series. Considering the low capital cost required to construct and maintain each spray unit, it is still a cost effective solution.

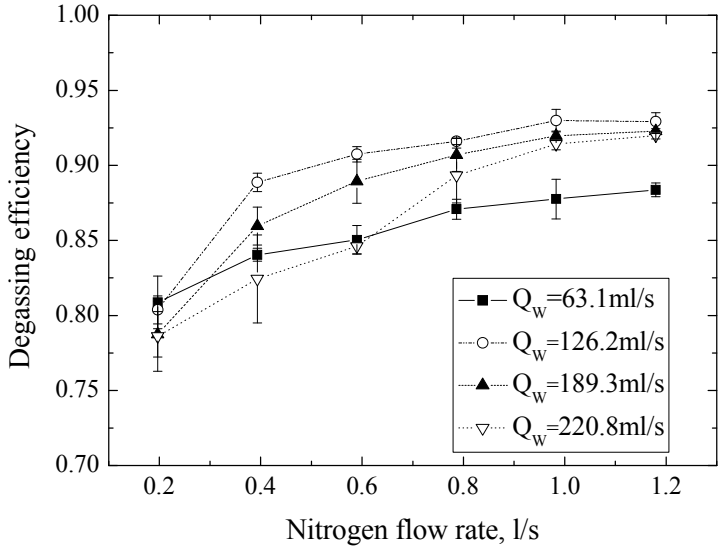

Figure 4-3 Effect of the water/inert gas flow rate.

3.1.2 Effect of vacuum/positive stagnant pressures

The gas pressure in the surrounding environment of the falling droplets was evaluated by their influence on the degassing efficiency. Figure 4-4 shows that positive nitrogen gas pressures in the surrounding environment decreased the water degassing efficiency by about 5%. However, the increase of this pressure did not show notable effect on the degassing efficiency. These observations were more obvious when argon gas was used as the sweep gas both at positive and vacuum pressures. A possible interpretation is that a positive pressure placed more mass transfer resistance at the interface, while the vacuum pressure had influence on the droplet size. Therefore, the degassing system is more favorable when it is open to the atmosphere.

Another interesting observation is that the degassing performance is better with nitrogen as the sweep gas, compared to argon. The authors believed that

more systematic studies are needed before the conclusion that different inert gases affect the degassing efficiency could be made. If this conclusion is supported, the definition of an "inert" gas needs to be re-evaluated. Molecular weight might come into play in this situation. With a great molecular weight, argon places a higher mass transfer resistance at the molecular level in the continuous phase. This factor should also be taken into consideration in the analytical mass transfer models. Since a better performance was achieved with use of nitrogen in this study, it was used for the rest experiments.

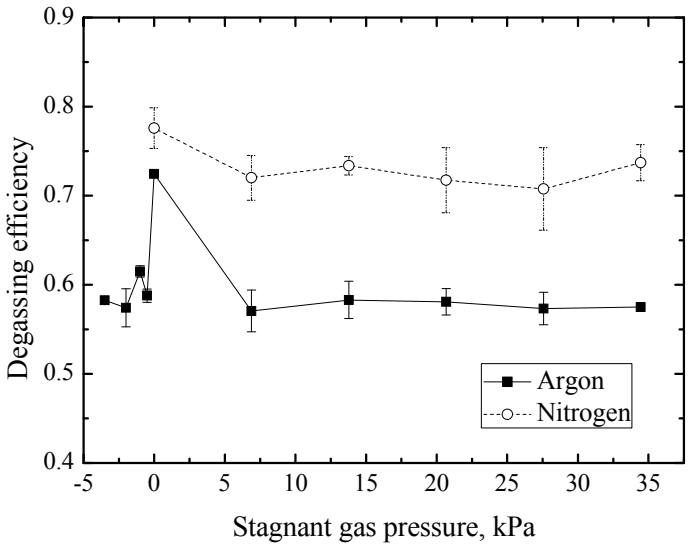

Figure 4-4. Effects of the inert gas pressure in the surrounding environment.

3.1.3 Effect of the inclined plates

Experiments also conducted toward verifying the influence of the inclined plates at the bottom. At two water flow rates, 126.2 and 220.8 ml/s, as shown in Figure 4-5, the existence of the inclined plates did increase the degassing efficiencies. The differences were around 2% to 3% for the smaller flow rate,

while its effect became less significant for larger flow rates. This improvement, although seemingly small, could make big impact lowering the capital cost when it is used in the up scaled industrial processes. The reasons why it improved the degassing efficiency are because it facilitated an extra film degassing process, increased the residence time, and straightened up the sweep gas flow for better interfacial droplet-sweep gas contacts.

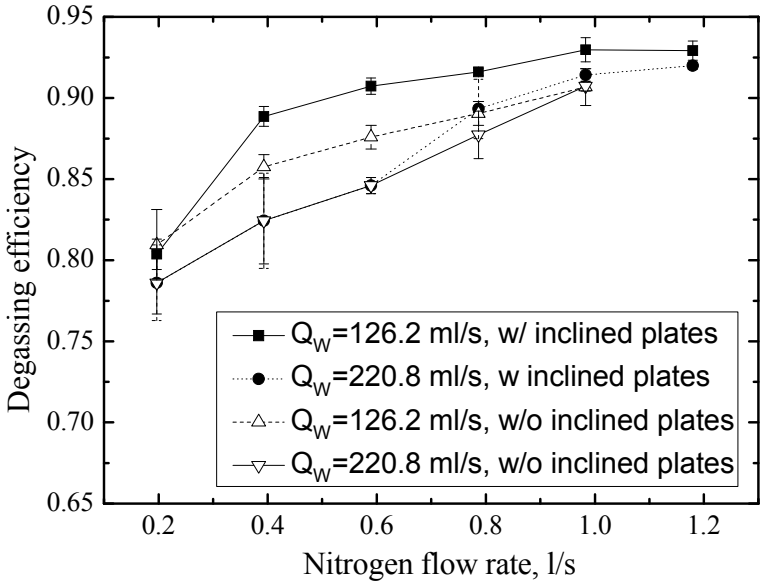

Figure 4-5 Effect of the inclined plates.

3.2 Degassing efficiency with mono-dispersed droplets

In the tests using mono-dispersed droplets, it was found that the degassing efficiency increased with the increase of the inlet nitrogen flow rates (0-5 LPM) for droplets of 265 μm in diameter (Figure 4-6). This is in accordance with the observations in the tests using poly-dispersed droplets. Again, this is resulted from the fact that the higher gas flow rate both increased the residence time and the extent of turbulent flow at the interface. It is also worth

mentioning that all the observations in this study were based on a medium Reynolds number range, which was calculated to be 10-100 for the falling droplets.

In addition, the degassing efficiency using mono-dispersed droplets were no better than 65%, obviously lower than that with poly-dispersed droplets, even with much higher gas to liquid flow ratios. This is most likely attributed to the lower residence time. Possible interactions between concentrated droplets and the enhanced turbulent flow could also contribute to the improvement.

The effect of the stagnant inert gas pressure was also tested in this system with mono-dispersed water droplets. Compared to a system open to the atmosphere, a positive stagnant nitrogen pressure of 6.89 kPa was found to decrease the degassing efficiency from 58.7% to 55.4%. This observation is also consistent with the previous finding in Figure 4-4.

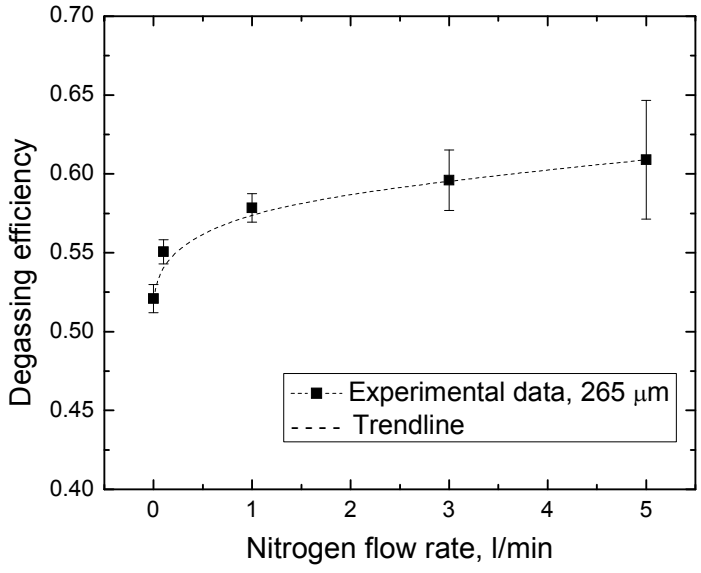

Figure 4-6. The effect of the nitrogen flow rate on a degassing system using mono-dispersed droplets.

4. Summary

A new laboratory water degassing system using poly-dispersed droplets falling in inert gas has been designed and evaluated in this study. With a low construction and operation cost, this system could achieve a degassing efficiency of 92% with a low sweep gas to water flow ratio. Higher degassing requirements could still be met in a cost-effective manner by operating multiple units in series. This system was also compared with performance of a laboratory bubbling degassing system and showed superiority. For the same inlet water flow rate and similar droplet/bubble size, the former system had an approximate 10% higher degassing efficiency at higher nitrogen flow rates while the difference became larger at lower sweep gas flow rates.

More systematic studies have been conducted, examining the effects of a few operation parameters. It was found that for inlet water flow rates up to 220.8 ml/s, the optimal inert gas flow rate was found to be around 1 l/s. Increased positive or vacuum stagnant inert gas pressure did not show obvious effects changing the degassing efficiency, but both of them were less favoured compared to an atmospheric pressure. Nitrogen gas exhibited better performances as a sweep gas than argon gas. However, this observation needs further studies to verify.

In addition, a water degassing system using mono-dispersed droplets was also studied. Preliminary experimental results such as the effects of the sweep gas flow rate and stagnant nitrogen pressure were in accordance with the

results from the system using poly-dispersed droplets. Further studies will include: a) modelling both degassing processes using poly-dispersed and mono-dispersed droplets, and b) means to improve the mass transfer rate (degassing efficiency) such as different nozzle types, surfactant addition, temperature or turbulence elevations, etc.

References

[1] D. B. Wilson, H. Y. Tsao, Journal of the Water Pollution Control Federation 46 (1974) 2209-2214.

[2] K. Li, I. Chua, W. J. Ng, W. K. Teo, Chemical Engineering Science 50 (1995) 3547-3556.

[3] T. Leiknes, M. J. Semmens, Separation and Purification Technology 22-23 (2001) 287-294.

[4] A. Sengupta, P. A. Peterson, B. D. Miller, J. Schneider, C. W. Fulk Jr., Separation and Purification Technology 14 (1998) 189-200.

[5] Z. G. Peng, S. H. Lee, T. Zhou, J. J. Shieh, T. S. Chung, Desalination 234 (2008) 316-322.

[6] V. I. Lebedeva, V. M. Gryaznov, I. V. Petrova, V. V. Volkov, G. F. Tereshchenko, E. I. Shkol'nikov, L. M. Plyasova, D. I. Kochubey, R. Van Der Vaart, E. L. J. Van Soest-Verecammen, Kinetics and Catalysis 47 (2006) 867-872.

[7] O. V. Abramov, Ultrasound in liquid and solid metals. CRC, London, 1994.

[8] H. Xu, T. T. Meek, Q. Han, Materials Letters 61 (2007) 1246-1250.

[9] A. Singer, S. Parnes, A. Gross, A. Sagi, A. Brenner, Aquacultural Engineering 39 (2008) 72-77.

[10] V. S. Warke, S. Shankar, M. M.Makhlouf, Journal of Materials Processing Technology 168 (2005) 119-126.

[11] R. Wu, D. Shu, B. Sun, J. Wang, F. Li, H. Chen, Y. Lu, Materials Science and Engineering A 408 (2005) 19-25.

[12] A. Turpin, A. Couvert, A. Laplanche, A. Paillier, Chemical Engineering and Processing: Process Intensification 47 (2008) 886-892.

[13] B. Dou, W. Pan, Q. Jin, W. Wang, Y. Li, Energy Conversion and Management 50 (2009) 2547-2553.

[14] B. Rajmohan, S. N. Reddy, B. C. Meikap, Industrial and Engineering Chemistry Research 47 (2008) 7833-7840.

[15] S. K. Mitra, A. U. Hannemann, Journal of Atmospheric Chemistry 16 (1993) 201-218.

[16] Y. Ji, H. Lei, Z. Tan, Separation and Purification Technology. (Submitted for publication)

[17] L. S. Peck, Journal of Experimental Marine Biology and Ecology 141 (1990) 53-62.

[18] R. Wu, B. Sun, D. Shu, Materials Science and Engineering A 456 (2007) 386-390.

CHAPTER 5 : LIQUID DEGASSING USING A COMBINATION OF MICRO-BUBBLES AND MECHANICAL AGITATION

1. Introduction

Liquid degassing is the key step in a number of industrial processes. For example, organic gases usually need to be removed from gasoline and crude oil, hydrogen gas is unwanted in molten aluminum alloys, and de-oxygen should be performed in beverages to prevent the negative effects on shelf life and taste. Moreover, toxic or corrosive gases such as ammonia, hydrogen sulfide, sulfur dioxide, and carbon dioxide are commonly found in industrial water systems— the water produced with crude oil and natural gas, the water used in power plant stack gas scrubbing processes, and the water processed in municipal wastewater treatment operations, etc. These gases, if not properly controlled before the water is released, can cause serious environmental and health issues.

Bubble column reactors have been widely adopted in chemical, pharmaceutical, and petroleum processing industries. Their large gas-liquid interfacial area to volume ratios leads to increased mass transfer rates, which can be taken advantage of in degassing processes. Compared to other existing techniques, such as mechanical agitation degassing, spray degassing, membrane contactor degassing [1-5] and ultrasonic degassing [6, 7], bubble column reactors are less costly to construct and easier to operate. In addition, despite the fact that the performances of existing degassing techniques distinctly vary from one to another, they are mainly designed to be batch reactors, therefore often call for a longer residence time. Bubble column

degassing units, on the other hand, can be designed as both continuous reactors and batch reactors. Combined with mechanical agitation (stirring), it is expected to match the most advanced degassing techniques in a cost effective manner.

Extensive research has been focused on the gas-liquid mass transfer between bubbles and the liquid in a bubble column. Volumetric mass transfer coefficient is the most widely used parameter to quantify this process. Akita and Yoshida [8, 9] studied oxygen bubble adsorption into several different organic and inorganic liquids using bubble columns of three different sizes. Empirical correlations were derived for the gas holdup, bubble size, and volumetric mass transfer coefficient with expressions of a number of dimensionless parameters. Hikita et al. [10] conducted a series of similar experiments. They qualified the effects of the physical properties of the gas and liquid and proposed another empirical correlation to fit their data. It was further pointed out that increased ionic strength would enhance the mass transfer rate. Vandu and Krishna [11] noted that the ratio of mass transfer coefficient over gas holdup is independent of the column diameter at high superficial velocities. This shed light on scale-up designs of industrial bubble columns. Lately, Jin et al. [12] derived their own empirical correlation for volumetric mass transfer coefficient, while they also qualitatively stated that the coefficient increases with increased temperatures and elevated pressures.

More recently, with the help of Computational Fluid Dynamics (CFD) and other numerical applications, more detailed studies have been made possible. Bubble breakup and coalescence were taken into consideration in predictions of the volumetric mass transfer coefficient [13, 14]. Nevertheless, the

simulation results did not show obvious superiorities over the existing analytical and empirical models. Another CFD model was developed by Krishna and van Baten [15] and the main assumption in their studies was that they categorized flows in bubble column into homogeneous and heterogeneous regimes. “Large” and “small” bubbles behaved differently in the heterogeneous regime. Dhaouadi et al. [16] derived an analytical model for the mass transfer in the bubble column, taking into account the effects of the probe time constant, and pressure on gas solubility. Their study demonstrated that all analytical, numerical, and selected correlations had good predictions of corresponding experimental data.

However, almost all the aforementioned theoretical and experimental studies were based on gas transfer from bubbles to the liquid; bubble columns have rarely been used in a liquid degassing process. The most similar process is rotary degassing with purging bubbles for the hydrogen gas removal from molten metals [17, 18].

There are also other reasons why more work needs to be done studying the mass transfer process in a bubble column. First of all, aside from the mass transfer coefficient, estimation of essential bubble dynamic parameters such as the gas holdup and bubble size has not been well addressed. These two are among the most important parameters that decide the mass transfer rate. In literature, there are generally two ways to estimate the bubble size and gas holdup besides imaging methods. The first is to use empirical correlations, of which there are many studies [8, 9, 19-22]. This method is often considered lacking in generality. An alternative starts with generally describing bubble and liquid movements in a bubble column using the Stokes law, which is to be

introduced in the next section. Nevertheless, these equations are only applicable to the Stokes region, and reliable photographic measurements and iterative calculations are required to verify the estimated data.

Another problem in using the method of mass transfer coefficient is that it tends to avoid the complexities of the physical process. A mass transfer coefficient is independent of the details of the convective-diffusive mechanism. Without addressing the physical mechanism, all the correlations naturally lack generality. The simplest yet most valid theory of interfacial mass transfer is the two-film theory, which is illustrated in Figure 5-1 for a single bubble in the liquid. It was first proposed by Nernst [23] and further developed by Lewis and Whitman [24]. Only diffusion is considered within the hypothetical stagnant gas and liquid films, while outside the bubble, oxygen transfer is dominated by convections. Since gas diffusion rate in the gas phase is generally several orders higher than that in the liquid phase, the main mass transfer resistance lies in the liquid phase. Therefore, usually only the thickness of the liquid film is of practical importance and is estimated herein.

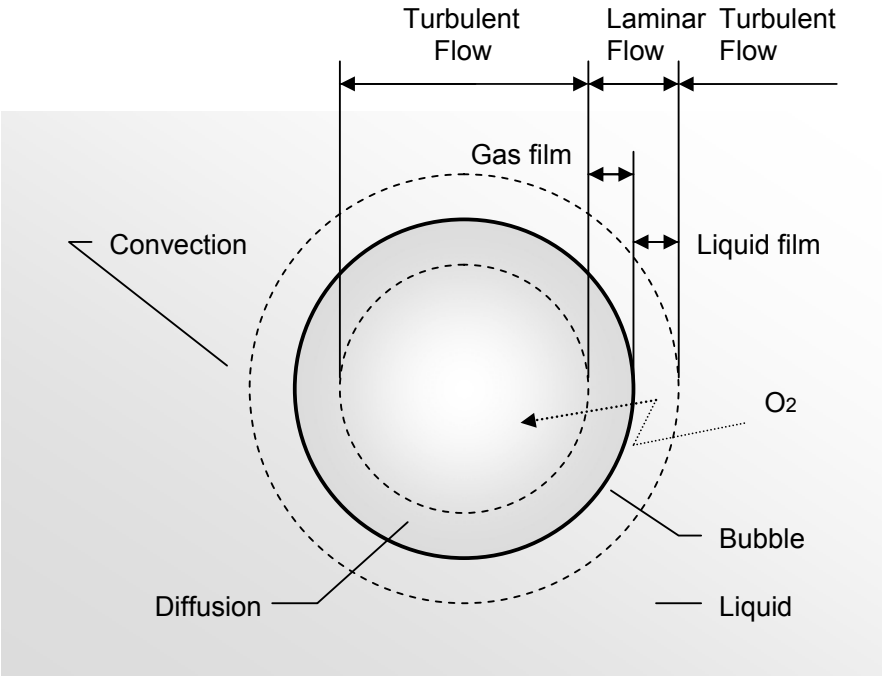

Figure 5-1 Film theory for mass transfer from a single bubble in the liquid.

The thickness of the hypothetical liquid film δ is expressed by:

$$\delta = \frac{D_g}{k} \tag{1}$$

where D_g is the gas diffusion coefficient in the liquid and k is the commonly used mass transfer coefficient.

Finally, the mass transfer coefficient is a unique parameter. Particularly, it is dependent on the dimensions of the system, and thus cannot be generalized [11, 12, 15]. One always needs to find a way to determine its unique mass transfer coefficient when it comes to a new or scaled up system.

To address these problems mentioned above, there are mainly three objectives in this study. The first is to apply proper knowledge of fluid mechanics and bubble dynamics to estimate parameters such as mean bubble size in a swarm and gas holdup in a bubble column degassing unit without

introducing redundant empirical correlations and using complicated photographic means. The second is to step further beyond mass transfer coefficient to see whether and how the two-film theory works for the new degassing system. Last but not least is to evaluate the degassing efficiency of a batch and a continuous reactor using the same degassing bubble tank combined with mechanical agitation. A batch reactor holds advantages in terms of estimating the mass transfer coefficient, evaluating the two-film theory, and verifying predictions of bubble size and gas holdup since less degrees of freedom are required. A continuous reactor, on the other hand, is the one aimed to be designed for the industrial degassing processes.

2. Theory

2.1 Bubble size and gas holdup

Hughmark [19] was among the first to develop and apply correlations to predict gas holdup and mass transfer rate in a bubble column. Whether or not the correlation for mass transfer from a single bubble is applicable to a swarm of bubbles is still a topic of discussion. Later, Akita and Yoshida [8, 9] proposed their correlations while studying the mass transfer from bubbles to liquids. Their proposed correlations (eq. 2 and 3) have been widely adopted:

$$\frac{d_b}{D} = 26\left(N_{Bo}\right)^{-0.5}\left(N_{Ga}\right)^{-0.12}\left(N_{Fr}\right)^{-0.12} \tag{2}$$

$$\frac{\varepsilon_g}{\left(1-\varepsilon_g\right)^4} = 0.2\left(N_{Bo}\right)^{-1/8}\left(N_{Ga}\right)^{1/12}\left(N_{Fr}\right) \tag{3}$$

where d_b and D are the volume-surface mean bubble diameter and bubble column cross-sectional diameter, respectively. (Bond

number $N_{Bo} = gD^2\rho_L/\gamma_L$, Galilei number $N_{Ga} = gD^3/\nu_L^2$, and Froude number $N_{Fr} = U_G/(gD)^{1/2}$)

However, unlike what Akita and Yoshida [9] stated, the velocity of bubble in a swarm can be estimated. Masliyah [25] developed an equation for relative particle velocities in a multi-species hindered settling system and it was later shown by Yianatos et al. [26] that this equation could be used for a swarm of rising bubbles:

$$V_{bs} = \frac{g d_b^{\,2}\left(1-\varepsilon_g\right)^{n-1}\rho_L}{18\mu_L\left(1+0.15\,\mathrm{Re}_b^{\,0.687}\right)} \tag{4}$$

where V_{bs} is the bubble slip velocity, n is a Reynolds number dependent number, and Re_b is the bubble Reynolds number:

$$\mathrm{Re}_b = \frac{\rho_L d_b V_{bs}\left(1-\varepsilon_g\right)}{\mu_L} \tag{5}$$

This method is generally preferred to the previous because it is less empirical and such finds more potential applications in bubble-fluid systems. Moreover, bubble-bubble interactions, analogous to hindered particles settling, should not be ignored because when the bubbles enter each other's wakes (drafting behind one another), it inevitably leads to bubble contact and even coalescences or breakups.

Following up on equation (4), for a degassing tank, the general slip velocity is written as:

$$V_{bs} = V_t(1-\varepsilon_g)^{n-1} \tag{6}$$

where n is a function of the terminal Reynolds number Re_t. Recommended values of n by Richardson and Zaki [27], taking the wall effect (column cross-sectional diameter D) into account, are summarized in Table 5-1.

Table 5-1 Parameter *n* as a function of the terminal Reynolds number.

Re_t	n
<0.2	$4.65+19.5d_b/D$
(0.2, 1)	$(4.35+17.5d_b/D)Re_t^{-0.03}$
(1, 200)	$(4.45+18d_b/D)Re_t^{-0.1}$
(200, 500)	$4.45Re_t^{-0.1}$
>500	2.39

$$\mathrm{Re}_t = \frac{\rho_L d_b V_t}{\mu_L} \tag{7}$$

To avoid iterative calculations, the easiest way to calculate the bubble terminal velocity is to use Galileo number method. Galileo number is expressed by:

$$Ga = \frac{g d_b^{\,3} \rho_L^{\,2}}{\mu_L^{\,2}} \tag{8}$$

while on the other hand it is related to the bubble Reynolds number at the terminal velocity by [28]:

$$\mathrm{Re}_t = (2.33Ga^{0.018} - 1.53Ga^{-0.016})^{13.3} \tag{9}$$

Furthermore, the slip velocity is also related to the gas and liquid superficial velocities, also known as the mean volumetric fluxes, by [26]:

$$V_{bs} = \frac{U_G}{\varepsilon_g} - \frac{U_L}{1-\varepsilon_g} \tag{10}$$

where the minus sign means the bubbles and the liquid travel in the same direction, and the gas and liquid superficial velocities are calculated as:

$$U_G = \frac{Q_G}{A} \tag{11}$$

$$U_L = \frac{Q_L}{A} \tag{12}$$

where Q_G and Q_L are the gas and liquid flow rates, respectively, and A is the cross-sectional area of the bubble degassing tank.

For a 1-D motion, conservation of mass and momentum in a slice of control volume along the flow direction are simplified as:

fluid: $$0 = -\frac{dP}{dz} - \rho_L g + f_{fb} \tag{13}$$

bubbles: $$0 = -\frac{dP}{dz} - \rho_b g + f_{bf} \tag{14}$$

so that

$$f_{fb} - f_{bf} = (\rho_L - \rho_b)g = \rho_L g \tag{15}$$

where f_{fs} and f_{sf} are the interfacial drag forces per unit volume of fluid and bubble, respectively. From their definitions, these two terms also have a relationship in equation (16) as:

$$\varepsilon_g f_{fb} + (1-\varepsilon_g) f_{bf} = 0 \tag{16}$$

In addition, Rowe et al. [29] derived a multi-particle relationship to evaluate the interfacial drag:

$$f_{bf} = \frac{3C_D \rho_L \left(V_f - V_b\right)^2}{4d_b (1-\varepsilon_g)^{1.7}} \tag{17}$$

where C_D is the drag coefficient of a single bubble in the liquid calculated as [30]:

$$C_D = \frac{24}{\mathrm{Re}}(1 + 0.15\,\mathrm{Re}^{0.687}) \tag{18}$$

and the bubble Reynolds number is expressed by:

$$\mathrm{Re} = \frac{\rho_L d_b V_{bs}}{\mu_L} \tag{19}$$

Given the equations above, the bubble size and gas holdup can be solved if the gas and liquid flow rates are known for a given bubble column degassing system.

2.2 Degassing in a batch reactor

Governed by the Fick's law of mass transfer, the flux of the solute, *j*, transferred from the liquid into the dispersed phase (inert gas bubbles) is expressed by:

$$j = k\left(c_l - c_b\right) \tag{20}$$

where k is the mass transfer coefficient, c_l and c_b are the dissolved gas concentrations in the liquid and within the bubble, respectively. Furthermore, the general mass balance of the degassing process is written as:

$$-V\frac{dc_l}{dt} = A_b j = A_b k(c_l - c_b) \tag{21}$$

where V is the volume of the liquid, and A_b is the total interfacial area between bubbles and the liquid.

Thermodynamically, the gas concentration within the bubble could be calculated using Henry's law:

$$c_b = P_{O_2} \cdot K_H \tag{22}$$

where Po_2 is the partial pressure of dissolved gas in the purging gas phase, and K_H is the Henry's law constant. This concentration increases as more and more dissolved gas is transferred into bubbles. If the concentrations are in the unit of ppmw, equation (22) can be further re-written as:

$$c_b = (P_0 + 4\gamma_L / r) \cdot \left[\left(c_i - c_l\right) \cdot \frac{\rho_l\left(1-\varepsilon_g\right)}{\rho_g \varepsilon_g} \right] \cdot K_H \tag{23}$$

where P_0 is the atmospheric pressure, γ_L is the surface tension of the liquid, r is the radius of the bubble, c_i is the initial dissolved gas concentration in the liquid, ε_g is the gas hold in the degassing unit, and ρ_l and ρ_g are the densities of the liquid and gas, respectively. Gas hold up ε_g refers to the total bubble volume over the sum of the bubble and the liquid volumes.

Considering the fact that the inert gas used is often not 100% pure in practice, equation (23) is revised by adding an initial concentration (in percentage) of the target gas *s%* in the inert gas bubble:

$$c_b = (P_0 + 4\gamma / r) \cdot \left[s + (c_i - c_l) \cdot \frac{\rho_l (1 - \varepsilon_g)}{\rho_g \varepsilon_g} \right] \cdot K_H \tag{24}$$

Substituting equation (24) into (21) and integrating equation (21) gives:

$$\frac{\left[1 + \frac{\rho_l}{\rho_g} \frac{1 - \varepsilon_g}{\varepsilon_g} \cdot K_H \cdot \left(P_0 + \frac{4\gamma}{r} \right) \right] \cdot (c_f - c_i) + \left[c_i - K_H \cdot s \cdot \left(P_0 + \frac{4\gamma}{r} \right) \right]}{\left[c_i - K_H \cdot s \cdot \left(P_0 + \frac{4\gamma}{r} \right) \right]} = \exp\left(- \frac{kA_b t}{V} \right)$$

(25)

where c_i and c_f are the dissolved gas concentrations at time 0 and t, respectively. Then the degassing efficiency can be expressed by:

$$\eta = 1 - \frac{c_f}{c_i} = \left[1 - \exp\left(- \frac{kA_b t}{V} \right) \right] \cdot \frac{\left[1 - \frac{K_H \cdot s \cdot \left(P_0 + \frac{4\gamma}{r} \right)}{c_i} \right]}{\left[1 + \frac{\rho_l}{\rho_g} \frac{1 - \varepsilon_g}{\varepsilon_g} \cdot K_H \cdot \left(P_0 + \frac{4\gamma}{r} \right) \right]} \tag{26}$$

Since A_b can be written in terms of the gas holdup, ε_g, as:

$$A_b = \frac{6V\varepsilon_g}{d_b} \tag{27}$$

Thus, equation (26) is re-written as:

$$\eta = \left[1 - \exp\left(-\frac{6k\varepsilon_g t}{d_b}\right)\right] \cdot \frac{\left[1 - \frac{K_H \cdot s \cdot \left(P_0 + \frac{4\gamma}{r}\right)}{c_i}\right]}{\left[1 + \frac{\rho_l}{\rho_g}\frac{1-\varepsilon_g}{\varepsilon_g} \cdot K_H \cdot \left(P_0 + \frac{4\gamma}{r}\right)\right]} \tag{28}$$

Similar to the analysis for the poly-dispersed droplet degassing system, this way of modeling for the bubble degassing does not taken the detailed size distribution into consideration either. This distribution is dependent on a number of factors such as the type of the bubble generator and the location of the bubbles and the gas to liquid flow ratio. Equation (28) infers that the degassing efficiency increases with the increase of the gas holdup and residence time and the decrease of the bubble size. It is also shown that theoretically the degassing efficiency could not reach 100% because of the second term in the right hand side, and the upper limit of the efficiency is even lower if s is not equal to 0. However, this usually is the case.

The unstirred film thickness is conceivably affected by the stirring rate and the inert gas injection rate. With proper experiments on a batch reactor, their influence could be quantified and those results were finally aimed to use for the continuous reactor evaluations.

2.3 Degassing in a continuous reactor

Consider the liquid with inert gas bubbles flows through a slice of control volume at a flow rate of Q_L as shown in Figure 5-2. The equation of continuity is expressed by:

$$Q_L c_z - M = Q_L c_{z+\Delta z} \tag{29}$$

where c_z and $c_{z+\Delta z}$ are dissolved gas concentrations at the inlet and outlet cross-sections, respectively. *M* is the total flux of oxygen transferred from the liquid into bubbles. If the two-film theory holds, *M* can be expressed as:

$$M = \frac{D_g}{\delta}\frac{6A\Delta Z\varepsilon_g}{d_b}\left(c_l - c_b\right) \tag{30}$$

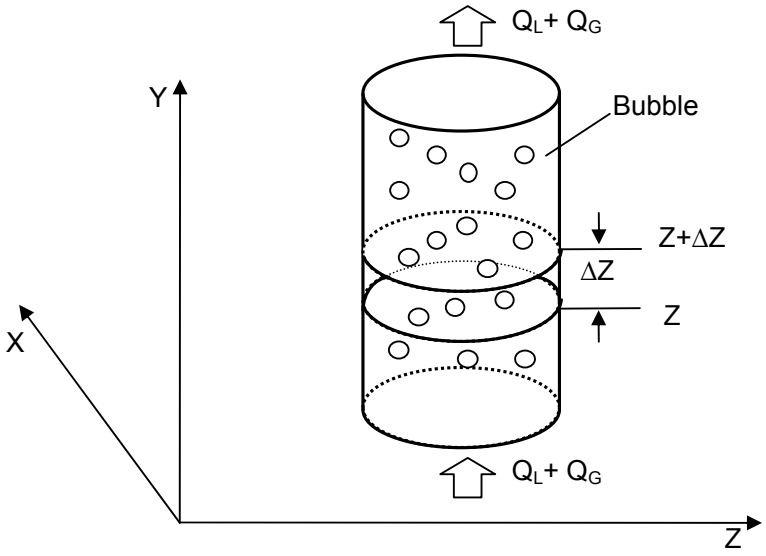

Figure 5-2 A slice of control volume with inert bubbles flows.

In addition, incorporating the function of δ with respect of the agitation rate and the inject gas flow rate derived from the aforementioned batch reactor experiments, equation (30) is re-written as:

$$\frac{dc_w}{dz} = -\frac{D_g}{\delta}\frac{6A\varepsilon_g(c_l - c_b)}{Q_L d_b}$$

(31)

Similar to the analysis for the batch reactor, considering the thermodynamic limitations and integrating equation (31) gives that:

$$\frac{\left[1+\frac{\rho_l}{\rho_g}\frac{1-\varepsilon_g}{\varepsilon_g}\cdot K_H\cdot\left(P_0+\frac{4\gamma}{r}\right)\right]\cdot(c_f-c_i)+\left[c_i-K_H\cdot s\cdot\left(P_0+\frac{4\gamma}{r}\right)\right]}{\left[c_i-K_H\cdot s\cdot\left(P_0+\frac{4\gamma}{r}\right)\right]} = \exp\left(-\frac{D_g}{\delta}\frac{6A\varepsilon_g Z}{Q_L d_b}\right)$$

(32)

Subsequently, the theoretical efficiency is expressed by:

$$\eta=\left[1-\exp\left(-\frac{D_g}{\delta}\frac{6A\varepsilon_g Z}{Q_L d_b}\right)\right]\cdot\frac{\left[1-\frac{K_H\cdot s\cdot\left(P_0+\frac{4\gamma}{r}\right)}{c_i}\right]}{\left[1+\frac{\rho_l}{\rho_g}\frac{1-\varepsilon_g}{\varepsilon_g}\cdot K_H\cdot\left(P_0+\frac{4\gamma}{r}\right)\right]} \qquad (33)$$

Both equations (28) and (33) indicate existence of a thermodynamic limit for the degassing efficiency. This is consistent with our observations as to be introduced shortly.

3. Experimental

In these experiments, nitrogen gas bubbles were used to remove dissolved oxygen from water to illustrate and verify the aforementioned analysis. The schematic diagram of the experimental setup with a photographic system is shown in Figure 5-3. As shown at the bottom, filtered laboratory tap water was introduced into the system through a water pump. This pump was only operated when the tap water pressure was not high enough to attain the desired flow rate. Nitrogen (industrial grade, >99% from Praxair) bubbles were generated using a porous bubble generator (Model 7610-1/2-06-2-AB, Mott). Water and nitrogen gas flow rates were regulated by a liquid (Cole-Parmer) and gas flowmeters (Cole-Parmer). In the batch reactor tests, the nitrogen gas

flow rates were 25, 50, and 75 SCFH (standard cubic foot per hour) with the agitation speed varying from 380 to 999 rpm (resolution per minute). In the continuous reactor experiments, water flow rate was set constant at 2GPM (gallon per minute), nitrogen injection rate at 50 SCFH, whereas the agitation rate ranged from 200 to 616 rpm.

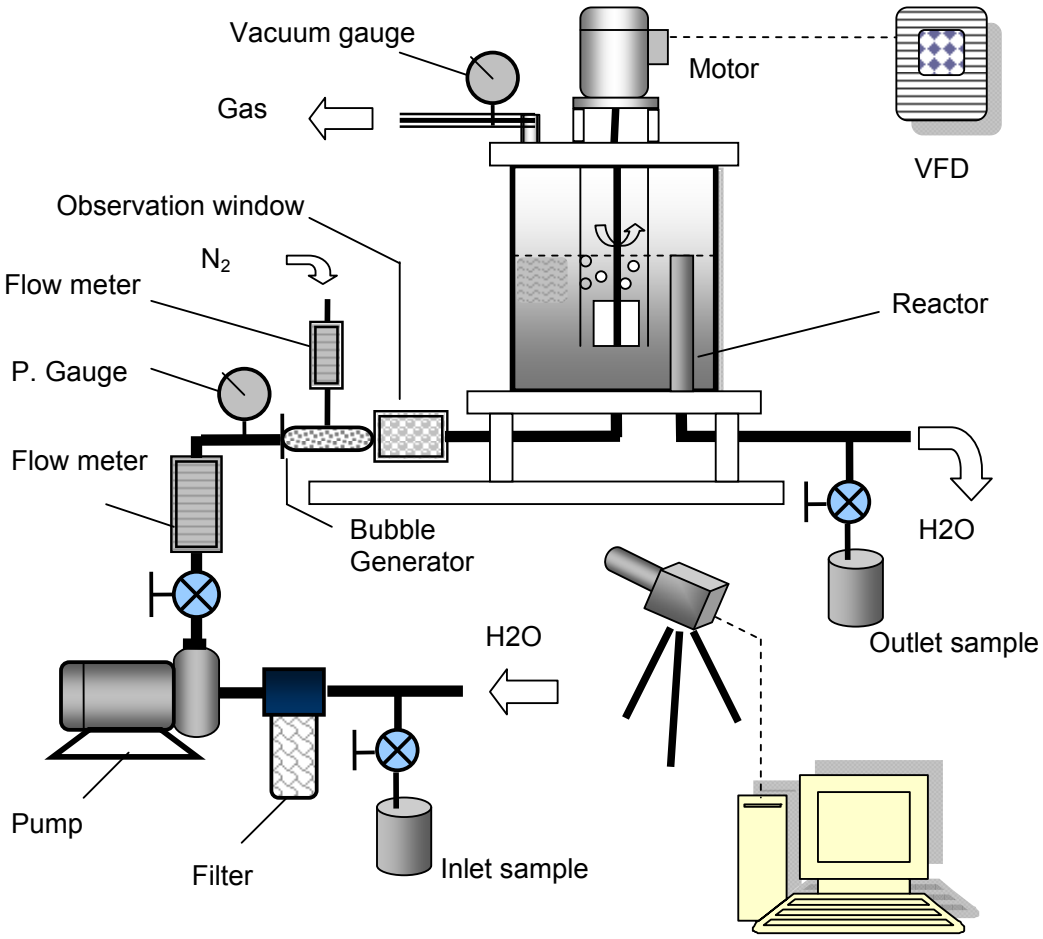

Figure 5-3 Experimental setup of the bubble degassing unit with mechanical agitation.

For practical considerations in picturing the bubble movements and monitoring the bubble size, breakup and coalescence, a transparent chamber was added at back of the generator. Its length was 15.24 cm and width was 5.08 cm. Degassing is expected to have happened when the bubbles and water

are travelling through this chamber. It, however, can be ignored because of the high flow velocity and low residence time.

Downstream the observation chamber, water with bubbles enters, through a 2.54 cm tubing, into the main part of the degassing unit—an acrylic bubble tank. The dimensions of the tank are a height of 45.72 cm, a length and a width of 40.64 cm. It was designed to be bigger in cross-sectional diameter than common bubble columns to minimize wall effects. As Akita and Yoshida [9] mentioned, a square bubble column has the same performance as a round one with a diameter the same as the distance from the centre to the wall in a square column. With a water outlet at the height of 30.48 cm, 15.24 cm was left as headspace. A secondary degassing/aeration process happens at the top interface of the water and headspace, inevitably, no matter the headspace is filled air or nitrogen. However, the rate is negligible compared to that at the bubble-water interface. In the tank, a home-made 4-straight-bladed Rushton impeller delimits the stirring area, which has a height and a diameter both of 10.16 cm. The impeller was driven by a DC motor provided with a Variable Frequency Driver (VFD) speed control unit.

Bubbles burst at the water surface, where both the nitrogen and oxygen gases were released into the headspace, subsequently vacuumed out of the system through the gas outlet. Meanwhile, the degassed water continuously flowed out from the outlet in the tank. Water was sampled at the inlet and outlet and analyzed by a Hach DO meter (Model WU-53013-10 from Cole-Parmer). Each DO measurement was repeated three times in parallel, and the experimental degassing efficiency was calculated as:

$$\eta_E = 1 - \frac{C_{outlet}}{C_{inlet}} \tag{34}$$

Finally, for comparisons purpose, the degassing performance of the same tank solely with mechanical agitations was also studied with a water flow of 2 GPM.

4. Results and Discussion

4.1 Bubble size and gas holdup

Without a water flow, this degassing systems acts like a batch reactor. Experiments were conducted toward this category under three different operation conditions—the nitrogen injection rates were of 25, 50, and 75 SCFH while the agitation rate changed from 380 rpm to 999 rpm. Residence time, defined as from the time when the nitrogen bubbles are first in contact with the water to the time of outlet water sampling, was tested until the degassing efficiency no longer increased. Some working conditions and other known experimental parameters were summarized in Table 5-2.

Table 5-2 Working conditions and other known experimental parameters.

Room temperature T, (K)	288
Oxygen diffusion coefficient in water D_g, $(m^2\ s^{-1}) \times 10^9$	2.3 [31]
Water density ρ_L, $(kg/m^3) \times 10^{-3}$	1
Oxygen density ρ_o, (kg/m^3)	1.3 [32]
Water surface tension γ, (mN/m)	73
Water kinematic viscosity v_L, (Pa s) $\times 10^6$	1
Water dynamic viscosity μ_L, (Pa s) $\times 10^3$	1

Following the aforementioned theoretical analysis, bubble dynamics parameters d_b, ε_g, U_G, and V_{bs} were solved and summarized in Table 5-3. It is

worth mentioning herein that the predicted bubble size and also the size of interest is for the bubbles rising in the degassing tank; bubbles leaving the orifice are different in size from those rising in the column [9]. Besides, volume to surface mean diameter was used here because mass transfer is essentially affected by the volume to surface ratio of the bubble.

Table 5-3 Bubble dynamics parameters calculated for a batch reactor (Q_L=0).

Nitrogen injection rate, (SCFH)	Agitation rate, (rpm)	d_b, (m)$\times 10^3$	ε_g, (%)	U_G, (m/s)$\times 10^3$	U_{bs}, (m/s)$\times 10^3$
25	380	1.34	94.8	1.19	1.25
50	618	3.01	96.8	2.38	2.42
75	999	5.26	96.7	3.54	3.75

As shown in Table 5-3, the size of the bubbles in this degassing unit were at the order of millimeters, which are comparable to those generated in other bubble columns described in literature. Calculations also show a high gas holdup over all test nitrogen injection rates, which is expected to improve the degassing efficiency in a shorter contact time due to increased contact area. Both of the predictions of gas holdup and mean bubble diameter were in accordance with preliminary photographic measurements. In addition, the small relative bubble velocity over the water ensures a longer residence (contact) time, and subsequently a better degassing performance.

4.2 Degassing efficiency of the batch reactor

Following up on equation (28) or (33), the thermodynamic limitation of the degassing efficiency could be calculated for our specific case. The mean initial dissolved oxygen concentration in the tap water measured in the experiments was 10 ppmw ca., atmospheric pressure 1.01325×10^{5} Pa, γ is the surface tension of tap water 73 mN/m, oxygen density is 1.3 kg/m^3, r is the radius of the bubble, K_H is 4.95×10^{-10} Pa^{-1} [33], and s depends on the purity of the nitrogen gas supply.

$$\frac{\left[1-\frac{K_H\cdot s\cdot\left(P_0+\frac{4\gamma}{r}\right)}{c_i}\right]}{\left[1+\frac{\rho_l}{\rho_g}\frac{1-\varepsilon_g}{\varepsilon_g}\cdot K_H\cdot\left(P_0+\frac{4\gamma}{r}\right)\right]} \tag{35}$$

Then the results of the degassing efficiencies versus residence time are shown in Figure 5-4. The mass transfer coefficients and the hypothetical film thicknesses were calculated from the best fit line for each set of tests with known and calculated parameters in Table 5-2 and Table 5-3.

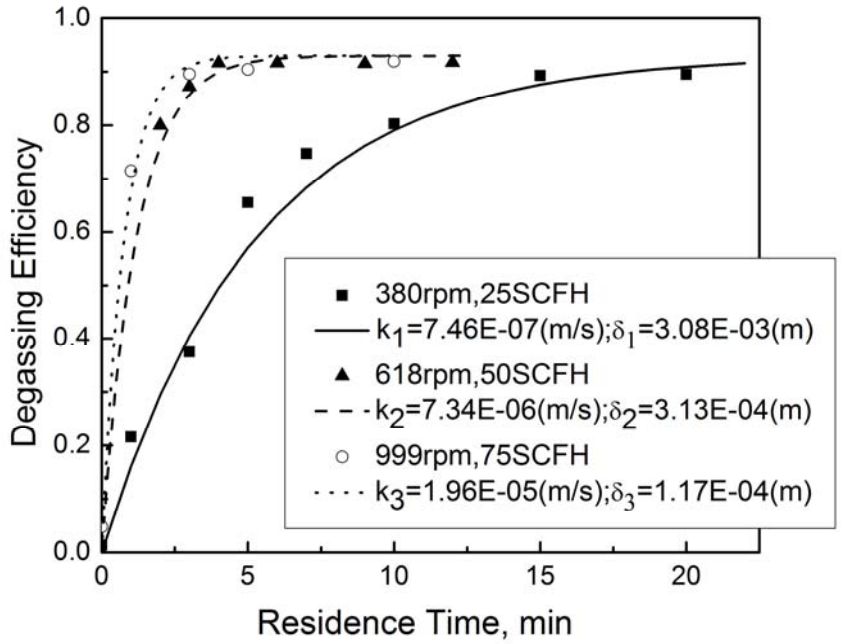

Figure 5-4 Degassing efficiency with respect to residence time using the batch reactor.

An important factor that decreases the film thickness is the agitation rate; the film thickness decreases about fifteen times as the agitation rate increases from 380 to 999 rpm. A thinner film leads to a higher mass transfer rate so that the system reaches the equilibrium more quickly with a higher agitation rate. The limit of the degassing efficiency (at the equilibrium), as explained with the thermodynamics theory and predicted in equation (35), was estimated to be no greater than 95%. This limit increased with the agitation rate, which can also be explained by the film theory - Figure 5-4 is conformed to the estimation. Similar methodology could be found in Jeannot and Cantwell's study [34] on the mass transfer using a single drop at the tip of a syringe needle. Nevertheless, the film thicknesses herein in our study are significantly thinner than those in their study. It is expected that the film thickness would decreases in tests of a single bubble in a more finite system.

4.3 Film thickness

It was found that the film thicknesses derived from the batch reactor experiments (Figure 5-4) can be most easily, yet very precisely (R^2=1), fitted with a linear equation (36).

$$\delta \times 10^4 = \frac{1.78 \times 10^8}{N \cdot Q_g{}^3} + 0.78 \qquad (36)$$

where the film thickness δ is in the unit of m, N is in rpm, and Qg is in SCFH.

Although this study was in a different and much more complex system, the fact that the film thickness is linearly proportional to *1/N* is still in accordance with the finding in Jeannot and Cantwell's single drop tests [34]. This conclusion is well founded because, again, the hypothetical film is essentially defined as the unstirred layer that thins as the stirring rate increases. Best-fit polynomial curves of higher orders also exist for the limited experimental data, but they are considered redundantly complex.

The reason why the film thickness decreases with the increase of the gas flow rate is because bubbles are in a more turbulent environment with a higher gas flow rate. This conclusion was also confirmed in Table 5-3 where it shows that the slip velocity increases with the gas flow rate, therefore leads to a higher bubble Reynolds number. It is also noted that the film thickness is more sensitive to the gas injection rate with an exponential order of two.

4.4 Degassing efficiency of the continuous reactor

With water flowing through, the degassing tank is operated as a continuous reactor. This is also what we aim to design for industrial degassing

processes. Similar to the batch reactor analysis, the bubble dynamic parameters were calculated first by solving the same set of equations and summarized in Table 5-4. In this study, the continuous reactor was operated at a water flow rate 2 GPM and a nitrogen injection rate 50 SCFH.

Table 5-4 Dynamic parameters calculated for a continuous reactor (Q_L=2 GPM).

Nitrogen injection rate, (SCFH)	d_b, (m)$\times 10^3$	ε_g, (%)	U_G, (m/s)$\times 10^3$	U_L, (m/s)$\times 10^4$	U_{bs}, (m/s) $\times 10^3$
50	3.00	92.6	2.38	7.64	7.75

The experimental data of the continuous reactor and the model predicted results of the degassing efficiency versus different impeller agitation rates were shown in Figure 5-5. The performance of equation (33) is based on the bubble dynamic parameters as listed in Table 5-4. The correlation derived in Figure 5-4 was used to calculate the new film thickness, which provides more information to evaluate the performance of the continuous reactor.

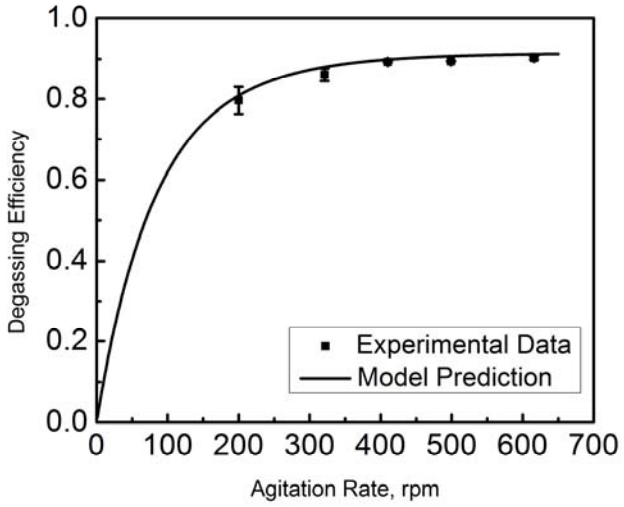

Figure 5-5 Experimental data and model predictions for the continuous reactor.

Figure 5-5 showed very positive results of model estimation with errors less than 3% at all experimental data points. There is very little over-prediction at higher agitation rates. It is very likely attributed to the fact that the system needs a bit longer residence time to reach the thermodynamic limit. This could be improved by re-designing the bubble column with a greater height. Bubble breakups and coalescences may also be a contributing factor, yet not significant. The system performances an 80% degassing efficiency at an agitation rate of around 200 rpm, whereas it could reach 90% after the agitation rate exceeds around 400 rpm. Finally, Figure 5-6 compared the degassing performances of this system with a system solely with mechanical agitation.

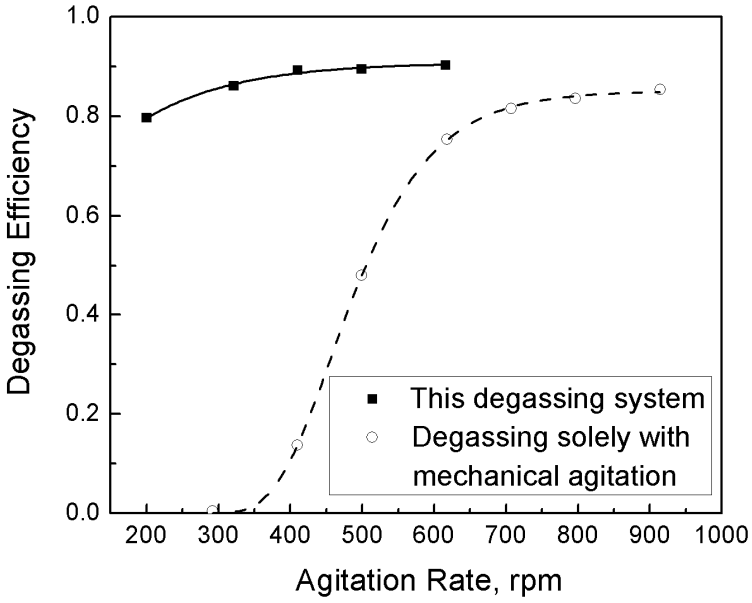

Figure 5-6 Comparison between the degassing system in this study with one solely with mechanical agitation.

Figure 5-6 showed obvious superiority of this new degassing system over the traditional system solely with mechanical agitations at all agitation rates. This difference was more significant at lower rates, which further highlighted the new system's efficient and cost-effective manner. Last but not least, higher and more special degassing efficiency requirements could be met by operating multiple units in series or using higher purity inert gases. Given the lower cost of the bubble columns, this would still be a cost effective solution.

5. Conclusions

A new bubble degassing system has been designed and its degassing efficiency has been both experimentally and analytically evaluated in this study. With a combination of micro bubbles and mechanical agitation at a low capital cost, this system could achieve a degassing efficiency of about 93%,

which showed significant superiority over the traditional system solely with mechanical agitations. A new way to estimate the bubble dynamics parameters such as the gas holdup and bubble size was developed by describing bubble movements and bubble-water interactions with a series of equations. Together with the equations of mass and momentum conservation, this method has a high generality. Consequently, these calculated parameters were coupled with the Fick's law mass transfer model to predict the degassing efficiency of a batch and a continuous reactor. Thermodynamic limit was taken into account and quantitatively described. Besides, two-film theory was used to complement the mass transfer coefficient theory which does not consider a diffusion-convection mechanism. Finally, the methodology of operating the bubble column as a batch reactor first to help evaluate the performance of it as a continuous reactor was proven to be valid and good agreement of the experimental and model-predicted data was obtained.

Nomenclature

A cross-sectional area of the degassing tank (m^2)

A_b total interfacial area between bubbles and the liquid (m^2)

c_b concentration of the target gas in the bubbles (ppmv)

c_i initial concentration of the dissolved gas in the liquid (ppmw)

c_f final concentration of the dissolved gas in the liquid (ppmw)

c_l concentration of the dissolved gas in the liquid (ppmw)

C_D drag coefficient of a single bubble rising in the liquid

d_b volume to surface mean diameter of bubbles (m)

D cross-sectional diameter of a bubble column (m)

D_g gas diffusion coefficient in a liquid ($m^2\ s^{-1}$)

f_{fb} interfacial drag per unit volume of liquid (N m^{-3})

f_{bf} interfacial drag per unit volume of bubble (N m^{-3})

g gravitational acceleration (m s^{-2})

j flux of the solute transferred from the liquid to the bubbles (kg m^{-2} s^{-1}).

k mass transfer coefficient (m s^{-1})

K_H Henry's law constant (Pa^{-1})

n Reynolds number dependent number in Richardson and Zaki experiments

N mechanical agitation rate (rpm)

N_{Bo} Bond number

N_{Fr} Froude number

N_{Ga} Galilei number

P_0 atmospheric pressure (Pa)

P_{O2} oxygen partial pressure (Pa)

Q_G gas flow rate (m^3 s^{-1})

Q_L liquid flow rate (m^3 s^{-1})

r radius of the bubble (m)

Re_b bubble Reynolds number

Re_t bubble Reynolds number at the terminal velocity

s initial concentration of the target gas in the inert gas bubble

T temperature (K)

U_G gas superficial velocity (m s^{-1})

U_L liquid superficial velocity (m s^{-1})

V volume of the degassing liquid (m^3)

V_b bubble velocity (m s^{-1})

V_{bs} bubble slip velocity (m s^{-1})

V_f fluid velocity (m s^{-1})

V_t bubble terminal velocity (m s^{-1})

Greek symbols

δ thickness of the hypothetical film (m)

ε_g gas holdup in a bubble column

ρ_g gas density (kg m^{-3})

ρ_L	liquid density (kg m^{-3})
γ_L	surface tension of a liquid (N m^{-1})
v_L	kinematic viscosity of a liquid (m^2 s^{-1})
μ_L	dynamic viscosity of a liquid (N m^{-2} s)
η	theoretical degassing efficiency
η_E	experimental degassing efficiency

References

[1] K. Li, I. Chua, W. J. Ng, W. K. Teo, Removal of dissolved oxygen in ultrapure water production using a membrane reactor, Chem. Eng. Sci. 50 (1995) 3547-3556.

[2] T. Leiknes, M. J. Semmens, Vacuum degassing using microporous hollow fiber membranes, Sep. Purif. Technol. 22-23 (2001) 287-294.

[3] A. Sengupta, P. A. Peterson, B. D. Miller, J. Schneider, C. W. Fulk Jr, Large-scale application of membrane contactors for gas transfer from or to ultrapure water, Sep. Purif. Technol. 14 (1998) 189-200.

[4] Z. G. Peng, S. H. Lee, T. Zhou, J. J. Shieh, T. S. Chung, A study on pilot-scale degassing by polypropylene (PP) hollow fiber membrane contactors, Desalination 234 (2008) 316-322.

[5] V. I. Lebedeva, V. M. Gryaznov, I. V. Petrova, V. V. Volkov, G. F. Tereshchenko, E. I. Shkol'nikov, L. M. Plyasova, D. I. Kochubey, R. Van Der Vaart, E. L. J. Van Soest-Verecammen, Porous Pd-containing polypropylene membranes for catalytic water deoxygenation, Kinet. Catal. 47 (2006) 867-872.

[6] O. V. Abramov, Ultrasound in liquid and solid metals, CRC, London, 1994.

[7] H. Xu, T. T. Meek, Q. Han, Effects of ultrasonic field and vacuum on degassing of molten aluminum alloy, Mater. Lett. 61 (2007) 1246-1250.

[8] K. Akita, F. Yoshida, Gas holdup and volumetric mass transfer coefficient in bubble columns: Effects of liquid properties, Ind. Eng. Chem. Process Des. Develop. 12 (1973) 76-80.

[9] K. Akita, F. Yoshida, Bubble size, interfacial area, and liquid-phase mass transfer coefficient in bubble columns, Ind. Eng. Chem., Process Des. Develop. 13 (1974) 84-91.

[10] H. Hikita, S. Asai, K. Tanigawa, K. Segawa, M. Kitao, The volumetric liquid-phase mass transfer coefficient in bubble columns, Chem. Eng. J. 22 (1981) 61-69.

[11] C. O. Vandu, R. Krishna, Volumetric mass transfer coefficients in slurry bubble columns operating in the churn-turbulent flow regime, Chem. Eng. Process. 43 (2004) 987-995.

[12] H. Jin, D. Liu, S. Yang, G. He, Z. Guo, Z. Tong, Experimental study of oxygen mass transfer coefficient in bubble column with high temperature and high pressure, Chem. Eng. Technol. 27 (2004) 1267-1272.

[13] M. Laakkonen, V. Alopaeus, J. Aittamaa, Validation of bubble breakage, coalescence and mass transfer models for gas-liquid dispersion in agitated vessel, Chem. Eng. Sci. 61 (2006) 218-228.

[14] K. Shimizu, S. Takada, K. Minekawa, Y. Kawase, Phenomenological model for bubble column reactors: Prediction of gas hold-ups and volumetric mass transfer coefficients, Chem. Eng. J. 78 (2000) 21-28.

[15] R. Krishna, J. M. Van Baten, Mass transfer in bubble columns, Catal. Today 79-80 (2003) 67-75.

[16] H. Dhaouadi, S. Poncin, J. M. Hornut, N. Midoux, Gas-liquid mass transfer in bubble column reactor: Analytical solution and experimental confirmation, Chem. Eng. Process. 47 (2008) 548-556.

[17] V. S. Warke, S. Shankar, M. M. Makhlouf, Mathematical modeling and computer simulation of molten aluminum cleansing by the rotating impeller degasser: Part II. Removal of hydrogen gas and solid particles, J. Mater. Process. Technol. 168 (2005) 119-126.

[18] Z. C. Hu, E. L. Zhang, S. Y. Zeng, Degassing of magnesium alloy by rotating impeller degasser Part 1 - Mathematical modelling, Mater. Sci. Technol. 24 (2008) 1304-1308.

[19] G. A. Hughmark, Holdup and mass transfer in bubble columns, Ind. Eng. Chem. Process Des. Dev. 6 (1967) 218-220.

[20] M. Martin, F. J. Montes, M. A. Galan, Mass transfer from oscillating bubbles in bubble column reactors, Chem. Eng. J. 151 (2009) 79-88.

[21] A. Kawahara, M. Sadatomi, F. Matsuyama, H. Matsuura, M. Tominaga, M. Noguchi, Prediction of micro-bubble dissolution characteristics in water and seawater, Exp. Therm Fluid Sci. 33 (2009) 883-894.

[22] F. Yazdian, S. A. Shojaosadati, M. Nosrati, M. Pesaran Hajiabbas, E. Vasheghani-Farahani, Investigation of gas properties, design, and operational parameters on hydrodynamic characteristics, mass transfer, and biomass production from natural gas in an external airlift loop bioreactor, Chem. Eng. Sci. 64 (2009) 2455-2465.

[23] W. Nernst, Zeitschrift fuer Physikalische Chemie 47 (1904) 52-55.

[24] W.K. Lewis, W.G. Whitman, Principles of Gas Absorption, J. Ind. Eng. Chem. 16 (1924) 1215-1220.

[25] J. H. Masliyah, Hindered settling in a multi-species particle system, Chem. Eng. Sci. 34 (1979) 1166-1168.

[26] J. B. Yianatos, J. A. Finch, G. S. Dobby, M. Xu, Bubble size estimation in a bubble swarm, J. Colloid Interface Sci. 126 (1988) 37-44.

[27] J. F. Richardson, W.N. Zaki, Sedimentation and fluidisation: Part I, Trans. Inst. Chem. Eng. 32 (1954) 35-53.

[28] J. H. Harker, J. F. Richardson, and J. R. Backhurst, Coulson & Richardson's chemical engineering, Fifth ed., Butterworth-Heinemann, London, 2002.

[29] P. N. Rowe, Drag forces in a hydraulic model of a fluidized bed-part 2, Trans. Inst. Chem. Eng. 39 (1961) 175-180

[30] W. C. Hinds, Aerosol Technology--properties behavior, and measurement of airborne particles, 2nd ed., John Wiley& Sons New York, 1999.

[31] P. T. H. M. Verhallen, L. J. P. Oomen, A. J. J. M. v. d. Elsen, J. Kruger, J. M. H. Fortuin, The diffusion coefficients of helium, hydrogen, oxygen and nitrogen in water determined from the permeability of a stagnant liquid layer in the quasi-s, Chem. Eng. Sci. 39 (1984) 1535-1541.

[32] J. G. Speight, Lange's Handbook of Chemistry 16th ed., McGraw-Hill New York, 2005.

[33] T. R. Rettich, R. Battino, E. Wilhelm, Solubility of gases in liquids. 22. High-precision determination of Henry's law constants of oxygen in liquid

water from T = 274 K to t d 328 Ka, J. Chem. Thermodyn. 32 (2000) 1145-1156.

[34] M. A. Jeannot, F. F. Cantwell, Mass Transfer Characteristics of Solvent Extraction into a Single Drop at the Tip of a Syringe Needle, Anal. Chem. 69 (1997) 235-239.

CHAPTER 6 : ADDITIONAL TECHNICAL DETAILS

6.1 Edson Gas Plant Field Test

Enersul Hyspec™ Degassing Process was considered to be one of the state-of-the-art liquid sulfur degassing technologies. A field trip was made to Talisman's gas plant at Edson to evaluate the real performance of the latest Hyspec™ units in order set up a base ground for this study.

6.1.1 Hyspec™ Degassing Process evaluation

Generally two series of experiments were conducted. The first one was to determine the sulfur degassing efficiency of each of the 4 degassing tanks. Liquid sulfur was sampled at the degasser inlet and each of the four tank outlets with a time interval equal to the residence time which is 10 minutes. Measurements were done using Fourier Transform Infrared Spectroscopy (FTIR) in a home-made cell at 135 ºC. Concentrations of three species, H_2S, H_2S_x, and the catalyst can be measured simultaneously. This series of tests was repeated 5 times and the results are shown in Figure 6-1.

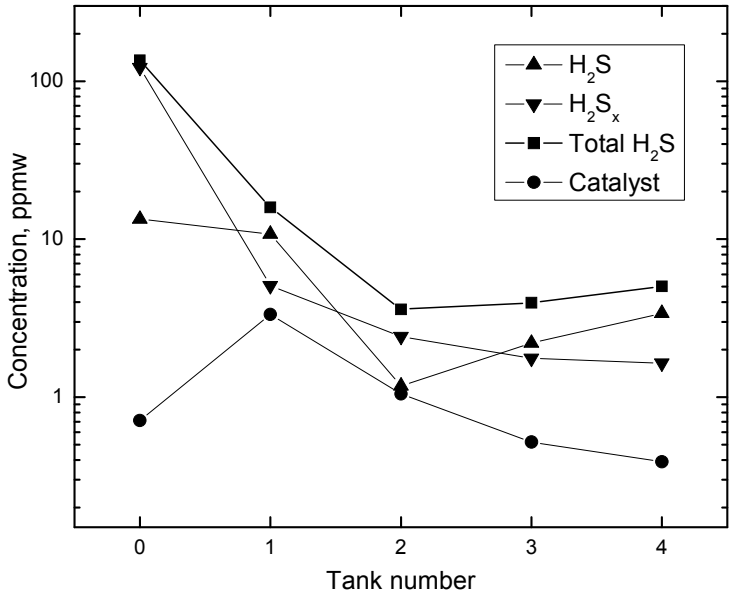

Figure 6-1 Concentrations of H_2S, H_2S_x, and the catalyst in the sulfur flowing through each of the 4 degassing tanks.

As shown in Figure 6-1, the sulfur transported from the upstream oil and gas plant contains about 150 ppmw total dissolved H_2S, a majority of which is in the form of H_2S_x. An amine-type catalyst was injected in the first tank while its concentration became negligible before it entered the forth tank. It, therefore, has negligible effects on the final sulfur product. Furthermore, this system shows a good degassing performance with the decomposition of H_2S_x. The sulfur product meets the quality requirement after two tank cells with a total H_2S concentration below 10 ppmw. The degassing efficiency of each tank is then plotted in Figure 6-2.

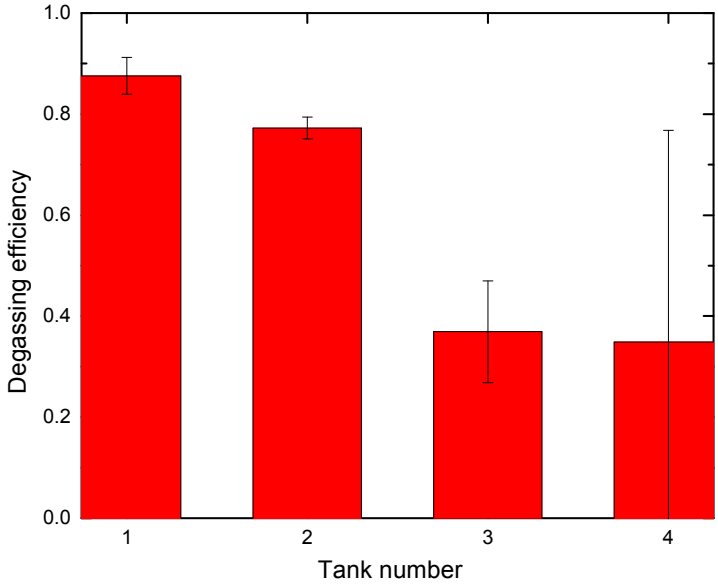

Figure 6-2 Degassing efficiency of each tank in Hyspec™ Process.

Either of the first two tanks is expected to reach the upper thermodynamic limit of one single tank unit's degassing performance, while the performance of the third and forth ones are significantly affected by the (low) inlet H_2S and catalyst concentrations. Therefore, it is concluded that the upper degassing efficiency of each tank unit is between 85% and 90%. The third tank ensures the purity of the sulfur and the forth one is mainly designed as a backup in case malfunction occurs to any of the first three tanks.

6.1.2 Effect of time and catalyst without sulfur agitation

The other part of the field test was to see if the degassing process can happen without catalyst addition or sulfur agitation. Sulfur was sampled at the inlet of the Hyspec™ unit. Tests were conducted in the measurement cell at 135 ºC. The sulfur sample was considered stagnant, free of any means of

external agitation. The result of the tests without catalyst addition is shown in Figure 6-3.

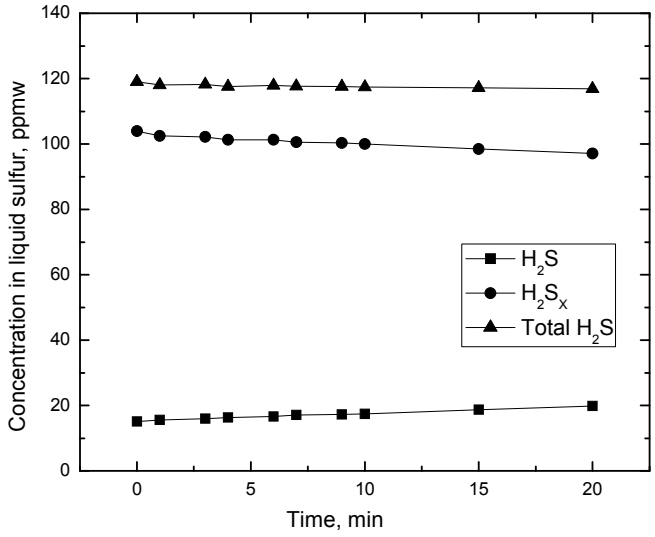

Figure 6-3 Concentrations of H_2S and H_2S_x with respect of time in stagnant liquid sulfur (without catalyst).

Figure 6-3, again, shows that without catalyst addition the H_2S_x is the dominant form of total dissolved H_2S. Decomposition of H_2S_x to H_2S is observed but obviously slow over the 20 min. The total dissolved H_2S (H_2S+H_2S_x) is more or less a constant amount, which indicates that, with a low surface to volume ratio and without any sulfur agitation, degassing is unlikely to happen in a short time during any industrial processes. The result for comparison is shown in Figure 6-4 where an amine-type catalyst was added in for every minute.

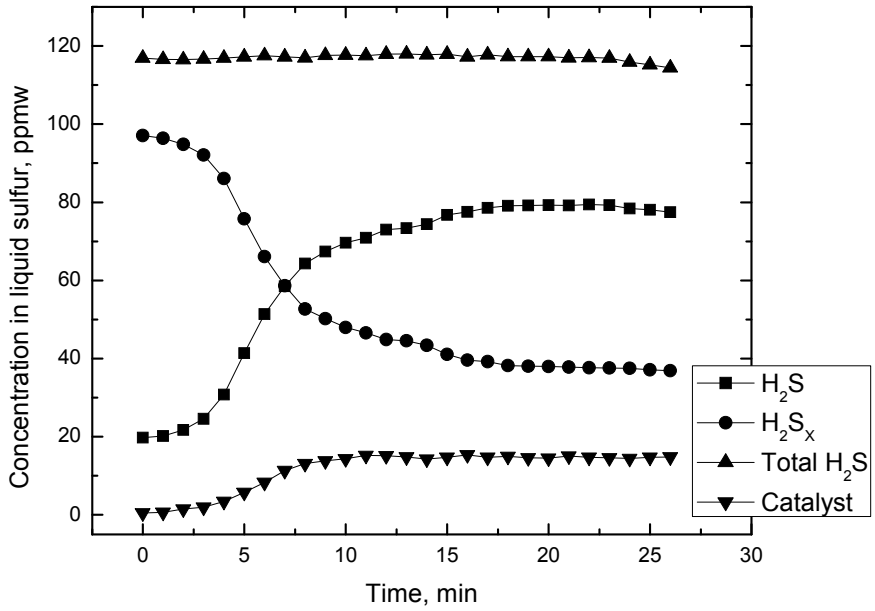

Figure 6-4 Concentrations of H_2S and H_2S_x with respect of time in stagnant liquid sulfur (with catalyst).

It is shown clearly in Figure 6-4 that the decomposition of H_2S_x to H_2S is perfectly correlated with the catalyst addition. However, the total amount of dissolved H_2S is still a constant—the catalyst can only facilitate the first step of a degassing process (reversible chemical reactions). A sound background of the effects of the catalyst and sulfur agitation was established through these series of experiments.

6.2 Design of a pilot degassing unit using poly-dispersed droplets

Since the laboratory degassing system using fine poly-dispersed droplets (spray) has demonstrated success, it is proposed herein that the project should move on to the stage of pilot tests. The purposes would be to further verify the fundamentals and give direct guidance to the industries. On top of a laboratory

degassing system design, three most important factors were considered in designing a pilot degassing unit: a) The system is operating at a high temperature (130-150 °C), above elemental sulfur's melting point; b) All the construction material should be H_2S-corrosion resistant; and c) Hot air is used instead of inert gas while the treatment load is also expected to be higher. The schematic of the design is shown in Figure 6-5.

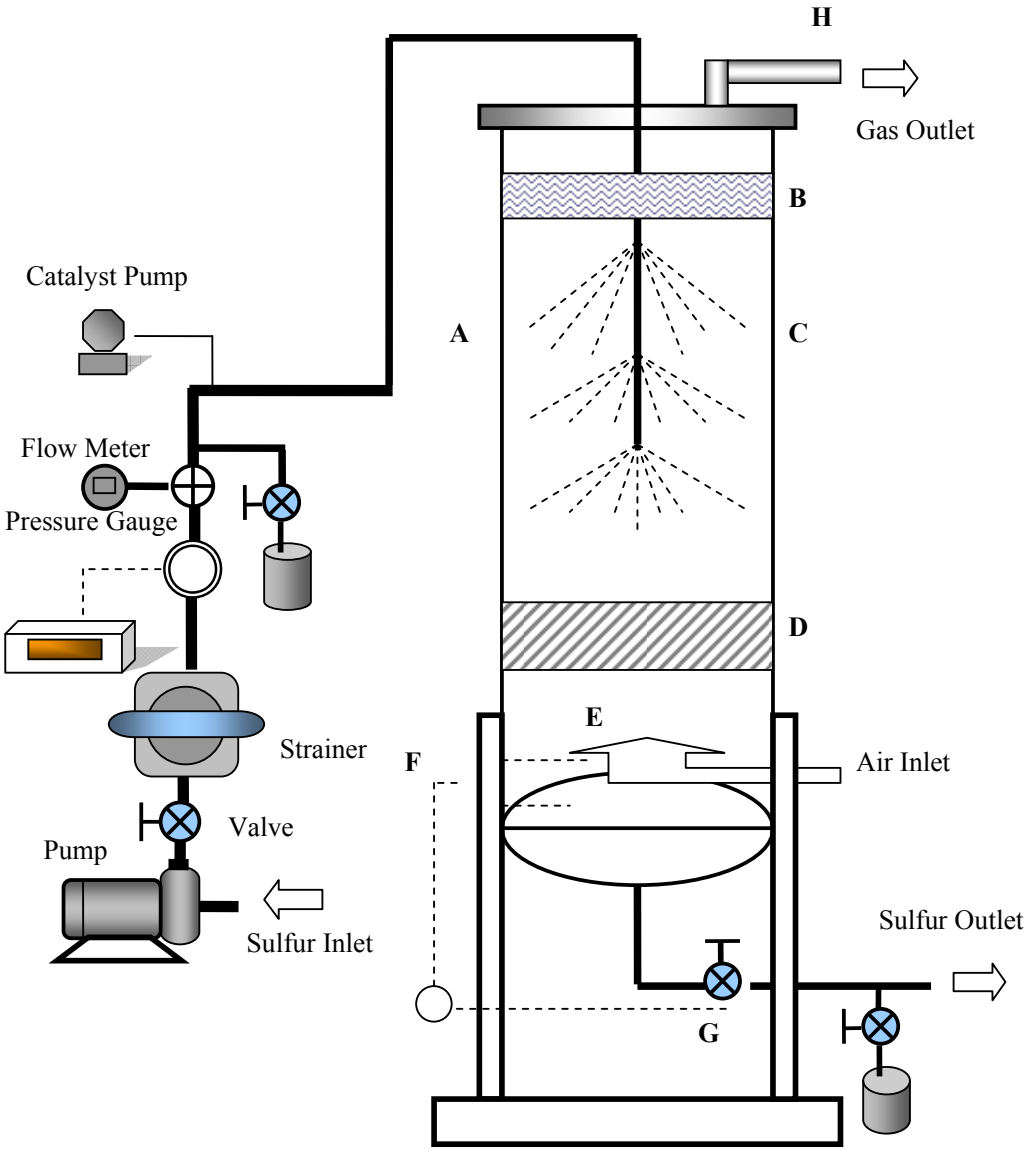

Figure 6-5 Design of a pilot sulfur degassing unit using fine poly-disperse droplets

More technical details about this pilot design are as the follows:

1) The spray angle of each nozzle, as shown in Chapter 3, is 90º. Considering the density difference between water and liquid sulfur, this angle should be corrected to about 88º (John Brooks, Inc.). In order to get 360º full space spray coverage, 4 nozzles are used on each of the 3 levels shown in Figure 6-5. There is a distance of 14 inches in between of each two adjacent nozzles.

2) A 24 inch stainless steel pipe with a vessel cap will be used to make the vessel body. The material is selected to have a pressure rating of 333 psi two different conditions can be set up. One is the atmospheric pressure environment, and the other is 40 psi pressurized system. A higher pressure is expected to facilitate the transfer (oxidization) of H_2S_x.

3) A unit with paralleled plates was proven to be of help to slightly increase the degassing efficiency, therefore the design is to be carried on in the pilot design, marked as "D". The whole system is continuously steam jacketed and insulated to maintain a high operation temperature (130-150 °C). This prevents the sulfur droplets and films from solidifying.

4) Pre-heated air will be introduced from the bottom of the vessel. A distributor "E" is used to get the air straightened and prevent liquid sulfur from clogging the air inlet openings.

5) Fine droplets are formed with use of a fog-type spray nozzle. Therefore, there is a distance designed in between of the top levels of nozzles and the top

cover of the vessel. As an additional protection, marked as “B”, a 4-inch high mesh pad is set to adsorb escaping droplets. Steam heat ensures that no solid sulfur is attached to the wire.

6) “H” is a pressure control valve. In the test under the atmospheric pressure, it is closed and one bypass is working as the air outlet; while for the pressurized system, it is opened to release the air when the system pressure is above 40 psi.

7) Similar function as valve “H”, a level control valve “G” is set up to release degassed liquid sulfur (sulfur outlet). Two-level liquid sensor “F” will monitor the liquid level. Only when the liquid reaches the top sensor, the valve will open to release the liquid; whereas when the liquid is below the bottom sensor, the valve will automatically close to keep the vessel chamber under certain air pressure.

6.3 Pressure decay method using a small reactor

Besides Chapter 5, the pressure decay method was also applied using a small reactor. The small reactor was cut from 1 inch tubing and had a volume of 54.7 cm^3. Similar to the tests using the big reactor, the gas to liquid ratio in the reactor was 3:2. Tests with two initial pressures and another test with overdosed catalyst (Steamate) were conducted at 130 ºC. Numerical optimization has not been performed and the raw pressure-decay data are shown in Figure 6-6 and 6-7.

Of more interests is Figure 6-7, which clearly shows that the catalyst addition dramatically enhanced the pressure decay rate given the same initial headspace pressure. This is interpreted by the fact that H_2S_x is a non-diffusive species in liquid sulfur, while the catalyst contained its formation path. The increased rate is mainly noticed at the beginning (t<8 ks)—after which the pressure decay rates (slops in Figure 6-7) of the two tests are almost identical. This is because the catalyst has a very short half life. In addition, combining the equilibrium data from the two no-catalyst tests in Figure 6-6 and 6-7 would result in a new Henry's law constant. As discussed in Chapter 5, this constant is also expected to be in accordance with the correlation recently derived by Alberta Sulfur Research Ltd. (ASRL). When it comes to analytical modeling, the system with catalyst addition to contain the forward chemical reaction between H_2S and sulfur is expected to follow the original Fick's law of diffusion.

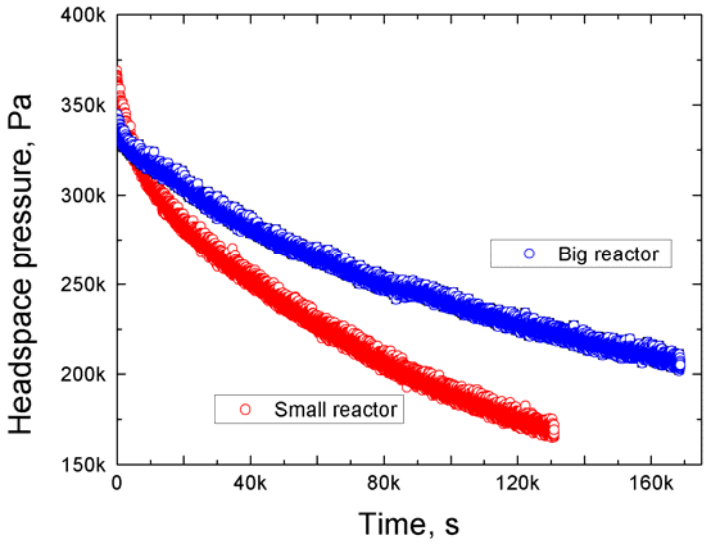

Figure 6-6 Raw pressure decay data for the big and small reactors

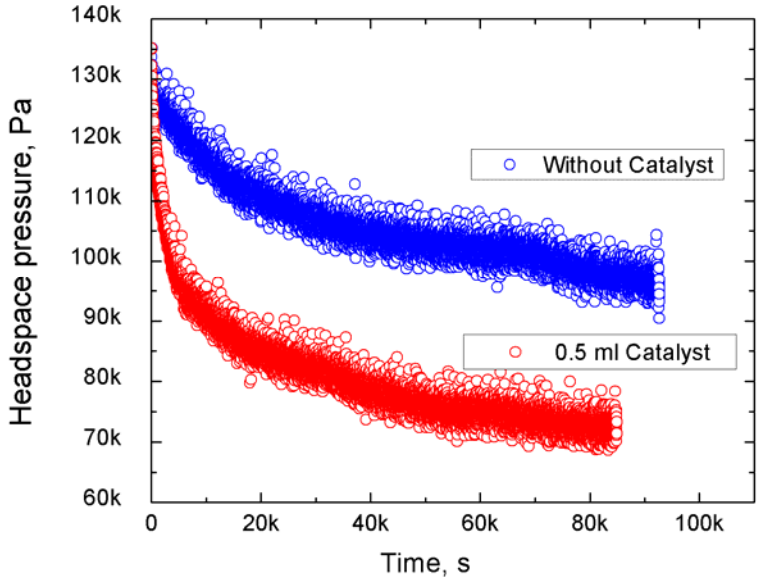

Figure 6-7 Raw pressure decay data for tests with and without the catalyst

6.4 High speed photo shots of mono-dispersed droplets

The degassing system using mono-dispersed droplets is one of the novel designs in this study. Considering that the droplet size is small and the droplet velocity coming out of the orifice is high, a high speed camera system was used to capture their movements. Figure 6-8 compares the shots before and the square wave excitation was sent to the system where a 50 μm orifice is used and the water flow rate is 66ml/hr. The picture on the left hand side shows a water stream without any disturbance, whereas, on the right hand, a 10.67 kHz excitation clearly breaks the water stream into a string of droplets, confirming successful generation of droplets.

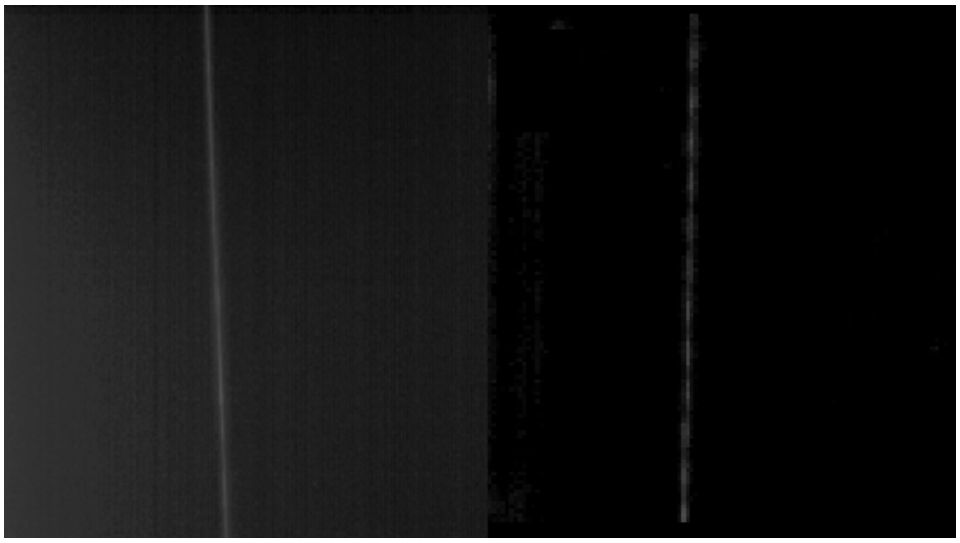

Figure 6-8 A mono-dispersed droplet system with (right) and without (left) square wave excitation.

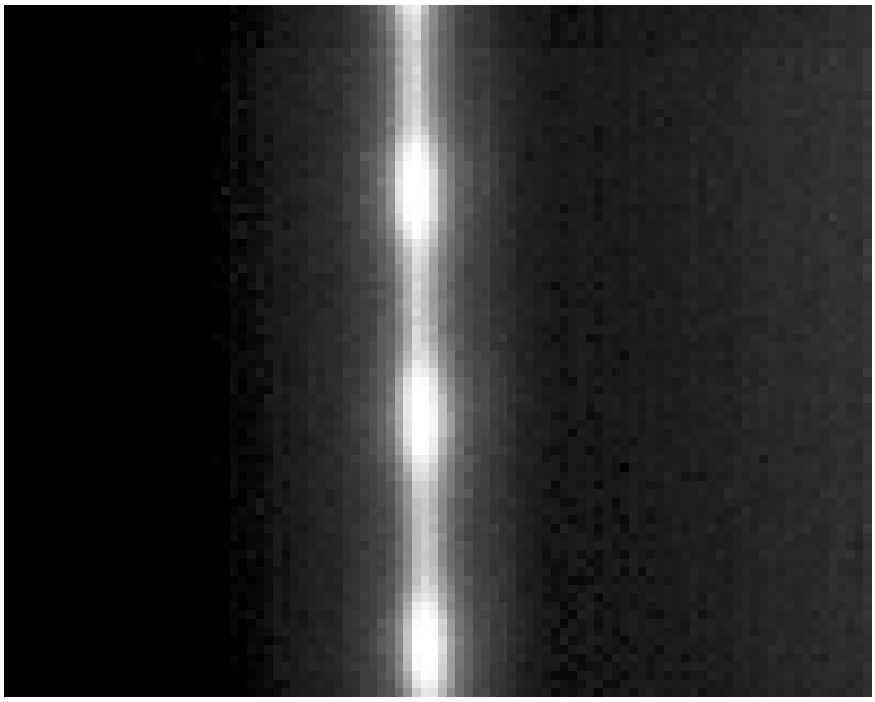

Figure 6-9 A high speed (1000 frames/s) shot of the mono-dispersed droplet.

Figure 6-9 gives a closer look at the mono-dispersed droplets with a high speed shot at 1000 frames/s. The gap between each two adjacent droplets is almost as large as one single droplet. Unfortunately, without a microscope-

assisted camera, it is still difficult to get a better view of each individual droplet which is supposed to be spherical.

CHAPTER 7 : CONCLUSIONS AND RECCOMENDATIONS

7.1 Conclusions

This work was motivated by a specific industrial problem to develop new de-H_2S techniques with new apparatus designs. It is to meet the quality requirement for sulfur production, and to prevent potential health or environmental problems caused by H_2S. The results are expected to have direct and instant impacts on improving degassing efficiencies and lowering capital/operating costs for sulfur production/purification companies. It also has a great potential for a variety of other industrial applications such as air pollution control. The experimental data and analytical analysis are of high generality, which can be applied for any mass transfer processes and various gas-liquid systems. A properly designed spray tower or bubble column should be able to work well not only for degassing, but also aeration, wet scrubbing, and liquid-liquid extraction, etc. The detailed conclusions for each Chapter are summarized as follows:

The diffusion coefficient of H_2S in liquid sulfur is a key kinetic parameter that so far has been missing in literature. In Chapter 2, a pressure decay method was applied to measure the diffusion coefficients of H_2S in liquid sulfur at 403 and 423 K. This pressure decay process was analytically modeled considering simultaneous diffusion and reversible chemical reactions between H_2S and liquid sulfur. With the headspace experimental pressure decay history, the diffusion coefficient and reaction rate constants were numerically determined from the best matched curve using Finite Element Method and Genetic Algorithm. The concentration distribution history was also shown using

numerical software such as Matlab and Comsol. The solubility of H_2S in liquid sulfur was also calculated and the result was in excellent accordance with the semi-empirical correlation derived lately in literature. Furthermore, this study extended the validity of this correlation to a higher partial pressure of H_2S.

In Chapter 3, liquid degassing using mono-dispersed and poly-dispersed fine droplets (148.6 and 264.8 μm) falling in inert gas was experimentally and analytically studied. The mono-dispersed droplet experiments indicated a significant increase with the decrease of the droplet size, while tests with poly-dispersed droplets revealed a system degassing limit of 93% when the inert gas to liquid flow ratio is above 15 and a fog-type nozzle was used. This degassing efficiency matched the most up-to-date degassing technique in a cost effective manner. Furthermore, simple linear correlations of the Sherwood number in relation to the Peclet number were derived for mono-dispersed droplets as $Sh = 0.0016\mathrm{Pe} + 15.297$ (20000<Pe<45000) and two adjacent Peclet number regions for poly-dispersed droplets as $Sh = 0.00136Pe + 15.822$ (Pe<7500) and $Sh = 0.00676Pe - 21.337$ (7500<Pe<200000). The experiments were conducted under medium Reynolds numbers (10-100). The correlation for the mono-dispersed droplets agreed well with the steady state mass transfer correlations derived previously based on both experiments and numerical simulations, especially at small Peclet numbers. The lower part of the correlation for the poly-dispersed droplets converged with that derived for mono-dispersed droplets, and the upper part of it fell in between of the steady state and the situation with fully-developed internal circulations.

Chapter 4 features a specific application of the new degassing technique. A new laboratory water-degassing (water treatment) system using poly-dispersed

droplets falling in inert gas has been designed and evaluated in this chapter. With a low construction and operation cost, this system could achieve a degassing efficiency of about 92%. It was superior over a laboratory bubbling degassing system by approximately 10% at higher nitrogen flow rates, and by even more at lower rates. For an inlet water flow rate up to 220.8 ml/s, the optimal inert gas flow rate was found to be around 1 l/s. Increased positive or vacuum stagnant inert gas pressure did not show obvious effects changing the degassing efficiency, but both of them were less favored than the atmospheric pressure. In addition, preliminary experiments with a system using mono-dispersed water droplets were consistent with the observations in the system using poly-dispersed droplets.

The theoretical and experimental performances of a new liquid degassing unit using a combination of micro-bubbles and mechanical agitation were evaluated in Chapter 5. Model predictions agreed well with the experimental degassing data with errors no greater than 3%. It was showed that while the gas to liquid flow ratio was up to 4.7, the degassing efficiency could reach a thermodynamic limit of 93% in less than 5 minutes when the unit was operated as a batch reactor. As a continuous reactor with a gas to liquid flow ratio of 3, the degassing efficiency increased with the increase of the mechanical agitation rate. Once the agitation rate was above 400 rpm, the degassing efficiency reached 90%. Higher degassing requirements could be met in a cost-effective manner by operating multiple units in series.

In addition, a new way to estimate the bubble size and gas holdup in the degassing unit by solving a series of mass/momentum-conservation and bubble-motion equations was developed with high generality. The two-film

theory was used to help interpret the diffusion-convection mechanism so as to complement the traditional method of using the volumetric mass transfer coefficient.

Finally, Chapter 6 complemented in all other important technical details. During a field trip to Talisman's gas plan at Edson, evaluation of Enersul's latest Hyspec^{TM} sulfur degassing process showed that each tank of the 4-tank series could achieve a degassing efficiency between 85% and 90%. The third and fourth tank units are mainly designed as backups as the sulfur after the first two units meets the 10 ppmw H_2S concentration requirements. The residence time in each tank unit was about 10min. An amine-type catalyst is continuously injected into the first tank unit, but it only has a trace amount after the forth unit and is unlikely to affect the quality of the final sulfur product. Besides, the effects of time and catalyst addition on the degassing efficiency were studied independently in a home-made measurement cell. It was found that the decomposition of H_2S_x to H_2S was perfectly correlated with the catalyst addition. However, without sulfur agitation, degassing was not noticed due to a limited surface to volume ratio.

Another set of pressure decay data using a small reactor was also reported in Chapter 6. Numerical optimization has not been performed but the data showed a consistent trend with those got from the big reactor. Addition of overdosed catalyst showed significant effect at the beginning, greatly enhancing the pressure decay rate by accelerating the decomposition of the non-diffusive species, H_2S_x, to H_2S. Changes were not noticeable to the pressure decay rates at longer times because the catalyst had a short half life.

7.2 Future work recommendations

Due to the time limitation of a Master's program, lots of work has not been completed and some of those were listed below as recommendations for future studies:

1. The tests using mono-dispersed droplets provided fundamentals for a degassing system using spray (poly-dispersed) droplets. Similar experiments should also be conducted for degassing using inert bubbles. This system is expected to be able to generate a stable string of mono-sized bubbles.
2. All the experiments were conducted using water-oxygen system. However, other different degassing systems (both organic and inorganic) should also be evaluated so that the validity of the analytical models can be verified.
3. To further bridge the differentials between a system using mono-dispersed droplets and one using poly-dispersed droplets, a system using two (or multiple) mono-dispersed droplet generator should be design and tested. Operating multiple mono-dispersed droplet generators with different droplet diameter can simulate a poly dispersed droplet system without droplet-droplet interactions.
4. The spray tower for the field degassing tests (H_2S-sulfur) have been designed but not been constructed. Field tests are needed to evaluate its performance and to further improving the design.
5. Numerical optimization should be performed to the pressure decay data achieved from the small reactor tests to further verify the diffusion coefficient derived from the big reactor tests. The system with catalyst

addition should be re-modeled using the traditional Fick's law of diffusion without considering reactions.

6. Kinetics of a H_2S- H_2S_x-sulfur is still a big project that is worth looking into. For example, the pressure decay experiments at 140 ºC led to an abnormally high diffusion coefficient (Figure 7-1). These experimental data need further verifications. Some reactions or transformations that were not accounted for in this study might need to be identified at this temperature.

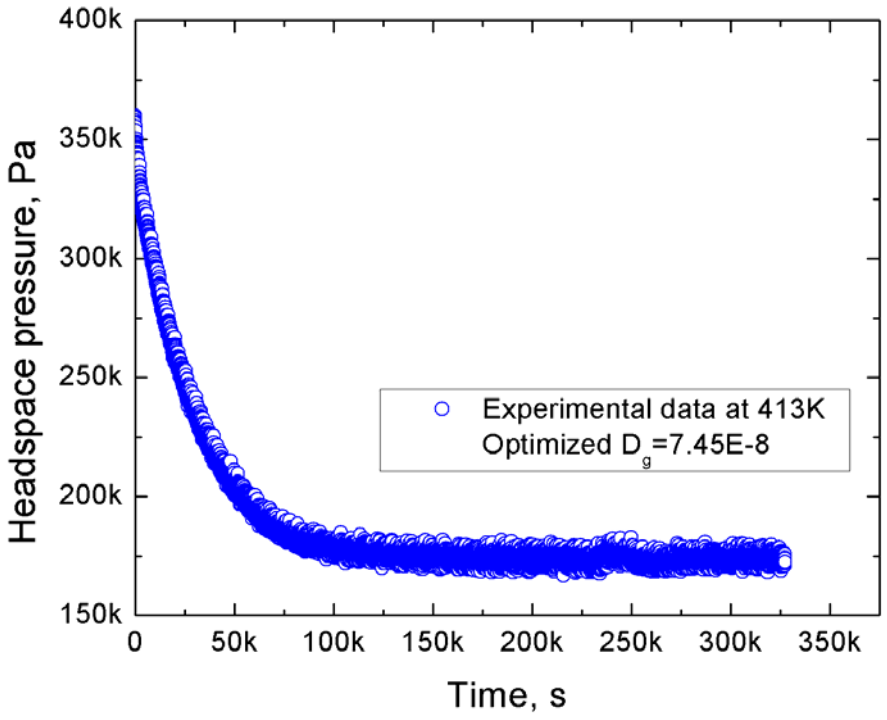

Figure 7-1 Pressure decay data at 140 ºC and its corresponding diffusion coefficient.